Area of Review and Corrective Action Plan

Orange text is from information provided by PNNL in February/March 2014

Facility Information

Facility name: FutureGen 2.0 Project: Morgan County Class VI UIC Wells 1, 2, 3, and 4

Facility contacts (names, titles, phone numbers, email addresses): Kenneth Humphreys, Chief Executive Officer, FutureGen Industrial Alliance, Inc., Morgan County Office, 73 Central Park Plaza East, Jacksonville, IL 62650, 217-243-8215
Telephone: 217/243-8215
Email: info@FutureGenAlliance.org
Homepage: www.FutureGenAlliance.org

Location (town/county/etc.): Morgan County, IL; 26−16N−9W; 39.800266ºN and 90.07469ºW"

~~Facility name: Alliance, the FutureGen 2.0~~

~~Facility contacts (names, titles, phone numbers, email addresses):~~
~~FutureGen Industrial Alliance, Inc.~~
~~73 Central Park Plaza East~~
~~Jacksonville, IL 62650~~

~~Location (town/county/etc.): Morgan County, Illinois~~

Computational Modeling

Model Name: STOMP -CO2 (Subsurface Transport Over Multiple Phases-CO_2) simulator
Model Authors/Institution: White et al. 2013; White and Oostrom 2006; White and McGrail 2005 / Pacific Northwest National Laboratory (PNNL)

Description of model:

The simulations conducted for this investigation were executed using the STOMP-CO2 simulator (White et al. 2013; White and Oostrom 2006; White and Oostrom 2000). STOMP-CO2 was verified against other codes used for simulation of geologic disposal of CO_2 as part of the GeoSeq code intercomparison study (Pruess et al. 2002).

Partial differential conservation equations for fluid mass, energy, and salt mass compose the fundamental equations for STOMP-CO2. Coefficients within the fundamental equations are related to the primary variables through a set of constitutive relationships. The salt transport equations are solved simultaneously with the component mass and energy conservation equations. The solute and reactive species transport equations are solved sequentially after the coupled flow and transport equations. The fundamental coupled flow equations are solved using an integral volume finite-difference approach with the nonlinearities in the discretized equations resolved

through Newton-Raphson iteration. The dominant nonlinear functions within the STOMP-CO2 simulator are the relative permeability-saturation-capillary pressure (k-s-p) relationships.

The STOMP-CO2 simulator allows the user to specify these relationships through a large variety of popular and classic functions. Two-phase (gas-aqueous) k-s-p relationships can be specified with hysteretic or nonhysteretic functions or nonhysteretic tabular data. Entrapment of CO_2 with imbibing water conditions can be modeled with the hysteretic two-phase k-s-p functions. Two-phase k-s-p relationships span both saturated and unsaturated conditions. The aqueous phase is assumed to never completely disappear through extensions to the s-p function below the residual saturation and a vapor pressure lowering scheme. Supercritical CO_2 has the function of a gas in these two-phase k-s-p relationships.

For the range of temperature and pressure conditions present in deep saline reservoirs, four phases are possible: 1) water-rich liquid (aqueous), 2) CO_2-rich vapor (gas), 3) CO_2-rich liquid (liquid-CO_2), and 4) crystalline salt (precipitated salt). The equations of state express 1) the existence of phases given the temperature, pressure, and water, CO_2, and salt concentration; 2) the partitioning of components among existing phases; and 3) the density of the existing phases. Thermodynamic properties for CO_2 are computed via interpolation from a property data table stored in an external file. The property table was developed from the equation of state for CO_2 published by Span and Wagner (1996). Phase equilibria calculations in STOMP-CO2 use the formulations of Spycher et al. (2003) for temperatures below 100°C and Spycher and Pruess (2010) for temperatures above 100°C, with corrections for dissolved salt provided in Spycher and Pruess (2010). The Spycher formulations are based on the Redlich-Kwong equation of state with parameters fitted from published experimental data for CO_2-H_2O systems. Additional details regarding the equations of state used in STOMP-CO2 can be found in the guide by White et al. (2013).

A well model is defined as a type of source term that extends over multiple grid cells, where the well diameter is smaller than the grid cell. A fully coupled well model in STOMP-CO2 was used to simulate the injection of supercritical CO_2 ($scCO_2$) under a specified mass injection rate, subject to a pressure limit. When the mass injection rate can be met without exceeding the specified pressure limit, the well is considered to be flow controlled. Conversely, when the mass injection rate cannot be met without exceeding the specified pressure limit, the well is considered to be pressure controlled and the mass injection rate is determined based on the injection pressure. The well model assumes a constant pressure gradient within the well and calculates the injection pressure at each cell in the well. The CO_2 injection rate is proportional to the pressure gradient between the well and surrounding formation in each grid cell. By fully integrating the well equations into the reservoir field equations, the numerical convergence of the nonlinear conservation and constitutive equations is greatly enhanced.

Model Inputs and Assumptions:

1. Conceptual Model

~~1.1 Model Domain~~

~~1.2~~1.1 ~~Site Geology~~Site Stratigraphy

The regional geology of Illinois is well known from wells and borings drilled in conjunction with hydrocarbon exploration, aquifer development and use, and coal and commercial mineral exploration. Related data are largely publicly available through the Illinois State Geological

Survey (ISGS)[1] and the U.S. Geological Survey. ~~(USGS)~~[2]. In addition, the U.S. Department of Energy ~~DOE~~ has sponsored a number of studies by the Midwest Geologic Sequestration Consortium[3] to evaluate subsurface strata in Illinois and adjacent states as possible targets for the containment of anthropogenic CO_2.

To support the evaluation of the Morgan County site as a potential carbon storage site, a deep stratigraphic well was drilled and extensively characterized. The FutureGen 2.0 stratigraphic well, located at longitude 90.05298W, latitude 39.80681N, is approximately 1.24 mi (2 km) northeast of the planned ~~storage~~ injection site. The stratigraphic well reached a total depth of 4,826 ft (1,471 m) bgs within the Precambrian basement (Figure 1~~(Figure 2.1))~~ ~~within the Precambrian basement~~. The well penetrated 479 ft (146 m) of the Eau Claire Formation and 512 ft (156 m) of the Mount Simon Sandstone. The stratigraphic well was extensively characterized, sampled, and geophysically logged during drilling. A total of 177 ft of whole core were collected from the lower Eau Claire Formation and ~~-~~upper Mount Simon Sandstone and 34 ft were collected from lower Mount Simon Sandstone and ~~-~~Precambrian basement interval. In addition to whole drill core, a total of 130 side-wall core plugs were obtained from the combined interval of the Eau Claire Formation, Mount Simon Sandstone, and the Precambrian basement. In Figure 2 ~~(Figure 2.11)~~, cored intervals are indicated with red bars; rotary side-wall core and core-plug locations are indicated to the left of the lithology panel. Standard gamma ray and resistivity curves are shown in the second panel. ~~The proposed injection interval (location of the horizontal wells' injection laterals) is highlighted on the geophysical log panels in Figure 2.~~

[1] http://www.isgs.uiuc.edu/
[2] http://www.usgs.gov/
[3] http://sequestration.org/

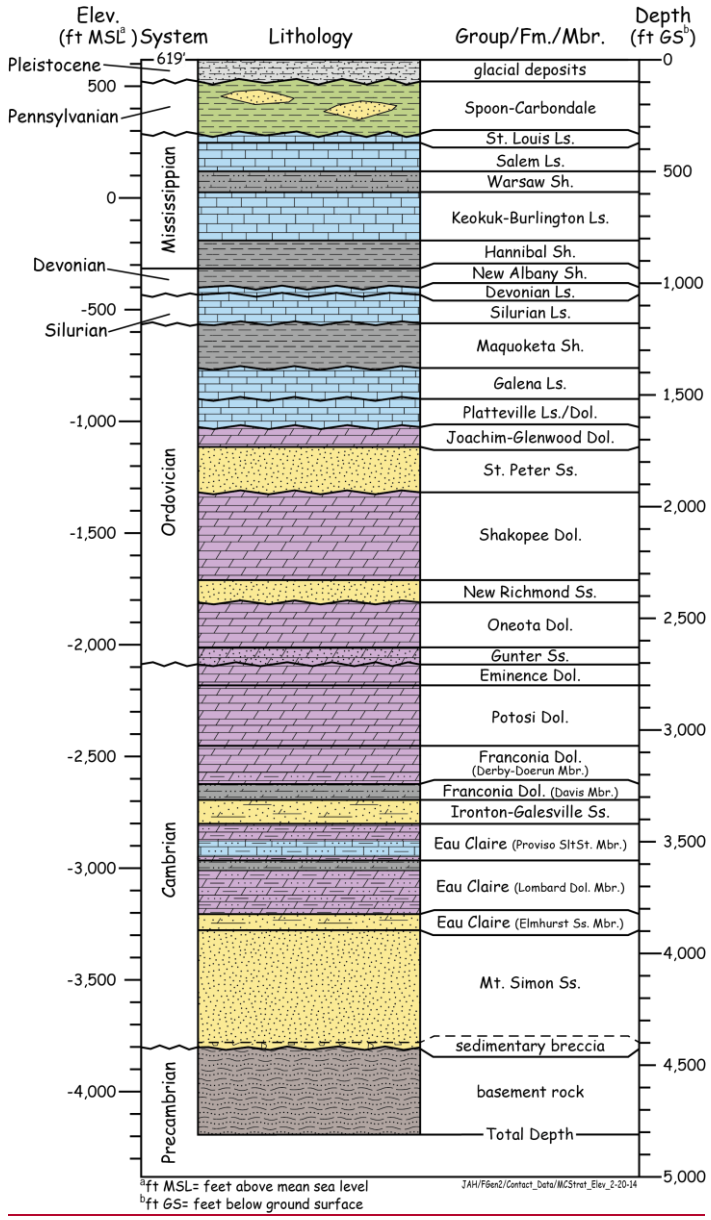
Elev.
(ft MSL[a])
System
Lithology
Group/Fm./Mbr.
Depth
(ft GS[b])
619'
Pleistocene
500
Pennsylvanian
0
Devonian
-500
Silurian
-1,000
-1,500
-2,000
-2,500
-3,000
-3,500
-4,000
Mississippian
Ordovician
Cambrian
Precambrian
glacial deposits
Spoon-Carbondale
St. Louis Ls.
Salem Ls.
Warsaw Sh.
Keokuk-Burlington Ls.
Hannibal Sh.
New Albany Sh.
Devonian Ls.
Silurian Ls.
Maquoketa Sh.
Galena Ls.
Platteville Ls./Dol.
Joachim-Glenwood Dol.
St. Peter Ss.
Shakopee Dol.
New Richmond Ss.
Oneota Dol.
Gunter Ss.
Eminence Dol.
Potosi Dol.
Franconia Dol. (Derby-Doerun Mbr.)
Franconia Dol. (Davis Mbr.)
Ironton-Galesville Ss.
Eau Claire (Proviso SltSt. Mbr.)
Eau Claire (Lombard Dol. Mbr.)
Eau Claire (Elmhurst Ss. Mbr.)
Mt. Simon Ss.
sedimentary breccia
basement rock
Total Depth
0
500
1,000
1,500
2,000
2,500
3,000
3,500
4,000
4,500
5,000
[a]ft MSL= feet above mean sea level
[b]ft GS= feet below ground surface
JAH/FGen2/Contact_Data/MCStrat_Elev_2-20-14

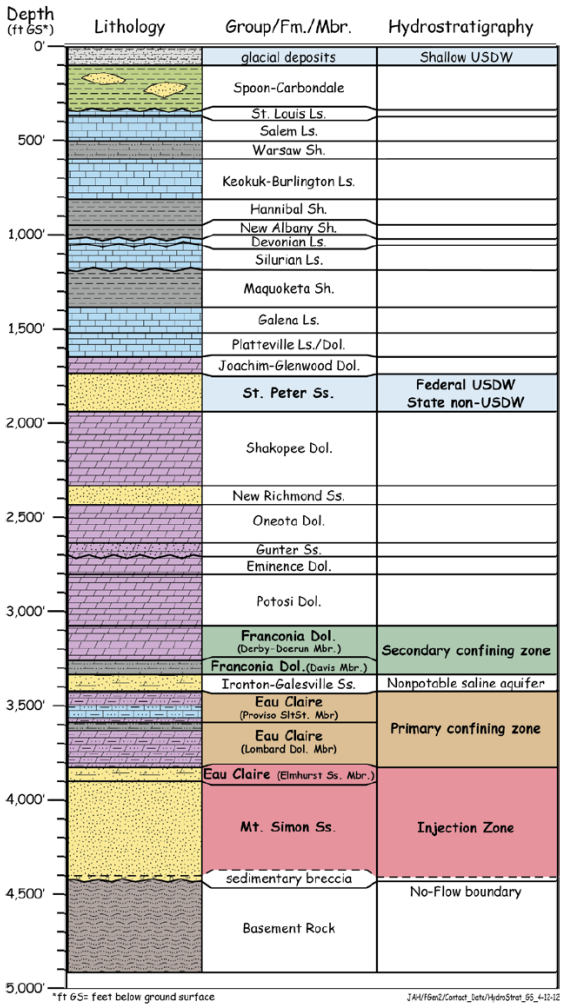

Stratigraphy and Proposed Injection and Confining Zones at the Morgan County CO_2 Storage Site

Figure 1. Stratigraphic Column of FutureGen 2.0 Stratigraphic Well

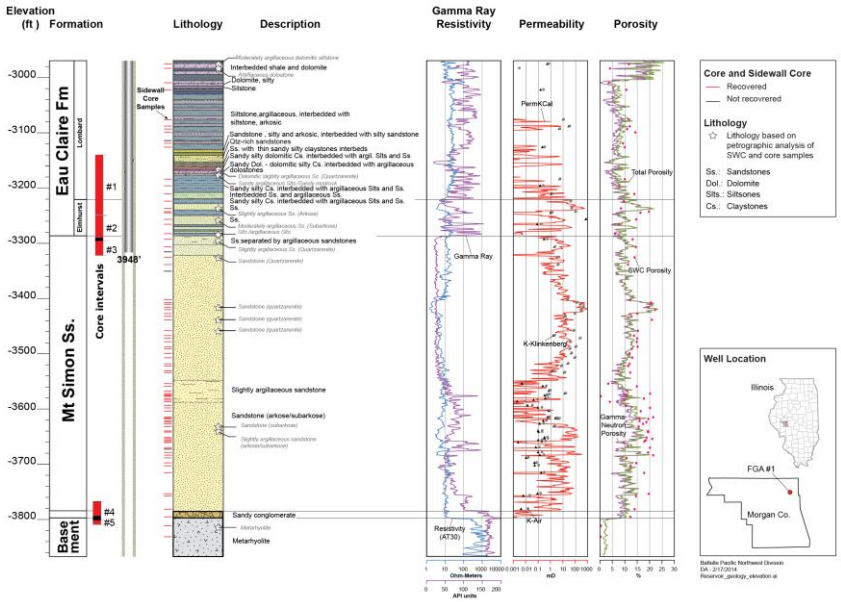

Figure 2. Lithology, Mineralogy, and Hydrologic Units of the Proposed Injection Zone (Mount Simon, Elmhurst and Lower Lombard member) and Lower Primary Confining Zone (Upper Lombard), as Encountered Within the Stratigraphic Well

~~1.3~~1.2 ~~1.1.1 Seismic profile~~Geologic Structures

Two orthogonal two-dimensional (2D) surface seismic lines, shown in Figure 3 ~~(Figure 2.14)~~, were acquired along public roads near the site and processed in January and February 2011. Surface seismic data were acquired as a single-component data. The seismic data are not of optimal quality due to loss of frequency and resolution below a two-way time depth of about 300 milliseconds (ms), approximately coincident with the top of the Galena limestone at a depth of 1,400 ft. However, they do not indicate the presence of obvious faults or large changes in thickness of the injection or confining zones. Both profiles indicate a thick sequence of Paleozoic-aged rocks with a contact between Precambrian and Mount Simon at 640 ms ~~ms~~ and a contact between Eau Claire and Mount Simon at 580 ms.

Some vertical disruptions, which extend far below the sedimentary basin, remain after reprocessing in 2012, but their regular spatial periodicity has a high probability of being an artifact during data acquisition and processing and is unlikely related to faults.

No discernable faults have been identified on the 2D data within the Area of Review (AoR). A small growth fault that affects the Mount Simon and Eau Claire formations is interpreted in the eastern part of the L201 profile at an offset 28,000 ft. This growth fault is more than 1.5 miles away from the outermost edge of the CO_2 plume and does not extend far upward in the overburden. For these reasons, it is highly unlikely that it could affect the integrity of the injection zone.

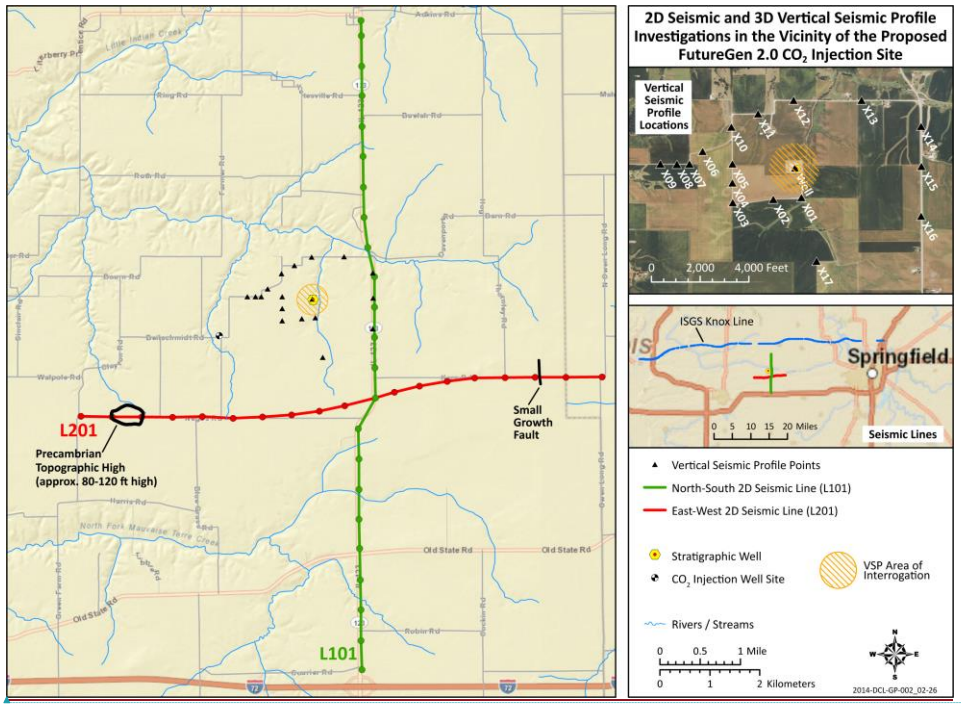

Figure 3. Locations of Two 2D Seismic Survey Lines, L101 and L201, Vertical Seismic Profile Locations, and the Knox Line Near the Proposed Morgan County CO_2 Storage Site. Line L101 is along Illinois Highway 123. The Knox line seismic profile completed in 2012 by the ISGS passes within 10 miles of the site. No discernable faults have been found within the extent of the simulated CO_2 plume.

A three-component vertical seismic profiling (VSP) data set (Figure 3) was acquired in the FutureGen stratigraphic well in March, 2013 and processed by Schlumberger Carbon Services. No discernable faults are present in the 15 short 2D seismic lines formed by the offset VSP locations. These lines represent a lateral interrogation extent of 800−1600 ft radially from the stratigraphic well. The high-resolution, low-noise VSP data also do not contain the vertical disruptions observed in the 2D surface seismic profiles (Hardage 2013[4]).

The ISGS recently shot a 120-mi long seismic reflection survey (the Knox Line) across central Illinois as part of a Department of Energy-sponsored research project to characterize rock units for geologic storage of CO_2. The continuous east-west line extends from Meredosia to southwestern Champaign County (Figure 3). FutureGen acquired these data from the ISGS with the intention of reprocessing the data, if needed, to identify regional faults that might impact the proposed Morgan County storage site. A review of the data by a geophysical expert on Illinois

[4] Bob Hardage, Personal Communication with Charlotte Sullivan, August 1, 2013.

Formatted: Font: 11 pt

reflection seismic data[5], indicated that there was no discernable faulting west of Ashland, Illinois; and that current plans to reprocess the ISGS Knox line would not likely result in a greatly improved image.

~~*1.3.1*~~

~~A fault can usually be recognized and interpreted in seismic data if it creates a quasi-vertical displacement of 20 ms or more in several successive reflection events. The amount of vertical fault throw that would produce a 20-ms vertical displacement would be (0.01 sec) X (P-wave interval velocity), for whatever interval velocity is appropriate local to a suspected fault. For the interval from the surface down to the Eau Claire at the FutureGen site in Morgan County, the P-wave interval velocity local to seismic lines L101 and L201 ranges from approximately 7,000 ft/s (shallow) to approximately 12,000 ft/s (deep). Thus, faults having vertical throws of 120 ft at the Eau Claire, and perhaps as little as 70 ft at shallow depths, should be detected if they traverse either profile. No faults with a clear vertical displacement have been identified; the only clear observation that can be made is the existence of a growth fault that affects Mount Simon and Eau Claire formations in the eastern part of the L201 profile at offset 28,000 ft. This growth fault is more than 1.5 miles away from the outermost edge of the CO_2 plume and does not extend far upward in the overburden. For these reasons, it is highly unlikely that it could affect the integrity of the reservoir~~injection zone~~.~~ The closest known earthquake to the FutureGen 2.0 Project site (Intensity VII, magnitude 4.8 – non-instrumented record) occurred on July 19, 1909, approximately 28 mi (45 km) north of the site; it caused slight damage. Most of the events in Illinois occurred at depths greater than~~ 3 km (~~1.9 mi (3 km). ~~ISGS recently acquired a new 120-mi-long seismic reflection survey across central Illinois as part of a DOE-sponsored research project to characterize reservoir rock units for geologic storage of carbon dioxide. The continuous east-west line extends from Meredosia to southwestern Champaign County (Figure 343). This line, which is currently under re-processing, will supply additional information about the structure of the sedimentary layers which will be correlated to the observations made on both profiles L101 and L201.~~

~~Figure 343~~

~~*1.4*~~*1.3 Conceptual ~~Model~~ Domain*

A stratigraphic conceptual model of the geologic layers from the Precambrian basement to ground surface was constructed using the EarthVision® software package. The geologic setting and site characterization data described in the Underground Injection Control (UIC) Permit Supporting Documentation and later in this section were the basis for the Morgan County CO_2 storage site computational model. Borehole data from the FutureGen 2.0 stratigraphic well and data from regional boreholes and published regional contour maps were used as input data~~. However, units below the Shakopee Dolomite and above the Eau Claire Formation were assumed to have a constant thickness based on the stratigraphy observed at the stratigraphic well. There is a regional dip of approximately 0.25 degrees in the east-southeast direction~~ (Figure 4, step 1). There is a regional dip of approximately 0.25 degrees in the east-southeast direction.

Preliminary simulations were conducted to determine the extent of the model domain so that lateral boundaries were distant enough from the injection location so as not to influence the model results and an expanded 100- x 100-mi conceptual model was constructed~~.~~

[5] John McBride. Personal Communication with Charlotte Sullivan, October 29, 2013

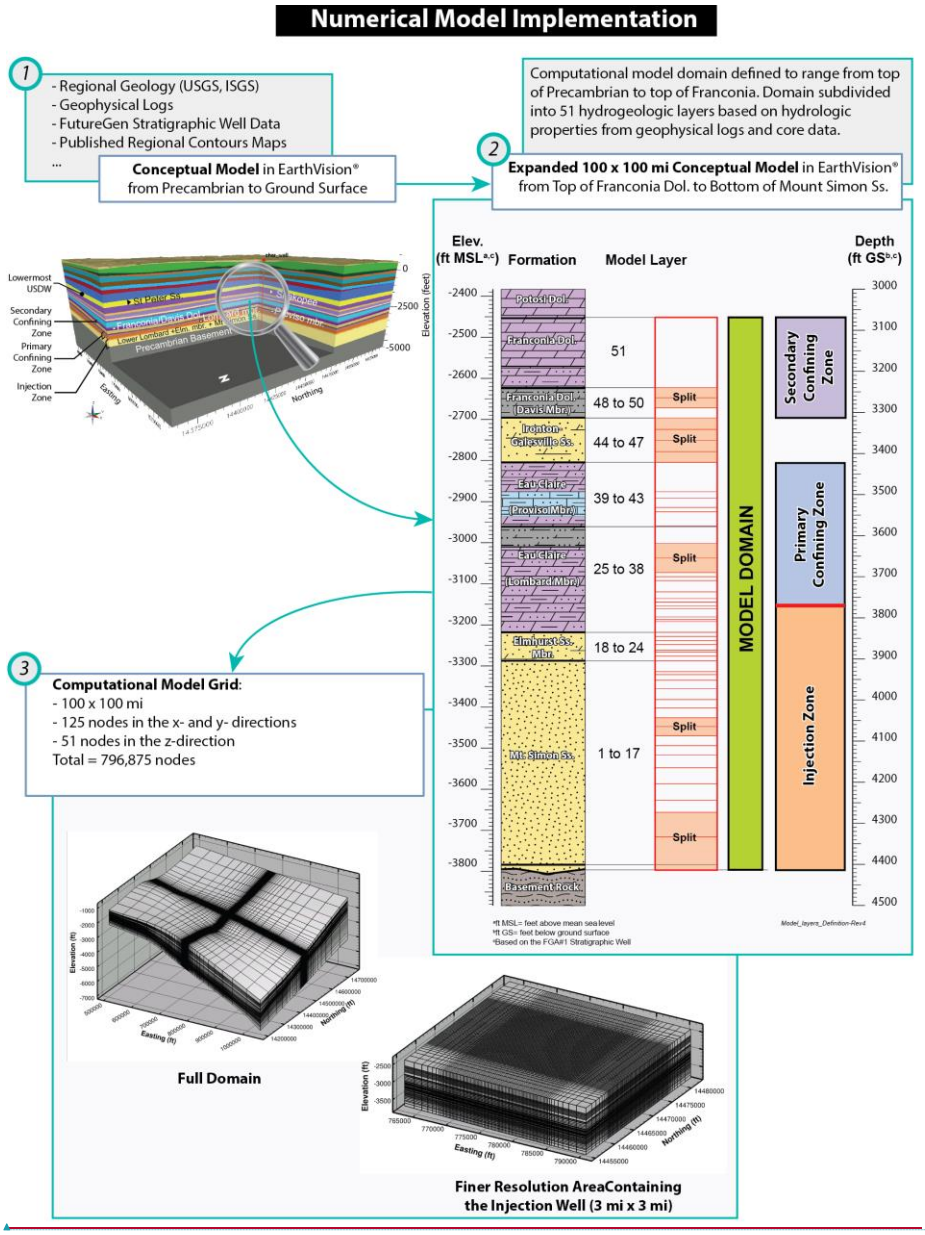

Figure 4. Implementation of the Numerical Model: From the Geological Conceptual Model to the Numerical Model

Formatted: Font: 10 pt, Bold

~~An expanded 100- x 100-mi conceptual model was constructed~~ (Figure 4, part 2). The model domain consists of the ~~to represent units below the Potosi dolomite interval including the Franconia, Ironton, Eau Claire (Proviso, Lombard, and Elmhurst), Mount Simon, and Precambrian formations.~~

~~The model domain for the Morgan County CO2 storage site consists of the~~ injection zone (the Mount Simon, the Elmhurst, and the lower part of the Lombard), the primary confining zone (the upper part of the Lombard and the Proviso), the Ironton-Galesville, and the secondary confining zone (Davis-Ironton and the Franconia). ~~Borehole data from the FutureGen 2.0 stratigraphic well and data from regional boreholes and published regional contour maps were used as input data. However, units below the Shakopee Dolomite and above the Eau Claire Formation were assumed to have a constant thickness based on the stratigraphy observed at the stratigraphic well. There is a regional dip of approximately 0.25 degrees in the east-southeast direction.~~

The tops of the Mount Simon and the Franconia and the bottom of Mount Simon in the simulation domain were gridded in EarthVision® based on borehole data and regional contour maps and make up the stratigraphic layers of the computational model. The formations above the Mount Simon top was further divided into multiple finer layers, whose thicknesses are proportional to those of the corresponding layers at the stratification well. The Mount Simon formation was divided into multiple layers and any intrusion of the Precambrian was considered inactive. The ~~three-dimensional,~~ boundary-fitted numerical model grid in the horizontal directions was designed to have constant grid spacing with higher resolution in the area influenced by the CO2 injection (3- by 3-mi area), with increasingly larger grid spacing moving out ~~in all lateral directions~~ toward the domain boundary.

The conceptual model hydrogeologic layers were defined for each stratigraphic layer based on zones of similar hydrologic properties. The hydrologic properties (permeability, porosity) were deduced from geophysical well logs and side-wall cores. The lithology, deduced from wireline logs and core data, was also used to subdivide each stratigraphic layer of the model. Based on these data, the Mount Simon Sandstone was subdivided into 17 layers, and the Elmhurst Sandstone (member of the Eau Claire Formation) was subdivided into 7 layers (Figure 4). The Lombard and Proviso members of the Eau Claire Formation were subdivided respectively into 14 and 5 layers. The Ironton Sandstone was divided into four layers, the Davis Dolomite into three layers, and the Franconia Formation into one layer. Some layers ("split" label in Figure 4, step 2) have similar properties but have been subdivided to maintain a reasonable thickness of layers within the injection zone as represented in the computational model. The thickness of the layers varies from 4 to 172 ft, with an average of 26 ft.

Based on knowledge of the regional and local geology, the Mount Simon Sandstone and the Elmhurst form the main part of the injection zone. However, the computational model results indicate that the Model Layer "Lombard 5" is the top unit containing a fraction of injected CO_2 during the 100-year simulation. Based on these results, the lower part of the Lombard (layers Lombard 1 to 5 of the Computational Model), is considered to be part of the injection zone (Figure 4). The top of the injection zone is set at 3,771 ft below ground surface (-3,153 ft elevation MSL) in the stratigraphic well. The upper part of the Lombard and the Proviso members form the primary confining zone.

Figure 4, step 3, shows the numerical model grid for the entire 100- by 100-mi domain and also for the 3- by 3-mi area with higher grid resolution and uniform grid spacing of 200 ft by 200 ft. The model grid contains 125 nodes in the x-direction, 125 nodes in the y-direction, and 51 nodes in the z-direction for a total number of nodes equal to 796,875. The expanded geologic model was queried at the node locations of the numerical model to determine the elevation of each surface for the stratigraphic units at the numerical model grid cell centers (nodes) and cell edges. Then each of those layers was subdivided into the model layers by scaling the thickness to preserve the total thickness of each stratigraphic unit. Once the vertical layering was defined, material properties were mapped to each node in the model.

~~Based on the current knowledge of the geology at the stratigraphic well, the top of the injection zone is set at 3,731 ft below ground surface, which is in the lower part of the model layer "Lombard 9" (Figure 5).~~

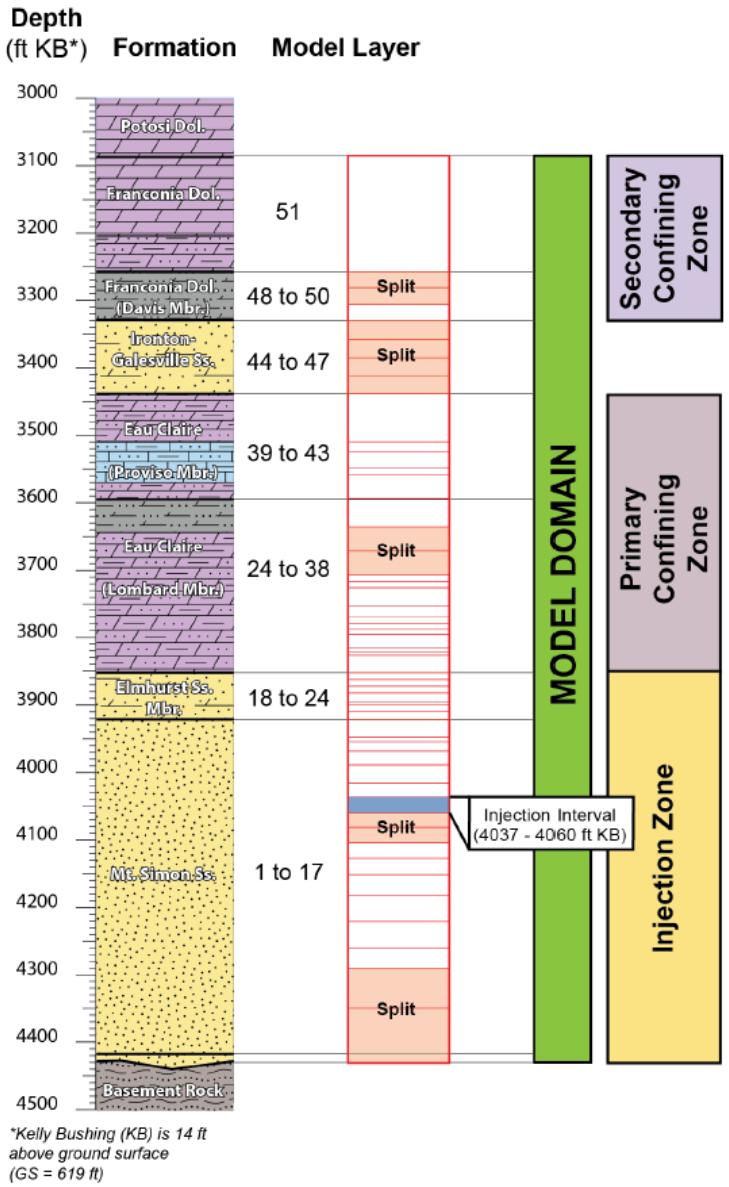

Division of Stratigraphic Layers to Create Computational Model Layers

~~Figure 4~~

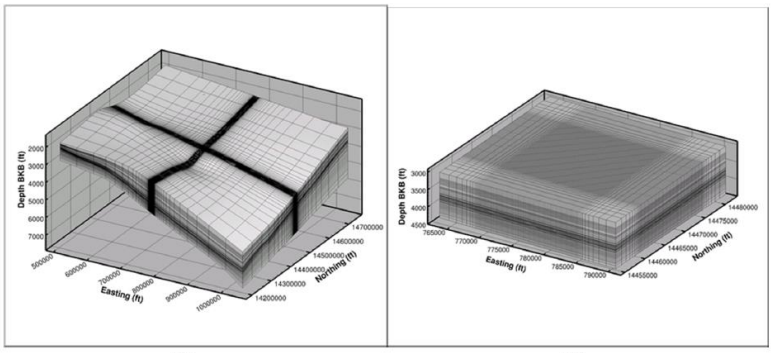

(a) (b)

Figure 3.14. Numerical Model Grid for a) Full Domain, and b) Finer Resolution Area Containing the Injection Wells

~~Figure 56~~

~~1.5~~1.4 *Simulation time period*

Based on measured pressures in the alluvial aquifer system and the injection zone, it was estimated that the pressure differential needed to force fluids from the injection zone into the surficial alluvial aquifer system through a hypothetical conduit was 31.45 psi. Therefore, once the pressure differential in the injection zone falls below this value, the simulation time period conditions are satisfied. The preliminary simulations show that, by year 60, the pressure differential is below 30 psi at the location of the injection well. Hence, the final representative case simulations were executed for a period of 100 years.

~~1.~~2. *Processes Modeled*

Physical processes modeled in the reservoir simulations included isothermal multi-fluid flow and transport for a number of components (e.g., water, salt, and CO_2) and phases (e.g., aqueous and gas). Isothermal conditions were modeled because it was assumed that the temperature of the injected CO_2 will be similar to the formation temperature. Formation salinity is considered because salt precipitation can occur near the injection well in higher permeability layers as the rock dries out during CO_2 injection. Porosity reduction due to salt precipitation is considered in the model, however permeability reduction was not modeled because the salinity is relatively low in the injection formations at this site, resulting in low levels of salt precipitation

Injected CO_2 partitions in the injection zone between the free (or mobile) gas, entrapped gas, and aqueous phases. Sequestering CO_2 in deep saline formations occurs through four mechanisms: 1) structural trapping, 2) aqueous dissolution, 3) hydraulic trapping, and 4) mineralization. Structural trapping is the long-term retention of the buoyant gas phase in the pore space of the permeable formation rock held beneath one or more impermeable or near impermeable confining zones. Aqueous dissolution occurs when CO_2 dissolves in the brine resulting in an aqueous-phase density greater than the ambient conditions. Hydraulic trapping is the pinch-off trapping of the gas phase in pores as the brine re-enters pore spaces previously occupied by the gas phase. Generally, hydraulic trapping only occurs upon the cessation of CO_2 injection. Mineralization is the chemical reaction that transforms formation minerals to carbonate minerals. In the Mount Simon Sandstone, the most likely precipitation reaction is the formation of iron carbonate precipitates. A likely reaction between CO_2 and shale is the dewatering of clays. Laboratory investigations are currently quantifying the importance of these reactions at the Morgan County

CO_2 storage site. Based on its experiments, the FutureGen Alliance (the Alliance) expects to see a small mass of precipitates (KCl, NaCl) forming near the injection well from the $scCO_2$ displacement of water, and does not expect to see the formation of any significant carbonate precipitates in the year (or years) time scale. Iron does precipitate, but concentrations are too low (<0.6 mmol/L) relative to carbonate mass to be a precipitate issue. Simulations by others (White et al. 2005) of $scCO_2$ injection in a similar sandstone (also containing iron oxides) shows that over significantly longer time scales (1000+ years), alumino silicate dissolution and alumino silicate precipitation incorporating significant carbonate (dawsonite) is predicted, as well as precipitation of some calcite. That predicted mineral trapping did permanently sequester 21 percent of the carbonate mass, thus decreasing $scCO_2$ transport risk (More details are presented in the response to NOD-December 10, 2013, Appendix A). Therefore, the simulations described here did not include mineralization reactions. However, the STOMP-CO2 simulator does account for precipitation of salt during CO_2 injection. The CO_2 stream provided by the plant to the storage site is no less than 97 percent dry basis CO_2. Because the amount of impurities is small, for the purposes of modeling the CO_2 injection and redistribution for this project, it was assumed that the injectate was pure CO_2.

~~2.~~3. Rock Properties

3.1 Intrinsic Permeability

3.1.1 Site characterization data

Permeability in the sandstones, as measured in rotary side-wall cores and plugs from whole core, appears to be dominantly related to grain size and abundance of clay. In Figure 2, ELAN (Elemental Log Analysis)-calculated permeability (red curve) is in the third panel, along with two different lab measurements of permeability for each rotary side-wall core. Horizontal permeability (K_h) data in the stratigraphic well outnumber vertical permeability (K_v) data, because K_h could not be determined from rotary side-wall cores. However, K_v/K_h ratios were successfully determined for 20 vertical/horizontal siliciclastic core-plug pairs cut from intervals of whole core. Within the Mount Simon Sandstone, the horizontal permeabilities of the lower Mount Simon alluvial fan lithofacies range from 0.005 to 0.006 mD and average ratios of vertical to horizontal permeabilities range from 0.635 to 0.722 (at the 4,318 to 4,388 ft KB depth or the elevation of -3,685 to -3,755 ft, Figure 2). Horizontal core-plug permeabilities range from 0.032 to 2.34 mD at the 3,852 to ~~–~~3,918 ft KB depth (elevation of -3,219 to -3,285 ft); K_v/K_h ratios for these same samples range from 0.081 to 0.833.

The computed lithology track for the primary confining zone indicates the upward decrease in quartz silt and increase in carbonate in the Proviso member, along with a decrease in permeability. The permeabilities of the rotary side-wall cores in the Proviso range from 0.000005 mD to 1 mD. Permeabilities in the Lombard member range from 0.001 mD to 28 mD, reflecting the greater abundance of siltstone in this interval, particularly in the lowermost part of the member. Whole core plugs and associated vertical permeabilities are available only from the lowermost part of the Lombard. Thin (few inches/centimeters), high-permeability sandstone streaks resemble the underlying Elmhurst; low-permeability siltstone and mudstone lithofacies have vertical permeabilities of 0.0004 to 0.465 mD, and K_v/K_h ratios of <0.0001 to 0.17.
The ELAN geophysical logs indicated permeabilities are generally less than the wireline tool limit of 0.01 mD throughout the secondary confining zone. Two rotary side-wall cores were taken from the Franconia, and three side-wall cores were cut in the Davis member. Laboratory-measured rotary side-wall core (horizontal) permeabilities are very low (~~0.001=~~0.000005 to 0.001 mD). The permeabilities of the two Franconia samples were measured with a special pulse decay permeameter; the sample from 3,140 ft bgs (~~957 m~~ 2521 ft elevation) has a permeability less than the lower instrument limit of 0.000005 mD. Vertical core plugs are required for directly

determining vertical permeability and there are no data from the stratigraphic well for vertical permeability or for determining vertical permeability anisotropy in the secondary confining zone. However, K_v/K_h ratios of 0.007 have been reported elsewhere for Paleozoic carbonate mudstones (Saller et al. 2004).

3.1.2 Model Parameters

Intrinsic permeability data sources for the FutureGen 2.0 stratigraphic well include computed geophysical wireline surveys (CMR and ELAN logs), and where available, laboratory measurements of rotary side-wall cores (SWC)~~s~~, core plugs from the whole core intervals, and hydrologic tests (including wireline [MDT]), and packer tests. For the Mount Simon and Elmhurst Sandstones model layers ~~within the injection reservoir~~ zone ~~section (i.e., Elmhurst Sandstone and Mount Simon Sandstone;~~ (3,852 to 4,432 ft KB depth or elevation of -3219 to -3799 ft at the stratigraphic well) wireline ELAN permeability model permKCal produced by Schlumberger (red curve on Figure 2) was used. This model, calibrated by rotary side-wall and core-plug permeabilities, provides a continuous permeability estimate over the entire injection zone. This calibrated permeability response was then slightly adjusted, or scaled, to match the composite results obtained from the hydrologic packer tests over uncased intervals. For injection zone model layers within the cased well portion of the model, no hydrologic test data are available, and core-calibrated ELAN log response was used directly in assigning average model layer permeabilities.

~~-~~The hydraulic packer tests were conducted in two zones of the Mount Simon portion of the injection zone. The Upper Zone (3,948 ft to 4,194 ft KB depth or -3,315 to -3,561 ft elevation) equates to layers 6 through 17 of the model, while the Lower Zone (4,200 ft to 4,512 ft KB depth or -3,567 to -3,879 ft elevation) equates to layers 1 through 5. The most recent ELAN-based permeability-thickness product values are 9,524 mD-ft for the 246-ft-thick section of the upper Mount Simon corresponding to the Upper Zone and 3,139 mD-ft for the 312-ft-thick section of the lower Mount Simon corresponding to the Lower Zone. The total permeability-thickness product for the open borehole Mount Simon is 12,663 mD-ft, based on the ELAN logs. Results of the field hydraulic tests suggest that the upper Mount Simon permeability-thickness product is 9,040 mD-ft and the lower Mount Simon interval permeability-thickness product is 775 mD-ft. By simple direct comparison, the packer test for the upper Mount Simon is nearly equivalent (~95 percent) to the ELAN-predicted value, while the lower Mount Simon represents only ~25 percent of the ELAN-predicted value.

Because no hydrologic test has been conducted in the Elmhurst Sandstone interval of the injection zone~~reservoir interval~~, a conservative scaling factor of 1 has been assigned to this interval, based on ELAN PermKCal data (The permeabilities used for this formation were the ELAN PermKCal values without applying a scaling factor). The sources of data for confining zones (Franconia to Upper part of the Lombard Formations) and the Upper part of the Injection zone (Lower part of the Lombard) are similar to those for the injection zone ~~reservoir~~, with the exception that no hydrologic or MDT test data are available. ELAN log-derived permeabilities are unreliable below about 0.01 mD (personal communication from Bob Butsch, Schlumberger, 2012). Because the average log-derived permeabilities (permKCal wireline from ELAN log) for most of the ~~caprock~~ confining zone layers are at or below 0.01 mD, an alternate approach was applied. For each model layer the core data were reviewed, and a simple average of the available horizontal Klinkenburg permeabilities was then calculated for each layer. Core samples that were noted as having potential cracks and/or were very small were eliminated if the results appeared to be unreasonable based on the sampled lithology. If no core samples were available and the arithmetic mean of the PermKCal was below 0.01 mD, a default value of 0.01 mD was applied (Lombard9 is the only layer with a 0.01-mD default value). Because the sandstone intervals of the Ironton-Galesville Sandstone have higher permeabilities that are similar in magnitude to the

modeled injection zone~~reservoir~~ layers, the Ironton-Galesville Sandstone model layer permeabilities were derived from the arithmetic mean of the PermKCal permeability curve. Because no hydraulic test has been conducted in the primary confining zone and the Upper part of the injection zone (Elmhurst Sandstone layers and lower part of the Lombard – Lombard 1 to Lombard 5), the scaling factor was assigned to be 100 percent in this interval and the overburden formations. Figure 5~~(Figure 3.3)~~ shows the depth profile of the horizontal permeability assigned to each layer of the model and actual values assigned are listed in Table 1~~Table 1 (Table 3.8)~~. Figure 6~~Figure 6 (Figure 3.15)~~ shows the distribution of horizontal and vertical permeability as it was assigned to the numerical model grid.

Because the anisotropy of the model layers is not likely to be represented by the sparse data from the stratigraphic well, the lithology-specific permeability anisotropy averages from literature studies representing larger sample sizes were used for the model layers (Table 2~~Table 2~~ and Table 3~~Table 3~~).

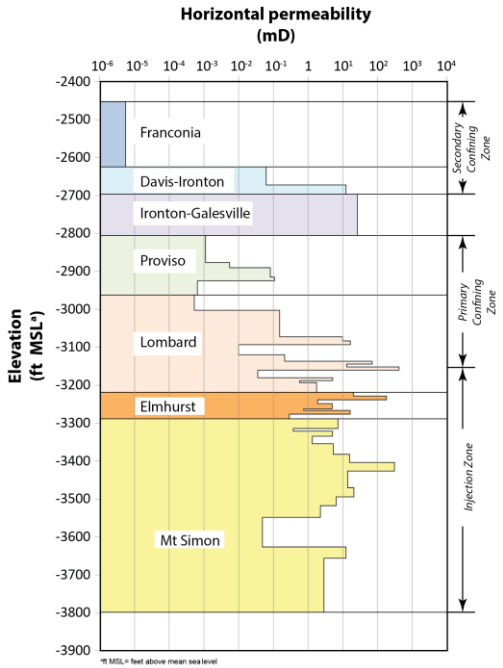

Figure 5. Vertical Distribution of the Horizontal Permeability in the Model Layers Stratigraphic Well Location

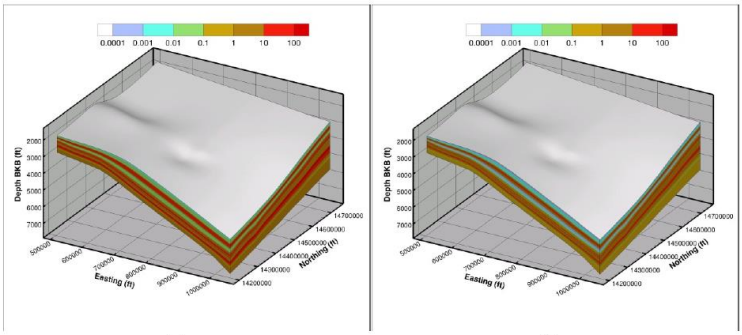

(a) (b)

Figure 3.15. Permeability Assigned to Numerical Model a) Horizontal Permeability; b) Vertical Permeability

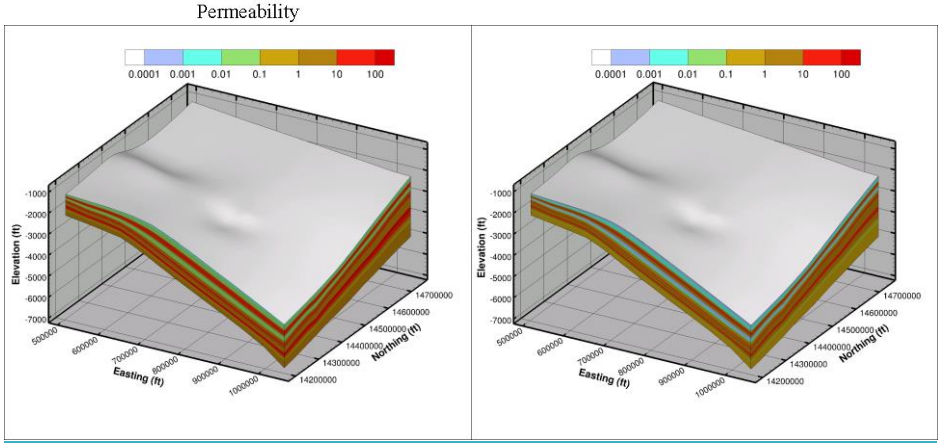

(a) (b)

Figure 6. Permeability Assigned to Numerical Model 1) Horizontal Permeability; b) Vertical Permeability

Table 3.8. Summary of the Hydrologic Properties Assigned to Each Model Layer

	Model Layer	Top Depth (ft bkb)	Top Elevation (ft)	Bottom Elevation (ft)	Thickness (ft)	Porosity	Horizontal Permeability (mD)	Vertical Permeability (mD)	Grain Density (g/cm3)	Compressibility (1/Pa)
Primary Conf. Zone	Franconia	3086.00	-2453	-2625	172	0.0358	5.50E-06	3.85E-08	2.82	7.42E-10
	Davis-Ironton3	3258.00	-2625	-2649	24	0.0367	6.26E-02	6.26E-03	2.73	3.71E-10
	Davis-Ironton2	3282.00	-2649	-2673	24	0.0367	6.26E-02	6.26E-03	2.73	3.71E-10
	Davis-Ironton1	3306.00	-2673	-2697	24	0.0218	1.25E+01	1.25E+00	2.73	3.71E-10
	Ironton-Galesville4	3330.00	-2697	-2725	28	0.0981	2.63E+01	1.05E+01	2.66	3.71E-10
	Ironton-Galesville3	3358.00	-2725	-2752	27	0.0981	2.63E+01	1.05E+01	2.66	3.71E-10
	Ironton-Galesville2	3385.00	-2752	-2779	27	0.0981	2.63E+01	1.05E+01	2.66	3.71E-10
	Ironton-Galesville1	3412.00	-2779	-2806	27	0.0981	2.63E+01	1.05E+01	2.66	3.71E-10
Primary Confining Zone	Proviso5	3439.00	-2806	-2877	71	0.0972	1.12E-03	1.12E-04	2.72	7.42E-10
	Proviso4	3510.00	-2877	-2891	14	0.0786	5.50E-03	5.50E-04	2.72	7.42E-10
	Proviso3	3524.00	-2891	-2916	25	0.0745	8.18E-02	5.73E-04	2.77	7.42E-10
	Proviso2	3548.50	-2916	-2926	10	0.0431	1.08E-01	7.56E-04	2.77	7.42E-10
	Proviso1	3558.50	-2926	-2963	38	0.0361	6.46E-04	4.52E-06	2.77	7.42E-10
	Lombard14	3596.00	-2963	-3003	40	0.1754	5.26E-04	5.26E-05	2.68	7.42E-10
	Lombard13	3636.00	-3003	-3038	35	0.0638	1.53E-01	1.53E-02	2.68	7.42E-10
	Lombard12	3671.00	-3038	-3073	35	0.0638	1.53E-01	1.53E-02	2.68	7.42E-10
	Lombard11	3706.00	-3073	-3084	11	0.0878	9.91E+00	9.91E-01	2.68	7.42E-10
	Lombard10	3717.00	-3084	-3094	10	0.0851	1.66E+01	1.66E+00	2.68	7.42E-10
	Lombard9	3727.00	-3094	-3121	27	0.0721	1.00E-02	1.00E-03	2.68	7.42E-10
	Lombard8	3753.50	-3121	-3138	17	0.0663	2.13E-01	2.13E-02	2.68	7.42E-10
	Lombard7	3770.50	-3138	-3145	8	0.0859	7.05E+01	7.05E+00	2.68	7.42E-10
	Lombard6	3778.00	-3145	-3153	8	0.0459	1.31E+01	1.31E+00	2.68	7.42E-10
	Lombard5	3785.50	-3153	-3161	9	0.0760	4.24E+02	4.24E+01	2.68	7.42E-10
	Lombard4	3794.00	-3161	-3181	20	0.0604	3.56E-02	3.56E-03	2.68	7.42E-10
	Lombard3	3814.00	-3181	-3189	8	0.0799	5.19E+00	5.19E-01	2.68	7.42E-10
	Lombard2	3821.50	-3189	-3194	5	0.0631	5.71E-01	5.71E-02	2.68	7.42E-10
	Lombard1	3826.50	-3194	-3219	26	0.0900	1.77E+00	1.77E-01	2.68	7.42E-10

Table 1. Summary of the Hydrologic Properties Assigned to Each Model Layer. Depths and Elevations Correspond to the Location of the Stratigraphic Well.

Simulation - CM22

	Model Layer	Top Depth (ft GS)	Top Elevation (ft MSL)	Bottom Elevation (ft MSL)	Thickness (ft)	Porosity	Horizontal Permeability (mD)	Vertical Permeability (mD)	Grain Density (g/cm3)	Compresibility (1/Pa)
Secondary Conf. Zone	**Franconia**	3086.00	-2453	-2625	172	0.0358	5.50E-06	3.85E-08	2.82	7.42E-10
	Davis-Ironton3	3258.00	-2625	-2649	24	0.0367	6.26E-02	6.26E-03	2.73	3.71E-10
	Davis-Ironton2	3282.00	-2649	-2673	24	0.0367	6.26E-02	6.26E-03	2.73	3.71E-10
	Davis-Ironton1	3306.00	-2673	-2697	24	0.0218	1.25E+01	1.25E+00	2.73	3.71E-10
	Ironton-Galesville4	3330.00	-2697	-2725	28	0.0981	2.63E+01	1.05E+01	2.66	3.71E-10
	Ironton-Galesville3	3358.00	-2725	-2752	27	0.0981	2.63E+01	1.05E+01	2.66	3.71E-10
	Ironton-Galesville2	3385.00	-2752	-2779	27	0.0981	2.63E+01	1.05E+01	2.66	3.71E-10
	Ironton-Galesville1	3412.00	-2779	-2806	27	0.0981	2.63E+01	1.05E+01	2.66	3.71E-10
Primary Confining Zone	**Proviso5**	3439.00	-2806	-2877	71	0.0972	1.12E-03	1.12E-04	2.72	7.42E-10
	Proviso4	3510.00	-2877	-2891	14	0.0786	5.50E-03	5.50E-04	2.72	7.42E-10
	Proviso3	3524.00	-2891	-2916	25	0.0745	8.18E-02	5.73E-04	2.77	7.42E-10
	Proviso2	3548.50	-2916	-2926	10	0.0431	1.08E-01	7.56E-04	2.77	7.42E-10
	Proviso1	3558.50	-2926	-2963	38	0.0361	6.46E-04	4.52E-06	2.77	7.42E-10
	Lombard14	3596.00	-2963	-3003	40	0.1754	5.26E-04	5.26E-05	2.68	7.42E-10
	Lombard13	3636.00	-3003	-3038	35	0.0638	1.53E-01	1.53E-02	2.68	7.42E-10
	Lombard12	3671.00	-3038	-3073	35	0.0638	1.53E-01	1.53E-02	2.68	7.42E-10
	Lombard11	3706.00	-3073	-3084	11	0.0878	9.91E+00	9.91E-01	2.68	7.42E-10
	Lombard10	3717.00	-3084	-3094	10	0.0851	1.66E+01	1.66E+00	2.68	7.42E-10
	Lombard9	3727.00	-3094	-3121	27	0.0721	1.00E-02	1.00E-03	2.68	7.42E-10
	Lombard8	3753.50	-3121	-3138	17	0.0663	2.13E-01	2.13E-02	2.68	7.42E-10
	Lombard7	3770.50	-3138	-3145	8	0.0859	7.05E+01	7.05E+00	2.68	7.42E-10
	Lombard6	3778.00	-3145	-3153	8	0.0459	1.31E+01	1.31E+00	2.68	7.42E-10

Table 1. (contd)

	Model Layer	Top Depth (ft GS)	Top Elevation (ft MSL)	Bottom Elevation (ft MSL)	Thickness (ft)	Porosity	Horizontal Permeability (mD)	Vertical Permeability (mD)	Grain Density (g/cm3)	Compresibility (1/Pa)
Injection Zone	**Lombard5**	3785.50	-3153	-3161	9	0.0760	4.24E+02	4.24E+01	2.68	7.42E-10
	Lombard4	3794.00	-3161	-3181	20	0.0604	3.56E-02	3.56E-03	2.68	7.42E-10
	Lombard3	3814.00	-3181	-3189	8	0.0799	5.19E+00	5.19E-01	2.68	7.42E-10
	Lombard2	3821.50	-3189	-3194	5	0.0631	5.71E-01	5.71E-02	2.68	7.42E-10
	Lombard1	3826.50	-3194	-3219	26	0.0900	1.77E+00	1.77E-01	2.68	7.42E-10
	Elmhurst7	3852.00	-3219	-3229	10	0.1595	2.04E+01	8.17E+00	2.64	3.71E-10
	Elmhurst6	3862.00	-3229	-3239	10	0.1981	1.84E+02	7.38E+01	2.64	3.71E-10
	Elmhurst5	3872.00	-3239	-3249	10	0.0822	1.87E+00	1.87E-01	2.64	3.71E-10
	Elmhurst4	3882.00	-3249	-3263	14	0.1105	4.97E+00	1.99E+00	2.64	3.71E-10
	Elmhurst3	3896.00	-3263	-3267	4	0.0768	7.52E-01	7.52E-02	2.64	3.71E-10
	Elmhurst2	3900.00	-3267	-3277	10	0.1291	1.63E+01	6.53E+00	2.64	3.71E-10
	Elmhurst1	3910.00	-3277	-3289	12	0.0830	2.90E-01	2.90E-02	2.64	3.71E-10
	MtSimon17	3922.00	-3289	-3315	26	0.1297	7.26E+00	2.91E+00	2.65	3.71E-10
	MtSimon16	3948.00	-3315	-3322	7	0.1084	3.78E-01	3.78E-02	2.65	3.71E-10
	MtSimon15	3955.00	-3322	-3335	13	0.1276	5.08E+00	2.03E+00	2.65	3.71E-10
	MtSimon14	3968.00	-3335	-3355	20	0.1082	1.33E+00	5.33E-01	2.65	3.71E-10
	MtSimon13	3988.00	-3355	-3383	28	0.1278	5.33E+00	2.13E+00	2.65	3.71E-10
	MtSimon12	4016.00	-3383	-3404	21	0.1473	1.59E+01	6.34E+00	2.65	3.71E-10
	MtSimon11	4037.00	-3404	-3427	23	0.2042	3.10E+02	1.55E+02	2.65	3.71E-10
	MtSimon10	4060.00	-3427	-3449	22	0.1434	1.39E+01	4.18E+00	2.65	3.71E-10
	MtSimon9	4082.00	-3449	-3471	22	0.1434	1.39E+01	4.18E+00	2.65	3.71E-10
	MtSimon8	4104.00	-3471	-3495	24	0.1503	2.10E+01	6.29E+00	2.65	3.71E-10
	MtSimon7	4128.00	-3495	-3518	23	0.1311	6.51E+00	1.95E+00	2.65	3.71E-10
	MtSimon6	4151.00	-3518	-3549	31	0.1052	2.26E+00	6.78E-01	2.65	3.71E-10
	MtSimon5	4182.00	-3549	-3588	39	0.1105	4.83E-02	4.83E-03	2.65	3.71E-10
	MtSimon4	4221.00	-3588	-3627	39	0.1105	4.83E-02	4.83E-03	2.65	3.71E-10
	MtSimon3	4260.00	-3627	-3657	30	0.1727	1.25E+01	1.25E+00	2.65	3.71E-10
	MtSimon2	4290.00	-3657	-3717	60	0.1157	2.87E+00	2.87E-01	2.65	3.71E-10
	MtSimon1	4350.00	-3717	-3799	82	0.1157	2.87E+00	2.87E-01	2.65	3.71E-10

Table 2. Lithology-Specific Permeability Anisotropy Averages from Literature

Facies or Lithology	Kv/Kh	Reference
1. Heterolithic, laminated shale/mudstone/siltstone/sandstone	0.1	Meyer and Krause (2006)
2. Herringbone cross-stratified sandstone. Strat dips to 18 degrees	0.4	Meyer and Krause (2006)
3. Paleo weathered sandstone (coastal flat)	0.4	Meyer and Krause (2006)
4. Accretionary channel bar sandstones with minor shale laminations	0.5	Ringrose et al. (2005); Meyer and Krause (2006)
6. Alluvial fan, alluvial braided stream plain to shallow marine sandstones, low clay content	0.3	Kerr et al. (1999)
7. Alluvial fan, alluvial plain sandstones, sheet floods, paleosols, higher clay content	0.1	Hornung and Aigner (1999)
8. Dolomite mudstone	0.007	Saller et al. (2004)

Table 3. Summary of the K_v/K_h Ratios Applied to Model Layers

Model Layer	Kv/Kh Applied to Model Layers[(a)]*	Kv/Kh Determined from Core Pairs[(b)]	Successfully Analyzed Core Pairs
Franconia carbonate	0.007	ND	ND
Davis-Ironton	0.1	ND	ND
Ironton-Galesville	0.4	ND	ND
Proviso (Layers 4 and 5)	0.1	ND	ND
Proviso ([carbonate] Layers 1 to 3)	0.007	ND	ND
Lombard Total Interval	0.1	0.029	12
Lombard (Layer 7)	0.1	.098	2
Lombard (Layer 6)	0.1	0.003	2
Lombard (Layer 5)	0.1	ND	ND
Lombard (Layer 4)	0.1	0.016	2
Lombard (Layer 3)	0.1	0.064	2
Lombard (Layer 2)	0.1	0.009	1
Lombard (Layer 1)	0.1	0.104	3
Elmhurst Total Interval	0.4	0.06	4
Elmhurst (Layer 7)	0.4	ND	ND
Elmhurst (Layer 6)	0.4	0.023	1
Elmhurst (Layer 5)	0.4	ND	ND
Elmhurst (Layer 4)	0.4	0.902	1
Elmhurst (Layer 3)	0.4	ND	ND
Elmhurst (Layer 2)	0.4	0.022	1
Elmhurst (Layer 1)	0.4	0.037	1
Mt. Simon (Layer 17)	0.4	0.233	2
Mt. Simon (Layer 16)	0.1	ND	ND
Mt. Simon (layer 13)	0.4	0.643	2
Mt. Simon (Layers 12, 14, and 15)	0.4	ND	ND
Mt. Simon (Layer 11, Injection) zone)	0.5	ND	ND
Mt. Simon (Layers 6, 7, 8, 9, 10)	0.3	ND	ND
Mt. Simon (Layers 1, 2, 3, 4, 5)	0.1	ND	ND

(a) Value from literature, referenced in the Supporting Documentation of the UIC permit application
(b) Geometric mean of successful core pairs.

3.2 Porosity

Total (or absolute) porosity is the ratio of void space to the volume of whole rock. Effective porosity is the ratio of interconnected void space to the volume of the whole rock. As a first step in assigning porosity values for the FutureGen 2.0 numerical model layers, Schlumberger ELAN ~~(elemental analysis)~~ porosity log results were compared with laboratory measurements of porosity as determined from SWC and core plugs for specific sampling depth within the Mount

Simon. The Schlumberger ELAN porosity logs examined include PIGN (Gamma-Neutron Porosity), PHIT (Total Porosity), and PIGE (Effective Porosity). The PIGN and PIGE wireline log surveys use different algorithms to identify clay- or mineral-bound fluid/porosity in calculating an effective porosity value. SWC porosity measurements are listed as "total porosity," but their measurement can be considered to be determinations of "effective porosity," because the measurement technique (weight measurements of heated/oven-dried core samples) primarily measures the amount of "free" or connected pore liquid contained within the SWC sample as produced by the heating process. It should be noted that the SWC porosity measurements were determined under ambient pressure conditions.

In Figure 2, neutron- and density-crossplot porosity is shown in the fourth panel, along with lab-measured porosity for core plugs and rotary SWC~~side-wall cores~~. An available porosity measurement data set for a conventional Mount Simon Sandstone core-plug sample taken near the top of the formation (depth of 3,926 ft KB or elevation of -3,293 ft) indicates only minor changes in porosity for measurements taken over a wide range in pressure (i.e., ambient to 1,730 psi). This suggests that ambient SWC porosity measurements of the Mount Simon may be representative of in situ formation pore pressure conditions. The ELAN porosity log results generally underestimate the SWC porosity measured values. As a result of the poor visual correlation of the PIGE survey results with SWC measurements, this ELAN log was omitted from subsequent correlation evaluations. To aid in the correlations, the gamma ray survey log (GR) was used as a screening tool for development of linear-regression correlation relationships between ELAN log responses and SWC porosity measurements. This helps account for the shale or clay content that can cause the inclusion of "bound water" porosity. To assign model layer porosities, the regression model relationships used to calibrate the ELAN measurement results (Figure 7~~ (Figure 3.9)~~) were applied to the ELAN survey results over the formational depths represented by the Mount Simon (3,918 to 4,430 ft KB depth or -3,285 to -3,797 ft elevation) and overlying Eau Claire-Elmhurst member (3,852 to 3,918 ft KB depth or -3,219 to -3,285 ft elevation) based on the gamma response criteria. The ELAN survey results are reported at 0.5-ft depth intervals. For stratigraphic units above the Elmhurst and/or depth intervals exhibiting gamma readings>64 API units, the un-calibrated~~calibrated~~, average ELAN log result for that depth interval was used. An average porosity was then assigned to the model layer based on the average of the calibrated ELAN values within the model layer depth range. Figure 8 (Figure 3.10) shows the depth profile of the assigned model layer porosities based on the average of the calibrated ELAN values. The actual values assigned for each layer are listed in Table 1.

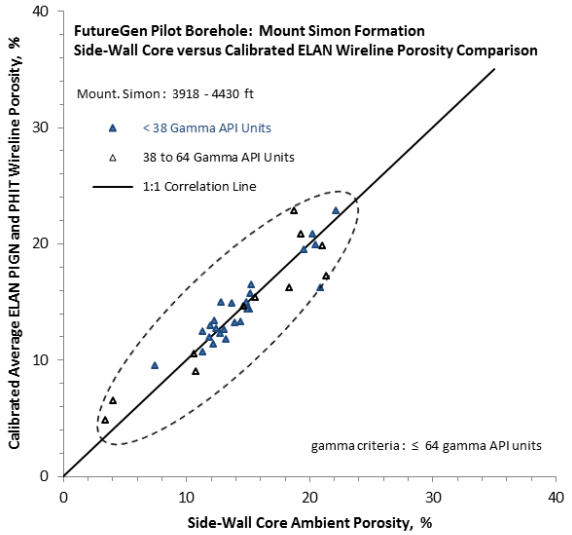

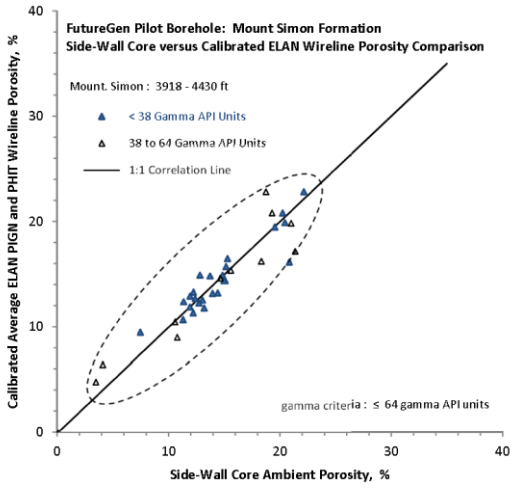

Comparison of SWC Porosity Measurements and Regression-Calibrated ELAN Log Porosities: ≤64 Gamma API Units

Figure 7. Comparison of SWC Porosity Measurements and Regression-Calibrated ELAN Log Porosities: ≤64 Gamma API Units

Formatted: Font: (Default) TimesNewRomanPSMT, 11 pt

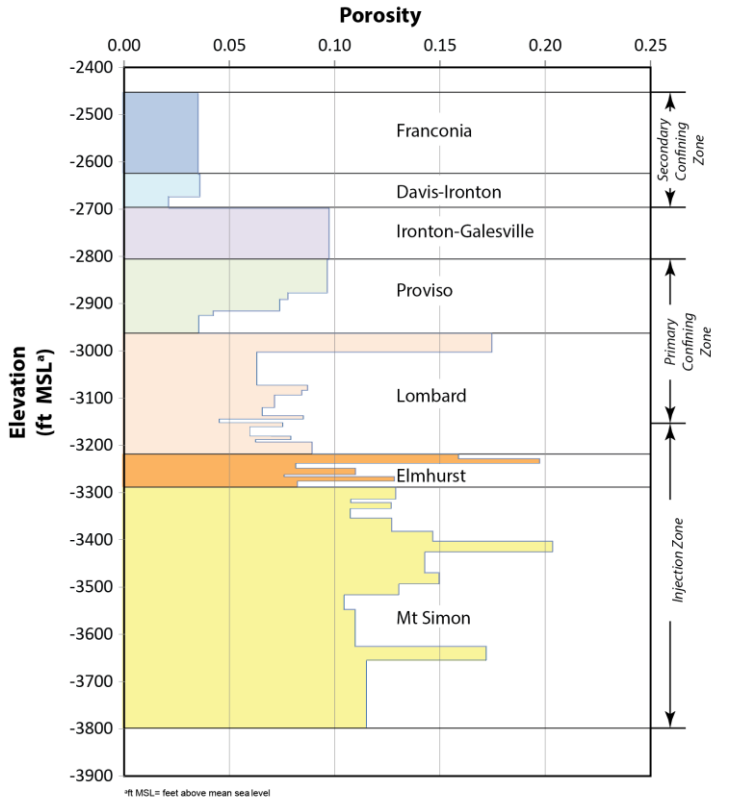
Porosity
0.00
0.05
0.10
0.15
0.20
0.25
Elevation (ft MSL[a])
-2400
-2500
-2600
-2700
-2800
-2900
-3000
-3100
-3200
-3300
-3400
-3500
-3600
-3700
-3800
-3900
Franconia
Davis-Ironton
Ironton-Galesville
Proviso
Lombard
Elmhurst
Mt Simon
Secondary Confining Zone
Primary Confining Zone
Injection Zone
[a]ft MSL= feet above mean sea level

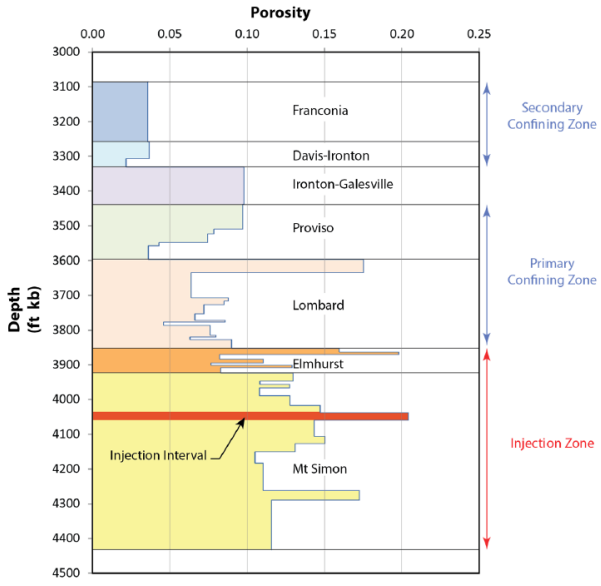

Figure 3.10. Porosity Versus Depth in Each Model Layer

Figure 8. Vertical Distribution of Porosity in the Model Layers at the Location of the Stratigraphic Well

3.3 Rock (bulk) Density and Grain Density

Grain density data were calculated from laboratory measurements of SWCs. The data were then averaged (arithmetic mean) for each main stratigraphic layer in the model. Only the Proviso member (Eau Claire Formation) has been divided in two sublayers to be consistent with the lithology changes. Figure 9~~(Figure 3.11)~~ shows the calculated grain density with depth. The actual values assigned to each layer of the model are listed in Table 1. Grain density is the input parameter specified in the simulation input file, and STOMP-CO2 calculates the bulk density from the grain density and porosity for each model layer.

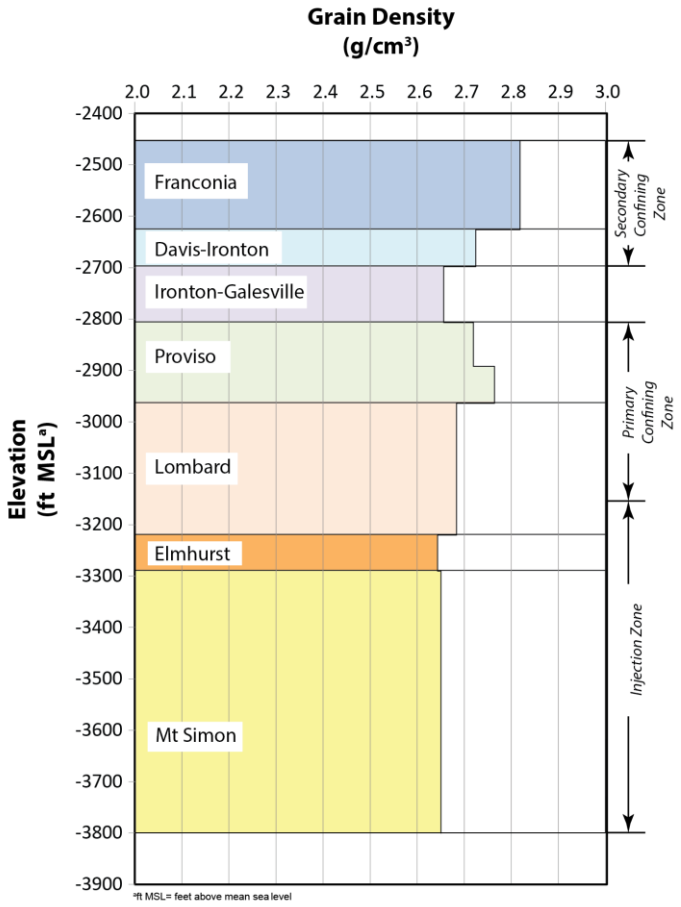
Grain Density
(g/cm³)
2.0 2.1 2.2 2.3 2.4 2.5 2.6 2.7 2.8 2.9 3.0
Elevation
(ft MSL[a])
-2400
-2500
-2600
-2700
-2800
-2900
-3000
-3100
-3200
-3300
-3400
-3500
-3600
-3700
-3800
-3900
Franconia
Davis-Ironton
Ironton-Galesville
Proviso
Lombard
Elmhurst
Mt Simon
Secondary Confining Zone
Primary Confining Zone
Injection Zone
[a]ft MSL= feet above mean sea level

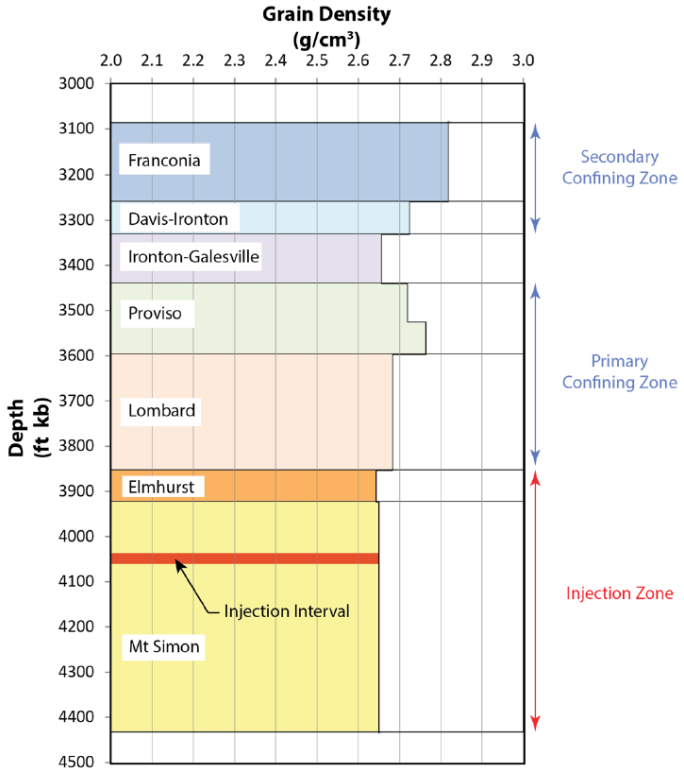

Figure 9. Vertical Distribution of the Grain Density in the Model Layer at the Location of the Stratigraphic Well

3.4 Formation compressibility

Limited information about formation (pore) compressibility estimates is available. The best estimate for the Mount Simon Sandstone (Table 4~~(Table 3.7)~~) is that back-calculated by Birkholzer et al. (2008) from a pumping test at the Hudson Field natural-gas storage site, found 80 mi (129 km) northeast of the Morgan County CO_2 storage site. The back-calculated pore-compressibility estimate for the Mount Simon Sandstone of 3.71E−10 Pa^{-1} was used as a spatially constant value for their basin-scale simulations. In other simulations, Birkholzer et al. (2008) assumed a pore-compressibility value of 4.5E−10 Pa^{-1} for aquifers and 9.0E−10 Pa^{-1} for aquitards. Zhou et al. (2010) in a later publication used a pore-compressibility value of 7.42E−10 Pa^{-1} for both the Eau Claire Formation and Precambrian granite, which were also used for these initial simulations (Table 4). Because the site-specific data are limited to a single reservoir sample, only these two published values have been used for the model. The first value (3.71E-10 Pa^{-1}) has been used for sands that are compressible because of the presence of porosity. The second value (7.42E-10 Pa^{-1}) is assigned for all other rocks that are less compressible (dolomite, limestone, shale, and rhyolite). Table 1 lists the hydrologic parameters assigned to each model layer.

Table 4. Formation Compressibility Values Selected from Available Sources

Table 3.5. Permeability Ranges Used to Assign Brooks-Corey Parameters to Model Layers

Permeability (mD)	Psi (ψ)	Lambda (λ)	Residual Aqueous Saturation
< 41.16	4.116	0.83113	0.059705
41.16 to 231	1.573	0.62146	0.081005
231 to 912.47	1.450	1.1663	0.070762
> 912.47	1.008	1.3532	0.044002

~~Table is missing~~

Hydrogeologic Unit	Formation (Pore) Compressibility, Pa^{-1}
Franconia	7.42E-10 Pa^{-1}
Davis-Ironton	3.71E-10 Pa^{-1}
Ironton-Galesville	3.71E-10 Pa^{-1}
Eau Claire Formation (Lombard and Proviso)	7.42E-10 Pa^{-1}
Eau Claire Formation (Elmhurst)	3.71E-10 Pa^{-1}
Mount Simon Sandstone	3.71E-10 Pa^{-1}

3.5 Constitutive Relationships

3.5.1 Capillary pressure and saturation functions

Capillary pressure is the pressure difference across the interface of two immiscible fluids (e.g., CO_2 and water). The entry capillary pressure is the minimum pressure required for an immiscible non-wetting fluid (i.e., CO_2) to overcome capillary and interfacial forces and enter pore space containing the wetting fluid (i.e., saline formation water). Capillary pressure data determined from site-specific cores were not available at the time the model was constructed. However, tabulated capillary pressure data were available for several Mount Simon gas storage fields in the Illinois Basin. The data for the Manlove Hazen well (FutureGen Alliance~~,~~ 2006) were the most complete. Therefore, these aqueous saturation and capillary pressure values were plotted and a user-defined curve fitting was performed to generate Brooks-Corey parameters for four different permeabilities (Figure 10~~ (Figure 3.12)~~). These parameters were then assigned to layers based on a permeability range as shown in Table 5~~(Table 3.5)~~.

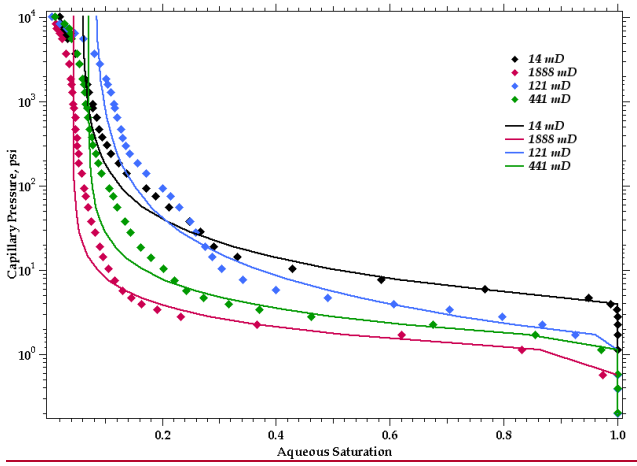

Figure 10. Aqueous Saturation Versus Capillary Pressure Based on Mercury Injection Data from the Hazen No. 5 Well at the Manlove Gas Field in Champagne County, Illinois

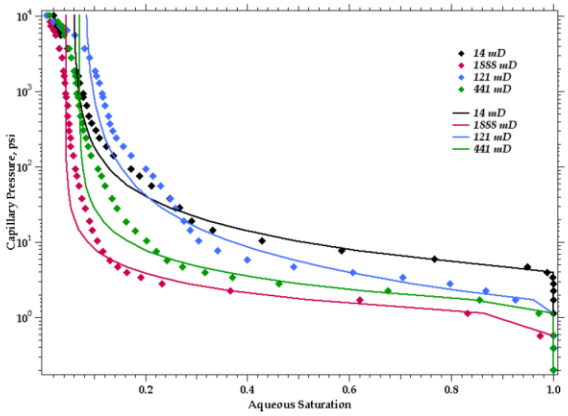

Aqueous Saturation Versus Capillary Pressure Based on Mercury Injection Data from the Hazen No. 5 Well at the Manlove Gas Field in Champagne County, Illinois

Table 5. Permeability Ranges Used to Assign Brooks-Corey Parameters to Model Layers

Permeability (mD)	Psi (ψ)	Lambda (λ)	Residual Aqueous Saturation
< 41.16	4.116	0.83113	0.059705
41.16 to 231	1.573	0.62146	0.081005
231 to 912.47	1.450	1.1663	0.070762
> 912.47	1.008	1.3532	0.044002

Table 3.5. Permeability Ranges Used to Assign Brooks-Corey Parameters to Model Layers

Permeability (mD)	Psi (ψ)	Lambda (λ)	Residual Aqueous Saturation
< 41.16	4.116	0.83113	0.059705
41.16 to 231	1.573	0.62146	0.081005
231 to 912.47	1.450	1.1663	0.070762
> 912.47	1.008	1.3532	0.044002

Table 3.9. Pressure Data Obtained from the Mount Simon Formation Using the MDT Tool. (Red line delimits the samples within the injection zone.)

Sample Number	Sample Depth (ft bkb)	Absolute Pressure (psia)
7	4130	1828
8	4131	1827.7
9	4110.5	1818.3
11	**4048**	**1790.2**
17	**4048 (duplicated)**	**1790.3**
21	4248.5	1889.2
22	4246	1908.8
23	4263	1896.5[a]

(a) Sample affected by drilling fluids (not representative)

The Brooks-Corey (1964) saturation function is given as

$$S_{ew} = \begin{cases} (P_e / P_c)^{\lambda} & \text{if} \quad P_c > P_e \\ 1 & \text{otherwise} \end{cases}$$

where S_{ew} is effective aqueous saturation, P_c is capillary pressure, P_e is gas entry pressure, and λ is the pore-size distribution parameter. Combined with the Burdine (1953) relative permeability model, the relative permeability for the aqueous phase, k_{rw}, and that for the non-aqueous phase, k_{rn}, are

$$K_{rw} = (S_{ew})^{3+2/\lambda}$$

$$K_{rn} = (1 - S_{ew})^2 (1 - S_{ew}^{1+2/\lambda})$$

Values for the residual aqueous saturation (S_{rw}) and the two other parameters used in the Brooks-Corey capillary pressure-saturation function (i.e., the non-wetting fluid entry pressure and a pore-size distribution parameter) were all obtained by fitting mercury (Hg) intrusion-capillary pressure data from the Manlove gas storage site in Champaign County. The fitting was applied after scaling the capillary pressures to account for the differences in interfacial tensions and contact angles for the brine-CO_2 fluid pair, relative to vapor-liquid Hg used in the measurements. This approach has the major advantage that the three fitted parameters are consistent as they are obtained from the same original data set. The use of consistent parameter values is not the norm for brine-CO_2 flow simulations in the Mount Simon Sandstone.

The S_{rw} values used in the modeling (~~Table 2~~Table 2~~Table 5~~) are indeed lower than the values found in the literature. The FutureGen Alliance was aware about these differences but opted to use a consistent data set for all retention parameter values instead of selecting parameter values from different data sources. An additional reason for using this approach is the considerable uncertainty in S_{rw} values for Mt. Simon rock in the literature. In general, using a lower S_{rw} value for the injection zone will possibly result in a somewhat smaller predicted CO_2 plume size and a

smaller spatial extent of the pressure front compared to using a higher value of S_{rw}. Variation of S_{rw} in the confining zone (cap rock) likely has relatively little impact on CO_2 transport and pressure development owing to the typically much lower permeability of this zone relative to the underlying formation.

3.5.2 *Gas entry pressure*

No site-specific data were available for gas entry pressure; therefore, this parameter was estimated using the Davies (1991) developed empirical relationships between air entry pressure, P_e, and intrinsic permeability, k, for different types of rock:

$$P_e = a\, k^b$$

where P_e takes the units of MPa and k the units of m^2, a and b are constants and are summarized below for shale, sandstone, and carbonate (Davies 1991; ~~Table 3~~ Table 3~~Table 6 (Table 3.6)~~). The dolomite found at the Morgan County site is categorized as a carbonate. The P_e for the air-water system is further converted to that for the CO_2-brine system by multiplying the interfacial tension ratio of a CO_2-brine system β_{cb} to an air-water system β_{aw}. An approximate value of 30 mN/m was used for β_{cb} and 72 mN/m for β_{aw}.

Table 6. Values for Constants a and b for Different Lithologies

	Shale	Sandstone	Carbonate
a	7.60E-07	2.50E-07	8.70E-07
b	-0.344	-0.369	-0.336

3.5.3 *CO_2 entrapment*

The entrapment option available in STOMP-CO2 was used to allow for entrapment of CO_2 when the aqueous phase is on an imbibition path (i.e., increasing aqueous saturation). Gas saturation can be free or trapped:

$$s_g = 1 - s_l = s_{gf} + s_{gt}$$

where the trapped gas is assumed to be in the form of aqueous occluded ganglia and immobile. The potential effective trapped gas saturation varies between zero and the effective maximum trapped gas saturation as a function of the historical minimum value of the apparent aqueous saturation. No site-specific data were available for the maximum trapped gas saturation, so this value was taken from the literature. Suekane et al. (2009) used micro-focused x-ray CT to image a chip of Berea Sandstone to measure the distribution of trapped gas bubbles after injection of $scCO_2$ and then water, under reservoir conditions. Based on results presented in the literature, a value of 0.2 was used in the model, representing the low end of measured values for the maximum trapped gas saturation in core samples.

~~3.4.~~ ~~Injection Zone~~~~Reservoir~~ Formation Properties

4.1 Fluid pressure

An initial fluid sampling event from the Mount Simon formation was conducted on December 14, 2011 in the stratigraphic well during the course of conducting open-hole logging. Sampling was attempted at 22 discrete depths using the MDT tool in the Quicksilver Probe configuration and from one location using the conventional (dual-packer) configuration. Pressure data were obtained at 7 of the 23 attempted sampling points, including one duplicated measurement at a depth of 4,048 ft KB or elevation of -3415 ft (Table 7~~Table 7~~ (Table 3.9)).

~~Regionally, Gupta and Bair (1997) presented borehole drill stem test (DST) data that indicated hydraulic heads within the Mount Simon Sandstone are near hydrostatic levels. Pressure depth measurements for the Mount Simon at the FutureGen stratigraphic well indicate a similar condition with a pressure gradient of ~0.4375 psi/ft, which is slightly higher than hydrostatic conditions (0.4331 psi/ft). Gupta and Blair (1997) also modeled the seepage velocity and flow direction of groundwater in the Mount Simon Formation across an eight state area that does not include the Morgan County area, but does include eastern Illinois. They concluded that for deep bedrock aquifers, the lateral flow patterns are away from regional basin highs arches, such as the Kankakee Arch, and toward the deeper parts of the Illinois Basin. With respect to vertical groundwater flow, Gupta and Blair (1997) surmised that within the deeper portions of the Illinois Basin, groundwater has the potential to flow vertically upward from the Mount Simon to the Eau Claire, and the vertical velocities are <0.01 in./yr. They estimated that 17 percent of the water recharging the Mount Simon basin wide migrates regionally into the overlying Eau Claire, while 83 percent flows laterally within the Mount Simon hydrogeologic unit.~~ Figure 11 shows the available regional potentiometric surfaces for the Mount Simon Sandstone. The figure contains pre-development hydraulic head measurements (e.g., before widespread pumping from the Mount Simon Sandstone, particularly in Northern Illinois) and simulation results for predicting the post-development (i.e., 1980) potentiometric surface. As shown in Figure 11, data are sparse around the area of the FutureGen 2.0 site, and it is situated in an area where the regional gradients are very low and the flow directions are not constrained (pre- or post-development). For these reasons, a regional horizontal flux for the Mount Simon Sandstone was not specified in the computational model.

Vertical flow potential at the FutureGen site was evaluated based on an analysis of discrete pressure/depth measurements obtained within the pilot characterization borehole over the depth interval of 1,148 to 4,263 ft KB depth (-515 to -3,630 ft elevation). The results indicate that there is a positive head difference in the Mount Simon that ranges from 47.8 to 61.6 ft above the calculated St. Peter observed static hydraulic head condition (i.e., 491.1 ft above MSL). This positive head difference suggests a natural vertical flow potential from the Mount Simon to the overlying St. Peter if hydraulic communication is afforded (e.g., an open communicative well). It should also be noted, however, that the higher head within the unconsolidated Quaternary aquifer (~611 ft above MSL), indicates a downward vertical flow potential from this surficial aquifer to both the underlying St. Peter and Mount Simon bedrock aquifers The disparity in the calculated hydraulic head measurements (together with the significant differences in formation fluid salinity) also suggests that groundwater within the St. Peter and Mount Simon bedrock aquifers is physically isolated from one another. This is an indication that there are no significant conduits (open well bores or fracturing) between these two formations and that the Eau Claire forms an effective confining layer.

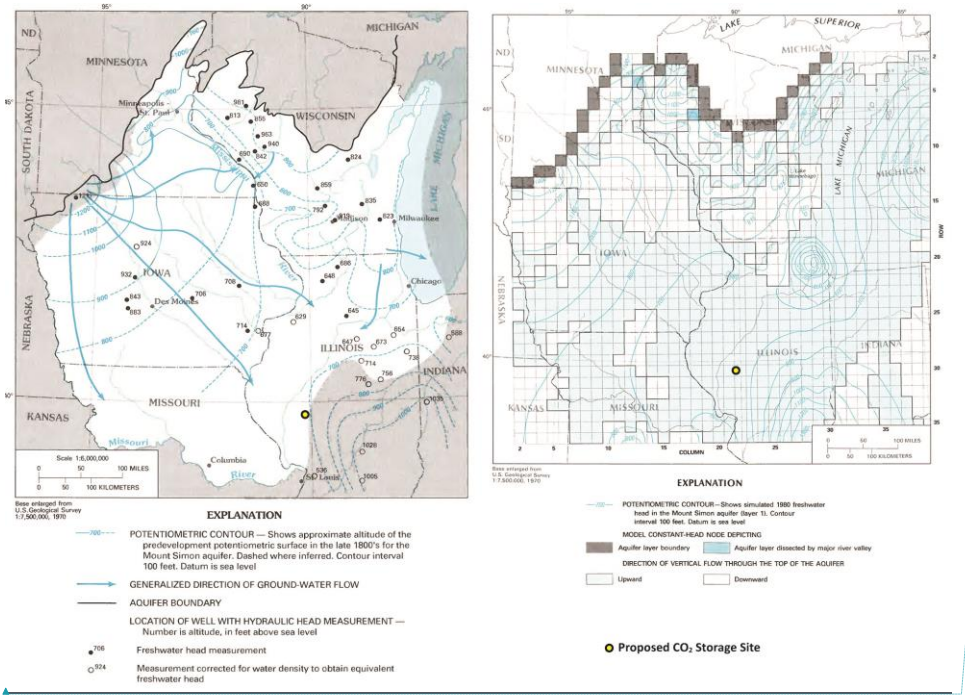

Figure 11. Approximate Pre-Development Potentiometric Surface (a) for the Mount Simon Aquifer (from Young 1992, modified from Mandel and Kontis 1992) and (b) Simulated 1980 Freshwater Head in the Mount Simon Aquifer showing Impact of Withdrawals in Northern portion of Illinois (Mandel and Kontis 1992).

Note: Permit applicants did not provide the regional groundwater flow map that shows groundwater flow direction. However, they indicated that the modeling results of Gupta and Blair (1997) in the Mount Simon formation that does not include the Morgan County area showed that for deep bedrock aquifers, the lateral flow patterns are away from regional basin highs arches.

Table 7. Pressure Data Obtained from the Mount Simon Formation Using the MDT Tool. (Red line delimits the samples within the injection zone.)

Formatted: Font: 10 pt, Bold, Font color: Accent 6

Commented [S1]: MDW attempted response by inserting Figure 13 and text on previous page. Removed the Gupta & Bair discussion and referred to this new figure.

Table 3.9. Pressure Data Obtained from the Mount Simon Formation Using the MDT Tool. (Red line delimits the samples within the injection zone.)

Sample Number	Sample Depth (ft bkb)	Absolute Pressure (psia)
7	4130	1828
8	4131	1827.7
9	4110.5	1818.3
11	**4048**	**1790.2**
17	**4048 (duplicated)**	**1790.3**
21	4248.5	1889.2
22	4246	1908.8
23	4263	1896.5[a]

(a) Sample affected by drilling fluids (not representative)

Sample Number	Sample Depth (ft bkb)	Absolute Pressure (psia)
7	4,130	1,828
8	4,131	1,827.7
9	4,110.5	1,818.3
11	**4,048**	**1,790.2**
17	**4,048 (duplicated)**	**1,790.3**
21	4,248.5	1,889.2
22	4,246	1,908.8
23	4,263	1,896.5[a]

(a) Sample affected by drilling fluids (not representative)

4.2 Temperature

The best fluid temperature depth profile was performed on February 9, 2012, as part of the static borehole flow meter/fluid temperature survey that was conducted prior to the constant-rate injection flow meter surveys. Two confirmatory discrete probe depth measurements that were taken prior to the active injection phase (using colder brine) corroborate the survey results. The discrete static measurement for the depth of 3,712 ft KB (elevation of -3,079 ft) was 95.9°F. The second discrete static probe temperature measurement is from the MDT probe for the successful sampling interval of 4,048 ft KB depth (elevation of -3,415 ft). A linear-regression temperature/depth relationship was developed for use by modeling. The regression data set analyzed was for temperature data over the depth interval of 1,300 to 4,547 ft KB (elevation of -667 to -3,914 ft). Based on this regression a projected temperature for the reference datum at the top of the Mount Simon (3,918 ft KB depth or -3,285 ft elevation) of 96.60°F is indicated. A slope (gradient) of 6.72×10^{-3} °F/ft and intercept of 70.27°F is also calculated from the regression analysis.

4.3 Brine density

Although this parameter is determined by the simulator using pressure, temperature, and salinity, based on the upper and lower Mount Simon injection zone tests, the calculated in situ injection zone fluid density is 1.0315 g/cm^3.

4.4 Salinity and water quality

During the process of drilling the well, fluid samples were obtained from discrete-depth intervals in the St. Peter Formation and the Mount Simon Formation using wireline-deployed sampling

tools (MDTs) on December 14, 2011. After the well had been drilled, additional fluid samples were obtained from the open borehole section of the Mount Simon Formation by extensive pumping using a submersible pump. The assigned salinity value for the Mount Simon (upper zone) 47,500 ppm is as indicated by both the MDT sample (depth 4,048 ft KB or elevation of -3,415 ft) and the multiple samples collected during extensive composite pumping of the open borehole section.

A total of 20 groundwater samples were collected between October 25 and November 10, 2011, including duplicate samples and blanks (Dey et al. in press). General water-quality parameters were measured along with organic and major inorganic constituents. Values of pH ranged from 7.08 to 7.66. Values for specific conductance ranged from 545 to 1,164 µS/cm, with an average of 773 µS/cm. Values of Eh ranged from 105 to 532 mV with an average of 411 mV. Values of dissolved oxygen (DO) ranged from below detection limit to 3.3 mg/L O_2. Most dissolved inorganic constituent concentrations are within primary and secondary drinking water standards. However, the constituent concentration in water is elevated with respect to iron (Fe), manganese (Mn), nitrate (NO_3), and the total dissolved salt (TDS). In some cases these constituents exceed the U.S. Environmental Protection Agency (EPA) secondary standards.

4.5 Fracture pressure in the injection zone

At the time the computational model was developed, no site-specific hydraulic fracturing tests had been conducted in the stratigraphic well and no site-specific fracture pressure values were available for the confining zone and the injection zone. Other approaches (listed below) have thus been chosen to determine an appropriate value for the fracture pressure.

- The geo-mechanical, un-calibrated anisotropic elastic properties log from Schlumberger performed in the stratigraphic well could give information about the minimum horizontal stress. However, several assumptions are made and a calibration with available mini-fracs or leak-off tests is usually required to get accurate values of these elastic parameters for the studied site. These data will not be considered here.
- Triaxial tests were also conducted on eight samples from the stratigraphic well. Samples 3 to 7 are located within the injection zone. Fracture gradients were estimated to range from 0.647 to 0.682 psi/ft, which cannot directly be compared to the fracture pressure gradient required for the permit. Triaxial tests alone cannot provide accurate measurement of fracture pressure.
- Existing regional values. Similar carbon storage projects elsewhere in Illinois (in Macon and Christian counties) provide data for fracture pressure in a comparable geological context. In Macon County (CCS#1 well at Decatur), about 65 mi east of the FutureGen 2.0 proposed site, a fracture pressure gradient of 0.715 psi/ft was obtained at the base of the Mount Simon Sandstone Formation using a step-rate injection test (EPA 2011a). In Christian County, a "conservative" pressure gradient of 0.65 psi/ft was used for the same injecting zone (EPA 2011b). No site-specific data were available.
- Last, the regulation relating to the "Determination of Maximum Injection Pressure for Class I Wells" in EPA Region 5 is based on the fracture closure pressure, which has been chosen to be 0.57 psi/ft for the Mount Simon Sandstone (EPA 1994).

Based on all of these considerations, a fracture pressure gradient of 0.65 psi/ft was chosen. The EPA GS Rule requires that "Except during stimulation, the owner or operator must ensure that injection pressure does not exceed 90 percent of the fracture pressure of the injection zone(s) so as to ensure that the injection does not initiate new fractures or propagate existing fractures in the injection zone(s)…" Therefore, a value of 0.585 psi/ft (90 percent of 0.65 psi/ft) was used in the model to calculate the maximum injection pressure permitted.

In November and December 2013, hydraulic tests were conducted in the Mount Simon Sandstone and in the Precambrian basement. The first results of these tests verify that the fracture gradient used in the model for the injection zone remains conservative and appropriate.

4.6 Site Evaluation of mineral resources

Other subsurface geochemical considerations include the potential for mineral or hydrocarbon resources beneath the proposed CO_2 storage site. While no significant mineral deposits are known to exist within Morgan County, natural gas has been recovered in the region, including at the Prentice and Jacksonville fields located within several miles of the stratigraphic well. ISGS oil and gas website data indicate that the Prentice Field contained more than 25 wells drilled during the 1950s; re-exploration occurred in the 1980s. Both oil and gas have been produced from small stratigraphic traps in the shallow Pennsylvanian targets, at depths of 250 to 350 ft (75 to 105 m) bgs. It is important to note that gas produced from these wells may contain around 16 percent CO_2 (Meents 1981). More than 75 wells have been drilled in the Jacksonville Field. Gas was discovered in the Jacksonville Field as early as 1890 (Bell 1927), but most oil and gas production from the Prentice and Jacksonville fields occurred between the late 1920s and late 1980s. The most productive formations in the Illinois Basin (lower Pennsylvanian and Mississippian siliciclastics and Silurian reefs) are not present in Morgan County. Only two boreholes in the vicinity of the Prentice Field and five boreholes near the Jacksonville Field penetrate through the New Albany Shale into Devonian and Silurian limestone. Cumulative production from the Prentice and Jacksonville fields is not available, and both fields are largely abandoned. The Waverly Storage Field natural-gas storage site in the southeast corner of Morgan County originally produced oil from Silurian carbonates. This field no longer actively produces oil, but since 1954 it has been successfully used for natural-gas storage in the St. Peter and the Galesville/Ironton Sandstone formations (Buschbach and Bond 1974).

The nearest active coal mine is approximately 10 mi (16 km) away in Menard County and does not penetrate more than 200 ft (61 m) bgs (ISGS 2012~~a~~). A review of the known coal geology within a 5-mi (8-km) radius of the proposed drilling site indicates that the Pennsylvanian coals, the Herrin, Springfield, and Colchester coals, are very thin or are absent from the project area (ISGS 2010, 2011; Hatch and Affolter 2008). During continuous coring of a shallow groundwater monitoring well~~,~~ located immediately adjacent to the stratigraphic well, only a single thin (5-ft [1.5-m]) coal seam was encountered at about 200 ft (61 m) deep.

~~4.~~5. Initial Conditions

The injection zone is assumed to be under hydrostatic conditions with no regional or local flow conditions. Therefore the hydrologic flow system is assumed to be at steady state until the start of injection. To achieve this with the STOMP-CO2 simulator one can either run an initial simulation (executed for a very long time period until steady-state conditions are achieved) to generate the initial distribution of pressure, temperature, and salinity conditions in the model from an initial guess, or one can specify the initial conditions at a reference depth using the hydrostatic option in the STOMP-CO2 input file, allowing the simulator to calculate and assign the initial conditions to all the model nodes. Site-specific data were available for pressure, temperature, and salinity, and therefore the hydrostatic option was used to assign initial conditions. A temperature gradient was specified based on the geothermal gradient, but the initial salinity was considered to be constant for the entire domain. A summary of the initial conditions is presented in Table 8~~Table 8Table 8Table 7~~ ~~Table 8((~~Table 3.10).

Table 8. Summary of Initial Conditions

Parameter	Reference Depth (ft KB)	Elevation (ft)	Value
Reservoir Pressure	4,048	-3,415	1,790.2 psi
Aqueous Saturation			1.0
Reservoir Temperature	3,918	-3,285	96.6 °F
Temperature Gradient			0.00672 °F/ft
Salinity			47,500 ppm

Table 2.17 List of Wells Located Within the AoR

Map ID	API Number	IBWS ID	Latitude NAD1983	Longitude NAD1983	Public Land Survey System	Total Depth ft	Elev ft	Completion Date	Owner	Well Num	Well Type	Status	Confining Zone Penetration Well	In AoR
0	12137221320		39.886964	-90.052919	T16n,R9w,Sec 25	4812	633	TBD	FutureGen Industrial Alliance, Inc.	1	Monitoring	Active	Yes	Yes
1	12137218200	116519	39.778074	-90.078443	T15N,R9W,Sec 2	25		19780712	A.A. Negus Estate	1	Water	Private Water Well	No	Yes
4	12137001870	115778	39.811025	-90.065241	T16N,R9W,Sec 25	115			Bellatchrist, William H.		Water		No	Yes
8	12137002850	115740	39.880661	-90.078306	T16N,R9W,Sec 26	127		1950	Martin, L. E.	1	Water		No	Yes
9		115741	39.880661	-90.078306	T16N,R9W,Sec 26	127			Martin, L. E.		Water		No	Yes
10	12137212600	115779	39.881129	-90.07342	T16N,R9W,Sec 26	25		19781213	Martin, Marvin & Jean	1	Water	Private Water Well	No	Yes
14		115763	39.792894	-90.078875	T16N,R9W,Sec 35	28			E Clemens		Water		No	Yes
15		115764	39.792894	-90.078875	T16N,R9W,Sec 35	25			B Bitter		Water		No	Yes
16		115765	39.792837	-90.060294	T16N,R9W,Sec 36	35			J M Dunlap		Water		No	Yes
17	12137005110		39.792093	-90.078904	T16N,R9W,Sec 35	1056	643		O'Rear, Judge	1	Oil & Gas / Water		No	Yes
18	12137010990		39.888545	-90.066614	T16N,R9W,Sec 25	1530	630	19391001	Bellatchrist, Wm.	1	Oil & Gas	Dry and Abandoned, No Shows	No	Yes
19	12137002350		39.779153	-90.077325	T15N,R9W,Sec 2	338	644	19231101	Conklin	1	Oil & Gas	Dry and Abandoned, No Shows	No	Yes
20	12137002360		39.781298	-90.075082	T15N,R9W,Sec 2	340	646	19231101	Conklin	2	Oil & Gas	Dry and Abandoned, No Shows	No	Yes
21	12137002370		39.778057	-90.080754	T15N,R9W,Sec 3	342	645	19231001	Harris, A. J.	1	Oil & Gas	Gas Producer	No	Yes
22	12137002390		39.7779	-90.080756	T15N,R9W,Sec 3	334	644	19231107	Harris, A. J.	3	Oil & Gas	Gas Producer	No	Yes
25	12137003630		39.885251	-90.075597	T16N,R9W,Sec 26	1205		19670330	Martin	1	Oil & Gas	Dry and Abandoned, No Shows	No	Yes
26	12137003630		39.885251	-90.075597	T16N,R9W,Sec 26	1403		19731029	Martin	1	Oil & Gas	Junked and Abandoned, Plugged	No	Yes
27	12137008580		39.880861	-90.073017	T16N,R9W,Sec 26	302	630				Coal Test		No	Yes
		115735	39.887386	-90.060378	T16N,R9W,Sec 25	27			Bellatchrist, William H.		Water		No	Potentially
		115736	39.887386	-90.060378	T16N,R9W,Sec 25	30			W R Foster		Water		No	Potentially
		115737	39.887386	-90.060378	T16N,R9W,Sec 25	28			Mason		Water		No	Potentially
		115739	39.887478	-90.079949	T16N,R9W,Sec 26	25			C H Mann		Water		No	Potentially
		115738	39.887478	-90.079949	T16N,R9W,Sec 26	22			T Goodall		Water		No	Potentially
		115650	39.887193	-90.041413	T16N,R9W,Sec 30	19		1930	R Allison		Water		No	Potentially
		115651	39.792765	-90.041512	T16N,R9W,Sec 31	28			W J Hutton		Water		No	Potentially
		115652	39.792765	-90.041512	T16N,R9W,Sec 31	28			E Robinson		Water		No	Potentially
		116450	39.777005	-90.052023	T15N,R9W,Sec 1	25			A Harris		Water		No	Potentially
		116453	39.776968	-90.070521	T15N,R9W,Sec 2	32			A Harris		Water		No	Potentially
		116451	39.776968	-90.070521	T15N,R9W,Sec 2	23			W R. Conklin		Water		No	Potentially
		116452	39.776968	-90.070521	T15N,R9W,Sec 2	30			B Negus		Water		No	Potentially
		116454	39.77688	-90.088996	T15N,R9W,Sec 3	28			C Negus		Water		No	Potentially
		116455	39.77688	-90.088996	T15N,R9W,Sec 3	30			L B Trotter		Water		No	Potentially
		115727	39.821881	-90.078925	T16N,R9W,Sec 23	30			D Pinn		Water		No	Potentially
		115728	39.821881	-90.078925	T16N,R9W,Sec 23	30			Hazel Dell School		Water		No	Potentially
		115729	39.821881	-90.078925	T16N,R9W,Sec 23	35			E. Haseline		Water		No	Potentially
		115733	39.821811	-90.060168	T16N,R9W,Sec 24	30			J L Jernagin		Water		No	Potentially
		115734	39.821811	-90.060168	T16N,R9W,Sec 24	30			O Lewis		Water		No	Potentially
		115775	39.821811	-90.060168	T16N,R9W,Sec 24	200		1944	E C Lewis		Water		No	Potentially
		115742	39.887531	-90.097566	T16N,R9W,Sec 27	23			J Brenart		Water		No	Potentially
		115743	39.887531	-90.097566	T16N,R9W,Sec 27	23			J J Brenart		Water		No	Potentially
		115761	39.792917	-90.097513	T16N,R9W,Sec 34	28			J Harrison		Water		No	Potentially
		115762	39.792917	-90.097513	T16N,R9W,Sec 34	30			J Mahon		Water		No	Potentially

Table 3.10. Summary of Initial Conditions

Parameter	Reference Depth (bkb)	Value
Reservoir Pressure	4,048 ft	1,790.2 psi
Aqueous Saturation		1.0
Reservoir Temperature	3,918 ft	96.6 °F
Temperature Gradient		0.00672 °F/ft
Salinity		47,500 ppm

~~5.~~6. *Boundary Conditions*

Boundary conditions were established with the assumption that the injection zone and confining zone are~~is~~ continuous throughout the region and that the underlying Precambrian unit is impermeable. Therefore, the bottom boundary was set as a no-flow boundary for aqueous fluids and for the CO_2-rich phase. The lateral and top boundary conditions were set to hydrostatic pressure using the initial condition with the assumption that each of these boundaries is distant enough from the injection zone to have minimal to no effect on the CO_2 plume migration and pressure distribution.

~~6.~~7. *Wells Within the Survey Area*

A survey area of 25 mi^2 (65 km^2) ~~that~~ is in Figure 12 (Figure 2.32). The survey area is centered on the proposed injection location (labeled "Injection Site") and encompasses the area of the expected CO_2 plume (the AoR) ~~is shown in Figure 12 (Figure 2.32)~~. Surface bodies of water and other pertinent surface features, administrative boundaries, and roads are shown. There are no subsurface cleanup sites, mines, quarries, or Tribal lands within this area.

Although numerous wells are located within ~~a 25 mi^2 (65 km^2)~~ the survey area ~~that includes the proposed injection location (Figure 12)~~, none but the Alliance's stratigraphic well penetrates the injection zone (Mount Simon Sandstone and the lower Eau Claire [Elmhurst Sandstone Member]), the confining zone (Lombard and Proviso members of the Eau Claire Formation), or the secondary confining zone (Franconia Dolomite).

A total of 129 wells (including the stratigraphic well) are within the survey area.~~; 51 42~~ Forty two wells are (or are potentially) within the AoR (Table 9~~Table 9Table 9Table 8 (Table 2.17)~~). ~~Indeed, 24~~Twenty~~-~~ ~~four~~ of these ~~51~~42 ~~water~~ wells are only identified with a general location (center of a section) in the ISWS database. If the section of those wells intersected the AoR borders, the wells were assumed to be within the AoR even though they could be beyond the border. Those wells are indicated with a "potentially" label in the last column of ~~the Table 8~~ Table 9~~Table 9~~~~Table 9~~ but are not shown on the map.

Shallow domestic water wells with depths of less than 50 ft (15 m) are the most common well type. Five slightly deeper water wells were identified that range in depths from 110 ft (33 m) to 405 ft (123 m). Other wells include stratigraphic test holes, coal test holes, and oil and gas wells (Figure 12).

Table 9~~Table 9Table 9Table 8~~ lists ~~these~~ wells located within the AoR with their unique API (American Petroleum Institute) identification number and ISWS well identification (ID), if available, well location, depth, elevation, completion date, well owner, well type, and identified status.

Attachment A ~~provides~~ is the list of wells within the survey Area ~~but not included in the AoR extent.~~ that are not within the AoR. ~~The map in Figure 12 134 shows the locations of four proposed injection wells for which permits are being sought. It also shows the location of the Alliance's stratigraphic well and abandoned hydrocarbon test holes, coal test holes, oil and gas wells, other plugged and abandoned wells, known water wells, and other surface features within a 25 mi^2 (65 km^2) area centered on the location of the proposed injection wells~~the survey a~~.~~

Table 2.17. List of Wells Located Within the AoR

Map ID	API Number	IWS ID	Latitude NAD1983	Longitude NAD1983	Public Land Survey System	Total Depth ft	Elev ft	Completion Date	Owner	Well Num	Well Type	Status	Confining Zone Penetration Wkl	In AoR
0	121372213200		39.806064	-90.052919	T16sR5w.Sec 25	4812	633	TBD	FutureGen Industrial Alliance, Inc.	1	Monitoring	Active	Yes	Yes
1	121372118200	116519	39.778074	-90.078443	T15N.R5W.Sec 2	25		19780712	A A Negus Estate	1	Water	Private Water Well	No	Yes
6	121370018700	115778	39.811025	-90.065241	T16N.R5W.Sec 25	115			Bellschmidt, William H.		Water		No	Yes
8	121370028500	115740	39.800661	-90.078386	T16N.R5W.Sec 26	127		1950	Martin, L. E.	1	Water		No	Yes
9		115741	39.800661	-90.078386	T16N.R5W.Sec 26	127			Martin, L. E.		Water		No	Yes
10	121372128600	115779	39.801129	-90.07342	T16N.R5W.Sec 26	25		19781213	Martin, Marvin & Jean	1	Water	Private Water Well	No	Yes
14		115763	39.792894	-90.078875	T16N.R5W.Sec 35	28			E Clemons		Water		No	Yes
15		115764	39.792894	-90.078875	T16N.R5W.Sec 35	25			B Sisne		Water		No	Yes
16		115765	39.792837	-90.066294	T16N.R5W.Sec 36	35			J M Dunlap		Water		No	Yes
17	121370051100		39.792893	-90.078984	T16N.R5W.Sec 35	1056	643		O'Kane, Judge	1	Oil & Gas / Water		No	Yes
18	121370009900		39.808545	-90.06614	T16N.R5W.Sec 25	1530	610	19381001	Bellschmidt, Wm.	1	Oil & Gas	Dry and Abandoned, No Shows	No	Yes
19	121370025500		39.779153	-90.077325	T15N.R5W.Sec 2	338	644	19231101	Conklin	1	Oil & Gas	Dry and Abandoned, No Shows	No	Yes
20	121370023600		39.781398	-90.075082	T15N.R5W.Sec 2	348	646	19231101	Conklin	2	Oil & Gas	Dry and Abandoned, No Shows	No	Yes
21	121370023700		39.778057	-90.080754	T15N.R5W.Sec 3	342	645	19231001	Harris, A. J.	1	Oil & Gas	Gas Producer	No	Yes
22	121370023900		39.7779	-90.080756	T15N.R5W.Sec 3	334	644	19231107	Harris, A. J.	3	Oil & Gas	Gas Producer	No	Yes
25	121370036100		39.805251	-90.075597	T16N.R5W.Sec 26	1205		19670330	Martin	1	Oil & Gas	Dry and Abandoned, No Shows	No	Yes
26	121370036101		39.805251	-90.075597	T16N.R5W.Sec 26	1400		19710029	Martin	1	Oil & Gas	Junked and Abandoned, Plugged	No	Yes
27	121372085500		39.800861	-90.073017	T16N.R5W.Sec 26	302	630		Coal Test				No	Yes
		115735	39.807386	-90.060378	T16N.R5W.Sec 25	27			Bellschmidt, William H.		Water		No	Potentially
		115736	39.807386	-90.060378	T16N.R5W.Sec 25	30			W B Fowler		Water		No	Potentially
		115737	39.807386	-90.060378	T16N.R5W.Sec 25	28			Mason		Water		No	Potentially
		115739	39.807478	-90.079049	T16N.R5W.Sec 26	25			C H Martin		Water		No	Potentially
		115738	39.807478	-90.079049	T16N.R5W.Sec 26	22			T Grenfell		Water		No	Potentially
		115650	39.807193	-90.041413	T16N.R5W.Sec 30	19		1930	R Allison		Water		No	Potentially
		115651	39.792765	-90.041512	T16N.R5W.Sec 31	28			W J Husten		Water		No	Potentially
		115652	39.792765	-90.041512	T16N.R5W.Sec 31	28			E Robinson		Water		No	Potentially
		116450	39.777005	-90.052023	T15N.R5W.Sec 1	25			A Harris		Water		No	Potentially
		116453	39.776968	-90.070521	T15N.R5W.Sec 2	32			A Harris		Water		No	Potentially
		116451	39.776968	-90.070521	T15N.R5W.Sec 2	22			W R Conklin		Water		No	Potentially
		116452	39.776968	-90.070521	T15N.R5W.Sec 2	30			B Negus		Water		No	Potentially
		116454	39.77688	-90.088996	T15N.R5W.Sec 3	28			C Negus		Water		No	Potentially
		116455	39.77688	-90.088996	T15N.R5W.Sec 3	30			L B Tretter		Water		No	Potentially
		115727	39.821881	-90.078925	T16N.R5W.Sec 23	30			D Flinn		Water		No	Potentially
		115728	39.821881	-90.078925	T16N.R5W.Sec 23	30			Hazel Dell School		Water		No	Potentially
		115729	39.821881	-90.078925	T16N.R5W.Sec 23	35			K. Hinshaw		Water		No	Potentially
		115733	39.821811	-90.060168	T16N.R5W.Sec 24	30			J L Icenogle		Water		No	Potentially
		115734	39.821811	-90.060168	T16N.R5W.Sec 24	30			G Lewis		Water		No	Potentially
		115775	39.821811	-90.060168	T16N.R5W.Sec 24	200		1944	E C Lewis		Water		No	Potentially
		115742	39.807531	-90.097566	T16N.R5W.Sec 27	23			J Stewart		Water		No	Potentially
		115743	39.807531	-90.097566	T16N.R5W.Sec 27	23			LJ Stewart		Water		No	Potentially
		115761	39.792917	-90.097513	T16N.R5W.Sec 34	28			T Harrison		Water		No	Potentially
		115762	39.792917	-90.097513	T16N.R5W.Sec 34	30			J Mahon		Water		No	Potentially

Formatted: Centered

Table 9~~Table 8~~. List of Wells Located Within the the AoR

Map ID	API Number	ISWS ID	Latitude NAD1983	Longitude NAD1983	Public Land Survey System	Total Depth ft	Elev ft	Completion Date	Owner	Well Num	Well Type	Status	Confining Zone Penetration Well	In AoR
0	121372213200		39.806064	-90.052919	T16n,R9w,Sec 25	4812	633	TBD	FutureGen Industrial Alliance, Inc.	1	Monitoring	Active	Yes	Yes
1	121372118200	116519	39.778074	-90.078443	T15N,R9W,Sec 2	25		19780712	A.A. Negus Estate	1	Water	Private Water Well	No	Yes
4	121370018700	115778	39.811025	-90.065241	T16N,R9W,Sec 25	115			Beilschmidt, William H.		Water		No	Yes
8	121370028500	115740	39.800661	-90.078386	T16N,R9W,Sec 26	127		1950	Martin, L. E.	1	Water		No	Yes
9		115741	39.800661	-90.078386	T16N,R9W,Sec 26	127			Martin, L. E.		Water		No	Yes
10	121372128600	115779	39.801129	-90.07342	T16N,R9W,Sec 26	25		19781213	Martin, Marvin & Jean	1	Water	Private Water Well	No	Yes
14		115763	39.792894	-90.078875	T16N,R9W,Sec 35	28			E Clemons		Water		No	Yes
15		115764	39.792894	-90.078875	T16N,R9W,Sec 35	25			B Sister		Water		No	Yes
16		115765	39.792837	-90.060294	T16N,R9W,Sec 36	35			J M Dunlap		Water		No	Yes
17	121370051100		39.792893	-90.078984	T16N,R9W,Sec 35	1056	643		O'Rear, Judge	1	Oil & Gas / Water		No	Yes
18	121370009900		39.808545	-90.06614	T16N,R9W,Sec 25	1530	630	19391001	Beilschmidt, Wm.	1	Oil & Gas	Dry and Abandoned, No Shows	No	Yes
19	121370023500		39.779153	-90.077325	T15N,R9W,Sec 2	338	644	19231101	Conklin	1	Oil & Gas	Dry and Abandoned, No Shows	No	Yes
20	121370023600		39.781298	-90.075082	T15N,R9W,Sec 2	348	646	19231101	Conklin	2	Oil & Gas	Dry and Abandoned, No Shows	No	Yes
21	121370023700		39.778057	-90.080754	T15N,R9W,Sec 3	342	645	19231001	Harris, A. J.	1	Oil & Gas	Gas Producer	No	Yes
22	121370023900		39.7779	-90.080756	T15N,R9W,Sec 3	334	644	19231107	Harris, A. J.	3	Oil & Gas	Gas Producer	No	Yes
25	121370036300		39.805251	-90.075597	T16N,R9W,Sec 26	1205		19670330	Martin	1	Oil & Gas	Dry and Abandoned, No Shows	No	Yes
26	121370036301		39.805251	-90.075597	T16N,R9W,Sec 26	1400		19731029	Martin	1	Oil & Gas	Junked and Abandoned, Plugged	No	Yes
27	121372088500		39.800861	-90.073017	T16N,R9W,Sec 26	302	630				Coal Test		No	Yes
		115735	39.807386	-90.060378	T16N,R9W,Sec 25	27			Beilschmidt, William H.		Water		No	Potentially
		115736	39.807386	-90.060378	T16N,R9W,Sec 25	30			W R Fowler		Water		No	Potentially
		115737	39.807386	-90.060378	T16N,R9W,Sec 25	28			Mason		Water		No	Potentially
		115739	39.807478	-90.079049	T16N,R9W,Sec 26	25			C H Matin		Water		No	Potentially
		115738	39.807478	-90.079049	T16N,R9W,Sec 26	22			T Gondall		Water		No	Potentially
		115650	39.807193	-90.041413	T16N,R8W,Sec 30	19		1930	R Allison		Water		No	Potentially
		115651	39.792765	-90.041512	T16N,R8W,Sec 31	28			W J Huston		Water		No	Potentially
		115652	39.792765	-90.041512	T16N,R8W,Sec 31	28			E Robinson		Water		No	Potentially
		116450	39.777005	-90.052023	T15N,R9W,Sec 1	25			A Harris		Water		No	Potentially
		116453	39.776968	-90.070521	T15N,R9W,Sec 2	32			A Harris		Water		No	Potentially
		116451	39.776968	-90.070521	T15N,R9W,Sec 2	22			W R Conklin		Water		No	Potentially
		116452	39.776968	-90.070521	T15N,R9W,Sec 2	30			B Negus		Water		No	Potentially
		116454	39.77688	-90.088996	T15N,R9W,Sec 3	28			C Negus		Water		No	Potentially
		116455	39.77688	-90.088996	T15N,R9W,Sec 3	30			L B Trotter		Water		No	Potentially

	115727	39.821881	-90.078925	T16N,R9W,Sec 23	30		D Flinn	Water	No	Potentially
	115728	39.821881	-90.078925	T16N,R9W,Sec 23	30		Hazel Dell School	Water	No	Potentially
	115729	39.821881	-90.078925	T16N,R9W,Sec 23	35		K Haneline	Water	No	Potentially
	115733	39.821811	-90.060168	T16N,R9W,Sec 24	30		J L Icenagle	Water	No	Potentially
	115734	39.821811	-90.060168	T16N,R9W,Sec 24	30		G Lewis	Water	No	Potentially
	115775	39.821811	-90.060168	T16N,R9W,Sec 24	200	1944	E C Lewis	Water	No	Potentially
	115742	39.807531	-90.097566	T16N,R9W,Sec 27	23		J Stewart	Water	No	Potentially
	115743	39.807531	-90.097566	T16N,R9W,Sec 27	23		l J Stewart	Water	No	Potentially
	115761	39.792917	-90.097513	T16N,R9W,Sec 34	28		T Harrison	Water	No	Potentially
	115762	39.792917	-90.097513	T16N,R9W,Sec 34	30		J Mahon	Water	No	Potentially

Table 8. (contd)

Map ID	API Number	ISWS ID	Latitude (NAD 83)	Longitude (NAD 83)	Public Land Survey System (PLSS)	Total Depth (ft)	Elevation (ft)	Completion Date	Owner	Well #	Well Type	Status	Confining Zone Penetration Well
79	-	115697	39.836221	-90.059875	T16N,R9W,Sec 13	27	-	-	U B Fox		Water		No
80	-	115698	39.836221	-90.059875	T16N,R9W,Sec 13	27	-	-	G W Lewis		Water		No
81	-	115699	39.836362	-90.078662	T16N,R9W,Sec 14	30	-	-	J Parrat		Water		No
82	-	115700	39.836362	-90.078662	T16N,R9W,Sec 14	28	-	-	C W Lewis		Water		No
83	-	115701	39.836362	-90.078662	T16N,R9W,Sec 14	28	-	-	J W Parrat		Water		No
84	-	115702	39.836362	-90.078662	T16N,R9W,Sec 14	32	-	-	J Hodgeson		Water		No
85	121372203900	356742	39.830101	-90.102984	T16N,R9W,Sec 15	47	-	20030910	Lomar Hager Construction		Water	Private Water Well	No
86	-	115703	39.836486	-90.097369	T16N,R9W,Sec 15	24	-	-	G Noulty		Water		No
87	-	115704	39.836486	-90.097369	T16N,R9W,Sec 15	30	-	-	L Lamkaular		Water		No
88	-	115705	39.836486	-90.097369	T16N,R9W,Sec 15	35	-	-	E E Hart		Water		No
89	-	115706	39.8365	-90.116151	T16N,R9W,Sec 16	23	-	-	S Jumper		Water		No
90	-	115707	39.8365	-90.116151	T16N,R9W,Sec 16	25	-	-	H Wester		Water		No
91	-	115722	39.821967	-90.116263	T16N,R9W,Sec 21	30	-	-	T J Ward		Water		No
92	-	115724	39.821967	-90.116263	T16N,R9W,Sec 21	30	-	-	C Trotter		Water		No
93	-	216249	39.821967	-90.116263	T16N,R9W,Sec 21	28	-	1934	Wm Noulty		Water		No
94	121370028400	-	39.822767	-90.073164	T16N,R9W,Sec 23	405	-	19540301	Keltner	1	Water		No
95	121372155100	237377	39.820978	-90.077895	T16N,R9W,Sec 23	42	-	19920414	Allen, John D.	1	Water	Private Water Well	No
96	121372207600	365042	39.822764	-90.075515	T16N,R9W,Sec 23	46	-	20040715	Burton, Larry		Water	Private Water Well	No
97	121372128400	115776	39.826288	-90.058992	T16N,R9W,Sec 24	40	-	19760220	Robinson, Leroy A.	1	Water	Private Water Well	No
98	121372128500	115777	39.828869	-90.059535	T16N,R9W,Sec 24	37	-	19781214	Romine, Buddy	1	Water	Private Water Well	No
99	121372211600	420169	39.813876	-90.103667	T16N,R9W,Sec 27	35	-	20060809	Donnan, Jeff		Water	Private Water Well	No
100	-	115744	39.807541	-90.116512	T16N,R9W,Sec 28	110	-	-	Noah B Fox		Water		No
101	-	115745	39.807541	-90.116512	T16N,R9W,Sec 28	28	-	-	Noah B Fox		Water		No
102	-	115746	39.807541	-90.116512	T16N,R9W,Sec 28	30	-	-	C Holdbrook		Water		No
103	-	115723	39.807541	-90.116512	T16N,R9W,Sec 28	28	-	-	W Noulty		Water		No
104	121372203000	348692	39.806645	-90.122622	T16N,R9W,Sec 28	42	-	-	Kendra Swain		Water		No
105	-	115759	39.792956	-90.116724	T16N,R9W,Sec 33	30	-	-	H Swain		Water		No
106	-	115760	39.792956	-90.116724	T16N,R9W,Sec 33	28	-	-	L L Hart		Water		No
107	121372155000	-	39.822856	-90.119949	T16N,R9W,Sec 21	-	-	-	Spradlin, Jack		Water		No
108	121370011400	-	39.833775	-90.10777	T16N,R9W,Sec 16	385	616	19551101	Wolfe, Eliz	1	Oil & Gas	Dry and Abandoned, No Shows, Plugged	No
109	121370011500	-	39.80091	-90.040421	T16N,R8W,Sec 30	420	635	19560101	Beilschmidt	1	Oil & Gas	Dry and Abandoned, No Shows, Plugged	No
110	121370011600	-	39.815108	-90.028322	T16N,R8W,Sec 20	365	610	19551201	Robinson, Howard	1	Oil & Gas	Dry and Abandoned, No Shows, Plugged	No
111	121370018900	-	39.825408	-90.062536	T16N,R9W,Sec 24	200	-	19440101	Lewis, E. C.		Oil & Gas	Dry Hole	No
112	121370024100	-	39.769077	-90.111454	T15N,R9W,Sec 4	580	-	-	Rayborn	1	Oil & Gas	Gas Producer	No
113	121370044200	-	39.770193	-90.110273	T15N,R9W,Sec 4	350	-	-	Rayburn	1	Oil & Gas	Gas Producer	No
114	121372086900	-	39.769679	-90.098565	T15N,R9W,Sec 4	301	-	-	-		Coal Test		No
115	121370024200	-	39.778927	-90.119618	T15N,R9W,Sec 5	423	-	-	Green, Laura & Effie	1	Oil & Gas	Gas Producer	No
116	121370024600	-	39.764523	-90.098492	T15N,R9W,Sec 9	293	-	-	Baxter	2	Oil & Gas	Dry and Abandoned, Gas Shows	No
117	121372094800	-	39.767065	-90.11144	T15N,R9W,Sec 9	325	-	-	Beilschmidt	1	Oil&Gas	Temporarily Abandoned	No
118	121372105200	-	39.763524	-90.104346	T15N,R9W,Sec 9	-	-	-	Leinberger	2	Oil&Gas	Permit to Drill Issued	No
119	121370007900	-	39.766464	-90.091366	T15N,R9W,Sec 10	295	-	-	Dunlap	8	Oil & Gas	Gas Producer	No
120	121372084800	-	39.766422	-90.065678	T15N,R9W,Sec 11	243	-	-	-		Coal Test		No
121	121370030900	-	39.806625	-90.105838	T16N,R9W,Sec 27	324	610	19591001	Fox, Lyman	1	Oil & Gas	Dry and Abandoned, No Shows, Plugged	No
122	121370033200	-	39.788212	-90.03349	T16N,R8W,Sec 31	323	641	19271001	Corrington	1	Oil & Gas	Dry and Abandoned, No Shows	No

Table 8. (contd)

Map ID	API Number	ISWS ID	Latitude (NAD 83)	Longitude (NAD 83)	Public Land Survey System (PLSS)	Total Depth (ft)	Elevation (ft)	Completion Date	Owner	Well #	Well Type	Status	Confining Zone Penetration Well
123	121370062300	-	39.828772	-90.06935	T16N,R9W,Sec 24	814	624	19700701	#MA-3		Stratigraphic or Structure Test	Structure Test, Plugged	No
124	121372068000	-	39.792709	-90.039363	T16N,R8W,Sec 31	142	641	19700518	Flynn, Robert		Coal Test		No
125	121372088400	-	39.829096	-90.098826	T16N,R9W,Sec 22	318	621	0			Coal Test		No
126	121372088600	-	39.801122	-90.108499	T16N,R9W,Sec 28	301	621	0			Coal Test		No
127	121372067800	-	39.814431	-90.023514	T16N,R8W,Sec 20	130	610	19700507	Newberry, Lucille		Coal Test		No
128	121372086000	-	39.83138	-90.055009	T16N,R9W,Sec 13	301	619	0			Coal Test		No

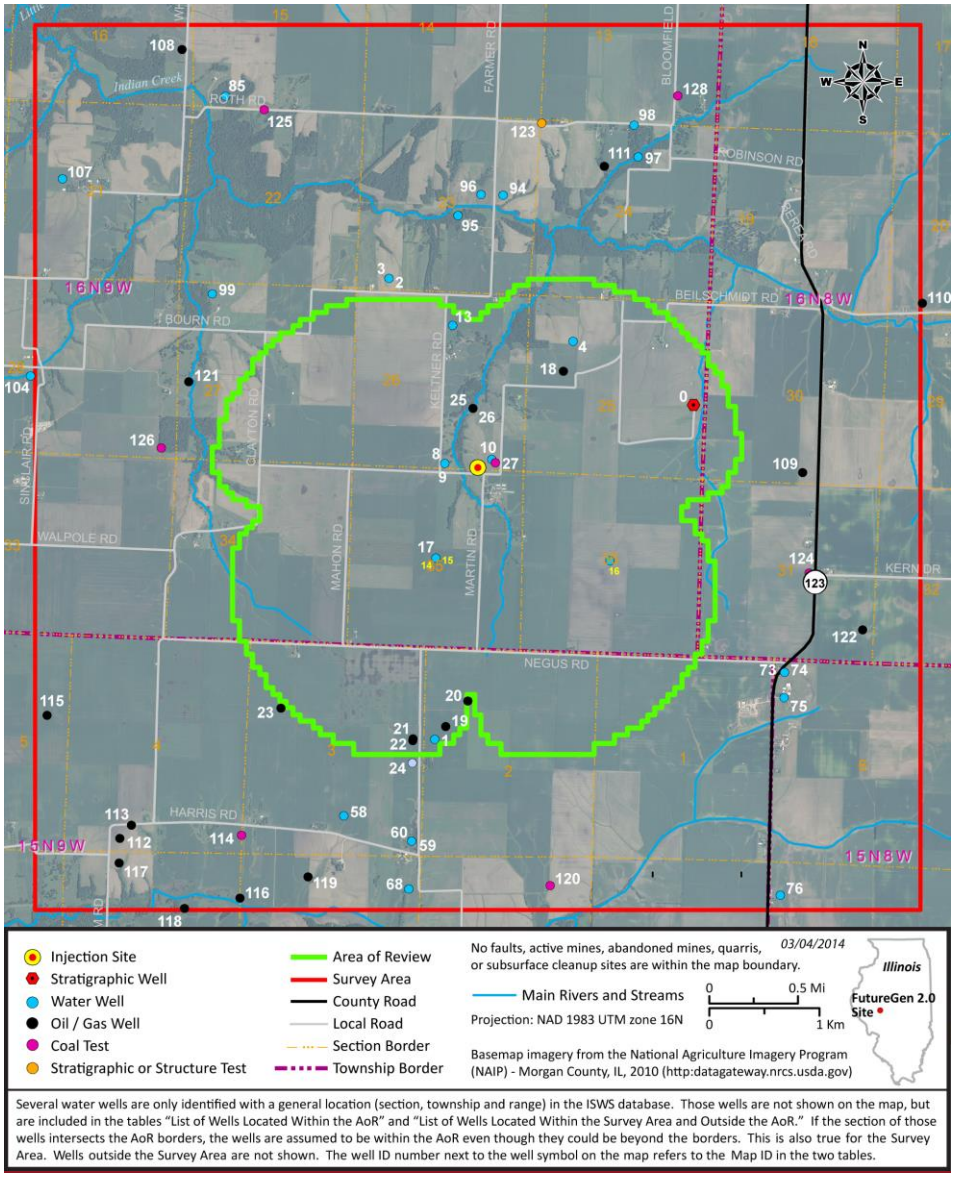
16N9W
16N8W
15N9W
15N8W
ROTH RD
BOURN RD
BEILSCHMIDT RD
ROBINSON RD
WALPOLE RD
NEGUS RD
HARRIS RD
KERN DR
FARMER RD
BLOOMFIELD
KELTNER RD
CLAYTON RD
MAHON RD
MARTIN RD
SINCLAIR RD
Indian Creek
Injection Site
Stratigraphic Well
Water Well
Oil / Gas Well
Coal Test
Stratigraphic or Structure Test
Area of Review
Survey Area
County Road
Local Road
Section Border
Township Border
No faults, active mines, abandoned mines, quarris, or subsurface cleanup sites are within the map boundary.
03/04/2014
Main Rivers and Streams
Projection: NAD 1983 UTM zone 16N
0 0.5 Mi
0 1 Km
Basemap imagery from the National Agriculture Imagery Program (NAIP) - Morgan County, IL, 2010 (http:datagateway.nrcs.usda.gov)
Illinois
FutureGen 2.0 Site
Several water wells are only identified with a general location (section, township and range) in the ISWS database. Those wells are not shown on the map, but are included in the tables "List of Wells Located Within the AoR" and "List of Wells Located Within the Survey Area and Outside the AoR." If the section of those wells intersects the AoR borders, the wells are assumed to be within the AoR even though they could be beyond the borders. This is also true for the Survey Area. Wells outside the Survey Area are not shown. The well ID number next to the well symbol on the map refers to the Map ID in the two tables.

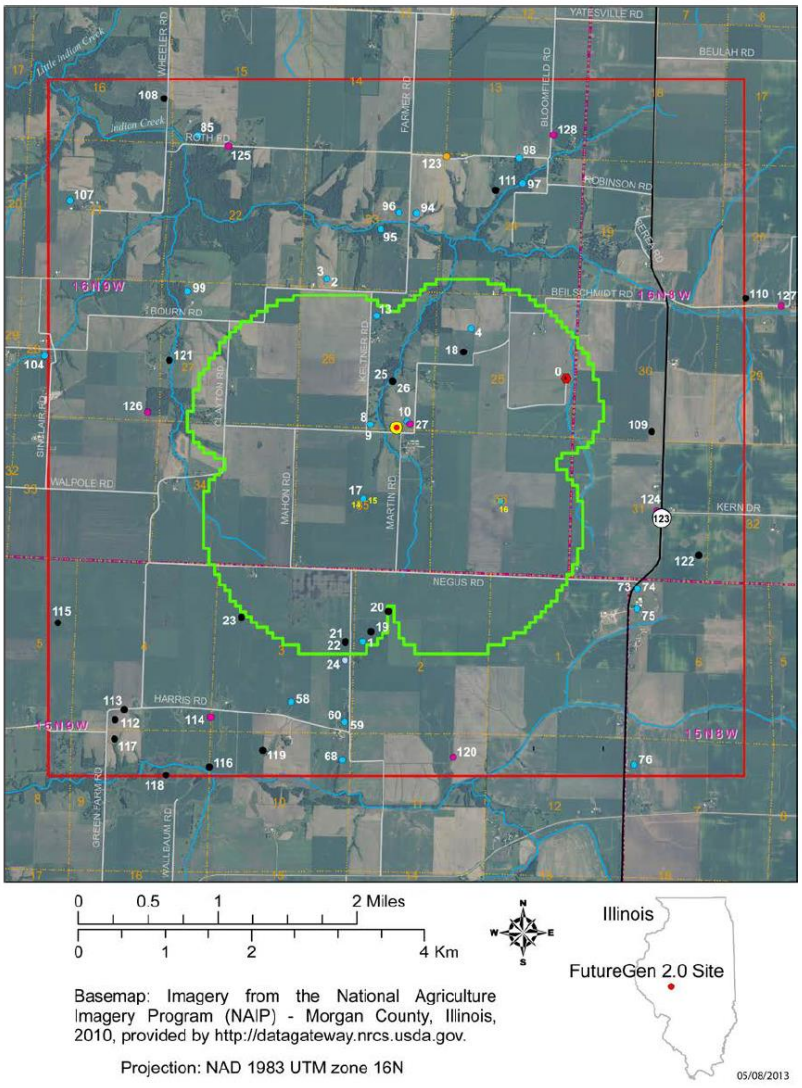

Figure 2.32. Wells Located Within the Survey Area. The map includes surface bodies of water, mines, quarries, faults, and other surface features. Tables of the data used to produce this map are provided in Table 2.17 and Appendix B.

Figure 12. Wells Located Within the Survey Area

~~7.~~8. *Proposed Operating Data (Operational Information)*

Figure 13 ~~(Figure 3.18)~~ and Figure 14 show~~s~~ the well design for the representative case for the refined area of the model domain in plan view ~~and~~, in 3D view, ~~or~~ and in cross section view, respectively. Injection into four lateral wells with a well-bore radius of 4.5 in. was modeled with the lateral leg of each well ~~being~~ located within the best layer of the injection zone to maximize injectivity. Only the non-cased open sections of the wells are specified in the model input file because only those sections are delivering CO_2 to the formation. The well design modeled in this case is the open borehole design, therefore part of the curved portion of each well is open and thereby represented in the model in addition to the lateral legs. The orientation and lateral length of the wells, as well as CO_2 mass injection rates, were chosen so that the resulting modeled CO_2 plume would avoid sensitive areas. The coordinates of the screened portion of the injection wells and the CO_2 mass injection rate was distributed among the four injection wells as shown in ~~Table 9~~ ~~Table 10~~ and Table 11~~Table 11~~~~Table 10~~ ~~(Table 3.11)~~ for a total injection rate of 1.1 MMT/yr for 20 years. The injection rate was assigned to each well according to the values in Table 11~~Table 11~~~~Table 10~~. A maximum injection pressure of 2,252.3 psi was assigned at the top of the open interval (depth of 3,850 ft bgs or an elevation of -3,231~~0~~ ft), based on 90 percent of the fracture gradient described in Section 3.5 (0.65 psi/ft).

Field Code Changed

Field Code Changed

3D View

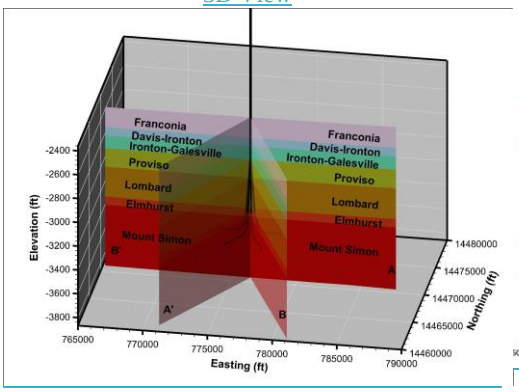

Plan View

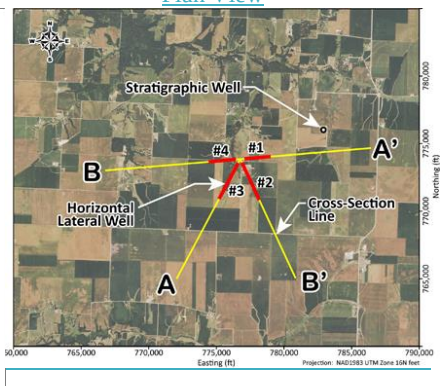

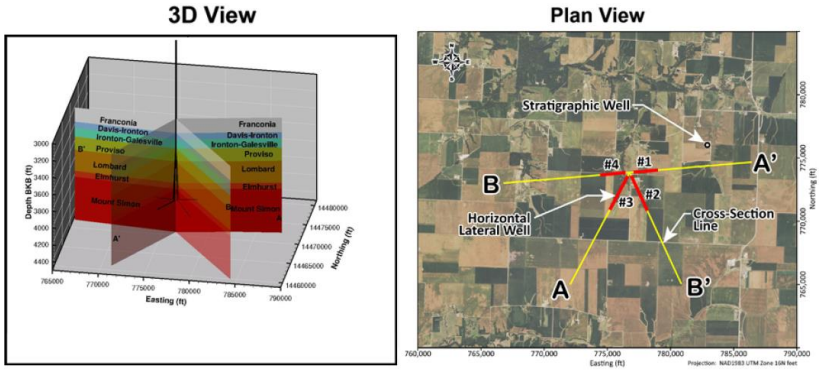

Figure 3.18. Operational Well Design for Representative Case Scenario as Implemented in the Numerical Model. The lateral legs of the injection wells are shown in red and the cross-section lines are shown in yellow.

Figure 13.

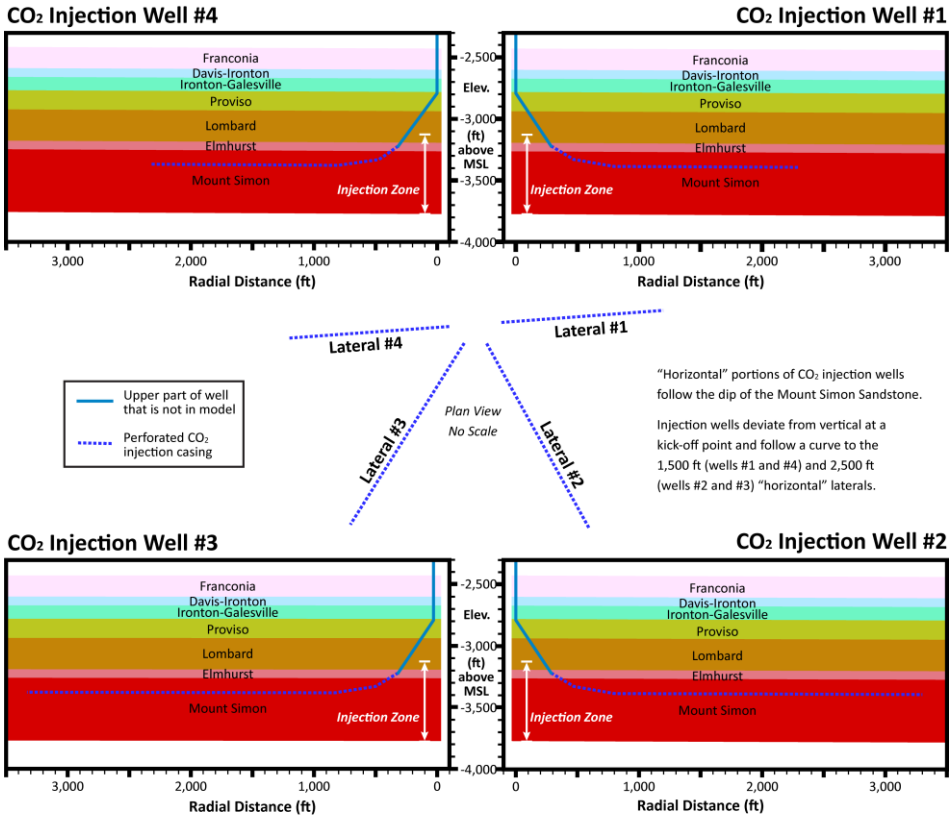

Figure 14. Cross Sections of CO_2 Injection Wells

Table 10.

~~Table 9.~~ Coordinates (NAD1983 UTM Zone 16N) of Open Portions of the Injection Wells

	Coordinate 1(ft)			Coordinate 2(ft)			Coordinate 3(ft)			Coordinate 4(ft)		
	x	y	z	x	y	z	x	y	z	x	y	z
Well 1	777079	14468885	-3200	777263	14468901	-3330	777592	14468929	-3392	779086	14469060	-3399
Well 2	776898	14468571	-3200	776976	14468404	-3330	777116	14468105	-3395	778172	14465839	-3463
Well 3	776617	14468578	-3200	776530	14468416	-3330	776375	14468124	-3389	775202	14465917	-3387
Well 4	776451	14468829	-3200	776267	14468813	-3330	775938	14468785	-3386	774444	14468654	-3379

Table 11. Mass Rate of CO_2 Injection for Each of the Four Lateral Injection Wells

Well	Length of Lateral leg (ft)	Mass Rate of CO_2 Injection (MMT/yr)
Injection well #1	1,500	0.2063
Injection well #2	2,500	0.3541
Injection well #3	2,500	0.3541
Injection well #4	1,500	0.1856

~~Table 8~~

Table 3.11. Mass Rate of CO_2 Injection for Each of the Four Lateral Injection Wells

Well	Length of Lateral leg (ft)	Mass Rate of CO_2 Injection (MMT/yr)
Injection well #1	1,500	0.2063
Injection well #2	2,500	0.3541
Injection well #3	2,500	0.3541
Injection well #4	1,500	0.1856

~~8.~~9. *Computational Modeling Results*

At the end of the simulation period, 100 years, most of the CO_2 mass occurs in the CO_2-rich (or separate-) phase, with 20 percent occurring in the dissolved phase. Note that residual trapping begins to take place once injection ceases, resulting in about 15 percent of the total CO_2 mass being immobile at the end of 100 years. The CO_2 plume forms a cloverleaf pattern as a result of the four lateral injection-well design. The plume grows both laterally and vertically as injection continues. Most of the CO_2 resides in the Mount Simon Sandstone. A small amount of CO_2 enters into the Elmhurst and the lower part of the ~~primary confining zone (~~Lombard~~)~~. When injection ceases at 20 years, the lateral growth becomes negligible but the plume continues to move slowly primarily upward. Once CO_2 reaches the low-permeability zone in the upper Mount Simon it begins to move laterally. There is no ~~additional~~ CO_2 entering the confining zone~~. from the injection zone. after injection ceases.~~

9.1 Pressure front A~~o~~R delineation

~~Note: AOR delineation using the pressure front method is missing~~

As shown in Figure 15, the calculated hydraulic heads from the pressures and fluid densities measured in the Mount Simon Sandstone during drilling of the stratigraphic well ranges from 47.8 to 61.6 ft higher than the calculated hydraulic head in the lowermost underground source of drinking water (USDW) (St. Peter Sandstone). Based on these measurements, it was expected that the approach suggested in the EPA AoR Guidance document (EPA 2013) for determination of the pressure front AoR would not be applicable for the FutureGen 2.0 site since it would be in the "over-pressured" category. Alternative methods for assessment of the impacts of the pressure front would be needed for the "over-pressured" case at the FutureGen 2.0 site. The sections below show the results of the EPA approach using the site parameters for an under-pressured case (demonstrating the need for alternative analyses) followed by a description and results of an alternative approach for this over-pressured case.

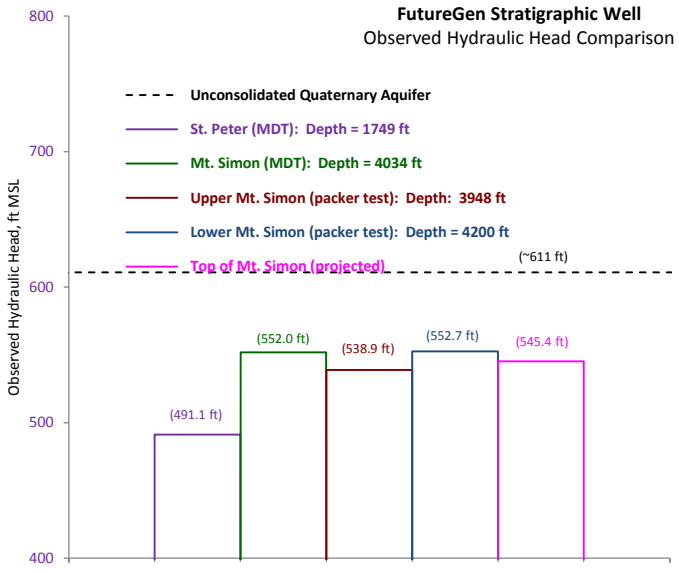

Figure 15. Observed Hydraulic Head Comparison between the Unconsolidated Quaternary Aquifer, St. Peter Sandstone, and Mount Simon Sandstone within the FutureGen Stratigraphic Well

9.1.1 -Pressure Front Calculation using EPA Method 1 (applicable for under-pressured cases)

The pressure front, as defined by EPA (2013, pg. 39), is "the minimum pressure within the injection zone necessary to cause fluid flow from the injection zone into the formation matrix of the USDW through a hypothetical conduit (i.e., artificial penetration) that is perforated in both intervals". Determining the pressure front ($P_{i,f}$) in "under-pressured" cases is calculated from Equation 1 of EPA (2013):

$$P_{i,f} = P_u + \rho_i \cdot g \cdot (z_u - z_i)$$

Where:

P_i, P_u Pressure (pre-injection) in injection zone and USDW (respectively), Pa

ρ_i Fluid density in injection zone, kg/m^3

z_i, z_u Elevation of injection zone and USDW (respectively), m

g Acceleration of Gravity

Table 12~~Table 12~~~~Table 11~~ lists the parameter values for this calculation for the Morgan County FutureGen 2.0 site from PNWD (2012). Based on these data, the threshold pressure ($P_{i,f}$) is 11.897 MPa. The pressure differential ($P_{i,f} - P_i$) is -0.34500 MPa. Since this value is negative, ambient conditions at the site already are over-pressured in the injection zone in relation to the lowermost USDW. Section 9.1.2 describes an alternative analysis for assessing the impacts of the pressure front on the lowermost USDW in this over-pressured case.

Table 12~~12~~~~11~~. Parameter Values for Pressure Front Calculation (pressure measurements from Battelle 2012)

Unit	Recorded Depth of Measurement (ft KB)	Elevation of Measurement (m MSL)	Pressure – gage (Pa)	Temperature	Fluid Density (kg/m^3)
St. Peter Sandstone	1,795.99	-354.5	4,951,600 (732.86 psia)	~82 F	999
Mt. Simon Sandstone	4,048	-1,041	12,242,400 (1,790.3 psia)	96.6 F	1,031.5

9.1.2 Alternative Approach for Analysis of Impacts of Pressure Front for Over-Pressured Cases

The objective of the analyses is to assess whether the AoR delineation, which is based on the maximum extent of the $scCO_2$ plume (see Section 9.2), is also protective of the lowermost USDW from the induced pressure front from $scCO_2$ injection. Additional details of this approach are described in Williams et al. (2014).

9.1.2.1 Description of Approach

This calculation must consider the potential for brine migration into aquifers and USDWs along plugged and abandoned or poorly constructed wells that penetrate the confining zone, driven by the injection zone pressure increases associated with $scCO_2$ injection. As noted by many authors, and shown in results from the FutureGen 2.0 injection modeling, the extent of the pressure increase during $scCO_2$ injection is larger than the extent of the $scCO_2$ plume. However, this extended region of increased pressure does not necessarily result in an increased risk to USDWs when mitigating factors are considered.

As discussed by Birkholzer et al. (2011), determination of a static critical threshold pressure for flow of brine up an open conduit or damaged borehole (e.g., substandard well completion, deteriorating seal in abandoned well, or near-borehole drilling-related formation damage) may not be applicable for cases where permeable units exist between a deep injection zone and lowermost USDW, because the open conduit approach does not account for lateral flow outside the conduit or casing and into these permeable zones. The effective permeability around a damaged plugged and abandoned or poorly constructed well would be smaller than in an unplugged well casing (i.e., open conduit) and would permit brine to flow into intervening permeable formations (i.e., thief zones). Birkholzer et al. (2011) stated that a model is required to analyze these dynamic and transient impacts.

At the FutureGen 2.0 site in Morgan County, Illinois, many potential thief zones exist between the injection zone and the lowermost USDW, including 1) the Ironton Sandstone; 2) the Potosi Dolomite (which was identified as a very challenging lost-circulation zone during drilling activities related to the

FutureGen 2.0 stratigraphic borehole [FGA#1], indicating extremely high-permeability conditions); and 3) the New Richmond Sandstone.

The analysis reported here followed the approach detailed by Birkholzer et al. (2013) for analyzing the impacts of the focused leakage of brine up a damaged, plugged, and abandoned or poorly constructed well based on the pressure buildup caused by $scCO_2$ injection. The analysis used by Birkholzer et al. (2013) applied an analytical model, ASLMA (Cihan et al. 2011, 2013, 2014), which was developed specifically for these types of focused leakage problems. The ASLMA analytical model was selected for this analysis because of its capabilities and published prior use, which included verification cases with other models for these types of problems. In this study for the FutureGen2.0 site, an assessment was conducted of the impacts on the lowermost USDW from focused leakage at the closest well outside the maximum extent of the $scCO_2$ plume that penetrates the confining zone; this well is the Criswell borehole at the Waverly field, which is 26 km from the center of the FutureGen 2.0 injection wells. Cases were also run for a stratigraphic borehole, FGA#1 (which will be completed as a monitoring well), that is located near the maximum extent of the predicted $scCO_2$ plume approximately 2 km from the centroid of the injection-well laterals. Figure 16 shows the location of the closest wells that penetrate the primary confining zone above the injection zone around the FutureGen 2.0 site. The results of the cases run at these two selected locations can provide guidance on the adequacy of the FutureGen 2.0 site AoR, which was defined based on the maximum predicted $scCO_2$ extent in the UIC Permit Application, to be protective of the lowermost USDW in the context of focused brine leakage from damaged, plugged, and abandoned or poorly constructed wells.

The ASLMA_V3 analytic model (Cihan et al. 2011, 2014), which is implemented as a Fortran 90 calculational code, was used for the analyses discussed in the report. Additional examples of the application of ASLMA_V3 are described by Cihan et al. (2013). Pacific Northwest National Laboratory has obtained the ASLMA_V3 source code, executable computer file, and sample problems from the authors at Lawrence Berkeley National Laboratory (LBNL). The model applies to single-phase, isothermal fluid flow for focused leakage around wells and/or diffuse leakage through aquitards in a multilayered aquifer system that results from the transient pressure field created during injection. The model requires specification of the permeability, specific storage, and unit thickness of the injection zone, aquifers, and aquitards. Because the simulation option of solving only for focused leakage into aquifers around a borehole was used in this analysis, aquitard permeability and specific storage were not used in the model. The model also requires borehole radii and effective permeabilities for the damaged zone around the borehole for each segment of the aquifers and aquitards it encounters. Initial conditions for the model assume a hydrostatic pressure gradient. The model does not account for brine density differences, but this simplifying assumption is conservative because the volume of freshwater leakage calculated for each permeable unit would be larger than if higher-density reservoir fluid were used in the calculation.

Runs were also conducted with another version of this code, ASLMA_V3_initialheads, which allows initial hydraulic head values to be specified for each of the aquifer units. This removes the hydrostatic head initial condition limitation of the ASLMA_V3 code. A description and test cases of this version of the ASMLA_V3 code are included in Cihan et al. (2014).

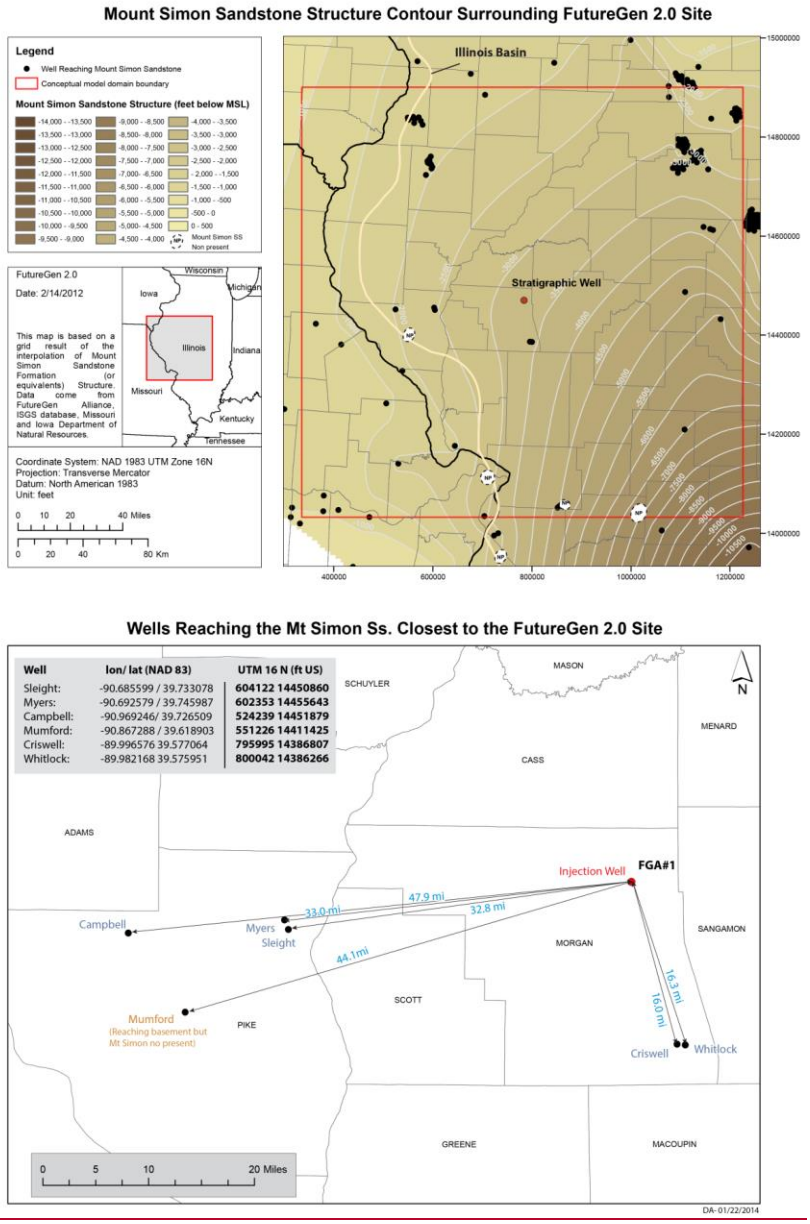

Figure 16. Location of the FutureGen 2.0 Site and Closest Wells that Penetrate the Mount Simon Sandstone

9.1.2.2 Model Parameters

Site data for the upper layers (Ironton to St. Peter) are limited at the FutureGen 2.0 site because the focus of the detailed characterization of the first stratigraphic borehole (FGA#1) was on the injection zone and confining zone. Detailed characterization of the upper layers is planned for the next drilling campaign. Some side-wall core permeability measurements of these upper layers were used, along with published regional values or conservative estimates (i.e., using lower ranges of permeability estimates for the aquifers below the USDW).

Direct measurements of the effective permeability of plugged and abandoned or poorly constructed wells are limited. Vertical Interference Tests have recently been used to help quantify this measurement for a range of wells (e.g., Crow et al. 2010; Gasda et al. 2013; Duguid et al. 2013). Effective permeability estimates for the damaged zone around a borehole for this study were based on published ranges of groupings of wells with different leakage potentials (low, medium, high, extreme), as reported in Table 2 of Celia et al. (2011), which used the categories defined by Watson and Bachu (2008). Celia et al. (2011) used a stochastic modeling study with a large number of realizations for wells in the Wabamun Lake area of Alberta, Canada. Data from Crow et al. (2010) were also used by Celia et al. (2011) to develop these effective permeability estimates, which also highlighted the few measurements available. The high end of the High Leakage Potential Category (0.5 to 8 mD) and Extreme Leakage Potential Category (8 to 10,000 mD) (Celia et al. 2011) were investigated in this modeling effort. Single values of effective permeability for the borehole were assigned for all the aquifer/aquitard segments (instead of variable borehole permeability for each segment), which provide conservative results based on the analysis of Celia et al. (2011).

The results from this analysis are reported as the volume of fluids leaked over time from the injection zone into each of the overlying aquifers (including the St. Peter, the lowermost USDW) for the two well distances (~2 km and 26 km) using conservative estimates for the site parameters and the borehole effective permeabilities, as discussed above. Well locations are shown in Figure 17. The two wells used in this analysis were 1) the Criswell borehole at the Waverly field 26 km southeast of the center of the FutureGen 2.0 injection wells (which is the closest borehole that penetrates the Mount Simon Formation outside the predicted $scCO_2$ plume), and 2) the FGA#1 borehole that will be completed as a monitoring well located at a distance of 2 km from the center of the injection wells, which is near the maximum extent of the predicted $scCO_2$ plume. Criswell and FGA#1 borehole diagrams are shown Williams et al. (2014) and Battelle (2012), respectively.

Thicknesses and properties for the layers in the model are shown in Table 13~~Table 13~~~~Table 1~~. Layer thicknesses are taken from the characterization/stratigraphic borehole (FGA#1) drilled at the FutureGen 2.0 site (Table 6.1 of Battelle [2012]). Adjacent aquitards are lumped into a single unit as required for the model because the code input structure only allows for a sequence of alternating aquifers and aquitards. The thickness of the injection zone was calculated by combining the upper permeable portion of the Mount Simon that was targeted in the UIC permit injection model and the Elmhurst member of the Eau Claire Formation.

Hydraulic properties are not listed in Table 13~~Table 12~~ for the aquitards because flow into these units is not calculated for the focused leakage-only model of ASLMA. Aquifer property determinations for the units other than the injection zone are listed in the footnotes of Table 12~~Table 12~~ Table 13~~Table 12~~. Hydraulic properties for the single-layer injection zone were based on fitting the simulated injection zone

pressure responses from the injection model used in the UIC Permit Application at the two well locations of interest (described in more detail below).

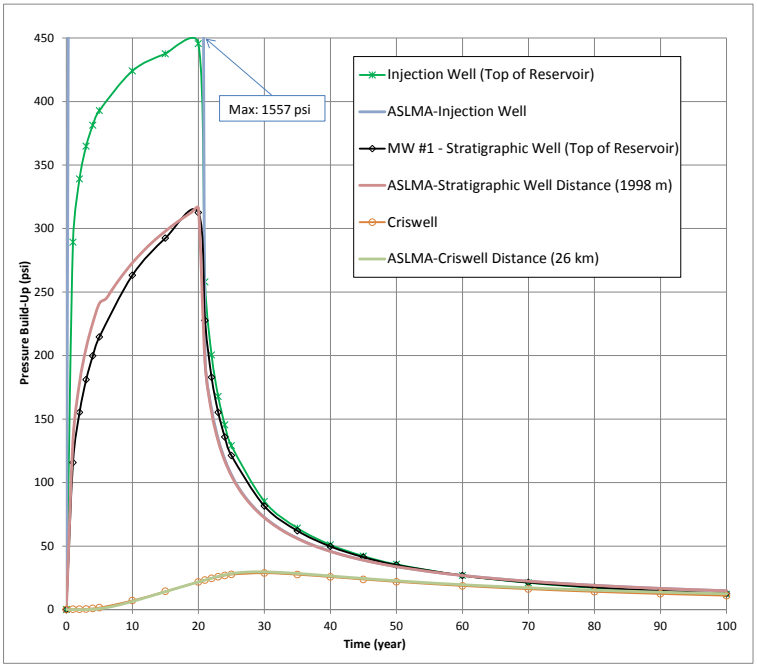

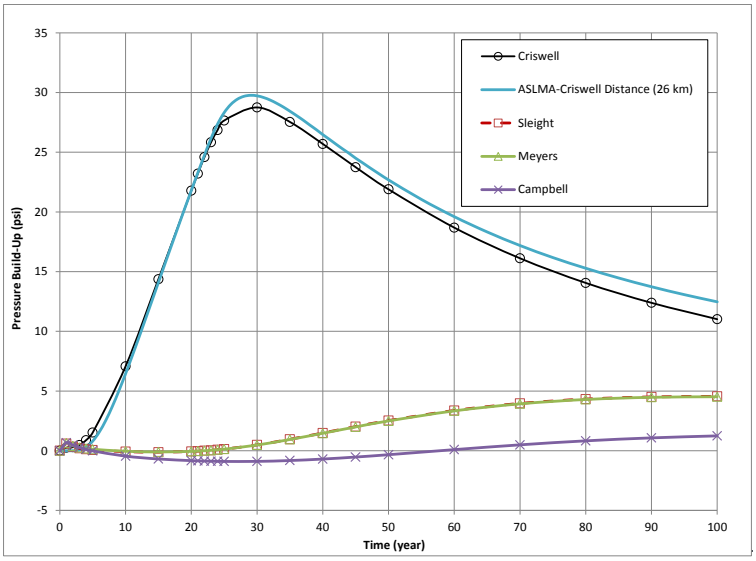

Figure 17. Comparison of Pressure Buildup within the Mount Simon Unit between UIC Permit Model and ASLMA Model Results for the FGA#1 Borehole (listed as MW#1 Stratigraphic Well in plot above) and the Criswell Borehole (Waverly field)

Permeability values for the Potosi Dolomite, potentially the most permeable unit between the confining zone and the lowermost USDW based on the five lost-circulation zones encountered during the initial characterization well drilling through this unit at the site, have not yet been determined for the site. Aquifer testing of this unit is planned during the next drilling campaign at the site. The Potosi Dolomite is described as a vuggy dolomite at the site and in other localities in the Illinois Basin. Preliminary estimates using a very conservative analysis based on the fluid losses during drilling indicate that the permeabilities of the lost-circulation zones are at least 5,000 mD. The permeability of the Potosi Dolomite at the Cabot waste injection well in Tuscola, Illinois, has been reported as 9,000 mD (Texas World Operations, Inc. 1995). Greb et al. (2009) listed permeabilities of core samples measurements for the Copper Ridge Formation, a vuggy dolomite similar to the Potosi, for a DuPont waste injection well in Louisville, Kentucky. The average horizontal permeability for the Copper Ridge Formation at the Louisville site, as reported by Greb et al. (2009), was 60 mD with the values ranging up to 632 mD. However, measurements of the permeability of core samples cannot capture the larger-scale permeability of solution cavities or fractures within this unit. The base case for this analysis uses the 9,000-mD value reported for the Tuscola site (see Table 13~~Table 13~~~~Table 12~~). Cases were also run using the much lower value of 60 mD based on the average for the Copper Ridge Formation at the Louisville, Kentucky site.

In addition to the lower Potosi Dolomite permeability case discussed above, sensitivity cases were developed using 50 percent of the Ironton Sandstone permeability and 200 percent of the St. Peter Sandstone permeability values shown in Table 13~~Table 13~~~~Table 12~~. Composite runs with all the parameter sensitivity adjustments were also developed.

Because the ASLMA model is a single-phase model, an equivalent water-injection rate was calculated from the $scCO_2$ injection rate of 1.1 MMT/yr for 20 years. The volumetric water-injection rate was calculated using $scCO_2$ densities at two pressures because the UIC permit model shows a significant pressure buildup around the injection well. The first $scCO_2$ density was applied for the first 5 years while injection pressures were rapidly increasing, and the second $scCO_2$ density (calculated at 400 psi higher) was applied from 5 to 20 years (see Williams et al. 2014 for details). The resulting water-injection rates were 0.0470 m^3/s (years 0 to 5) and 0.0439 m^3/s (years 5 to 20).

Table 13~~13~~12. Summary of Properties used in ASLMA Focused Leakage Model for the FutureGen 2.0 Site

Unit	Thickness	Hydraulic Conductivity	Specific Storage[(a)]
St. Peter Sandstone	202 ft (61.6 m)	1.18E-5 m/s (1,220 mD)[(b)]	1.0E-6 m^{-1}
Shakopee Dolomite	390 ft (119 m)	Aquitard	Aquitard
New Richmond Sandstone	102 ft (31.1 m)	2.2E-6 m/s (230 mD)[(c)]	1.0E-6 m^{-1}
Oneota Dolomite, Gunter Dolomite, Eminence Dolomite	362 ft (110 m)	Aquitard	Aquitard
Potosi Dolomite	276 ft (84.1 m)	9.E-5 m/s (9,000 mD)[(d)]	1.0E-6 m^{-1}
Franconia Dolomite, Davis Dolomite	244 ft (74.3 m)	Aquitard	Aquitard
Ironton Sandstone	109 ft (33.2 m)	2.9E-7m/s (30 mD)[(e)]	1.0E-6 m^{-1}
Upper Eau Claire (Proviso and Lombard)	413 ft (126 m)	Aquitard	Aquitard
Lower Eau Clair (Elmhurst) and Upper Mount Simon	330 ft (100 m)	7.6E-7 m/s (79 mD)[(f)]	2.2E-6 m^{-1}[(f)]

(a) Specific storage for units other than ~~reservoir~~injection zone: default value calculated based on mid-range of compressibility for sound rock (Table 2.5 of Freeze and Cherry [1979]). Specific storage not used for aquitards.

(b) St. Peter: Permeability from Waverly Project listed by Buschbach and Bond (1967, 1974). Measurement could be air permeability (water permeability would be lower).

(c) New Richmond: Geometric mean of a large number of samples (38) analyzed for air permeability (water permeability would be lower) from the New Richmond Formation at the Waverly site (Core Laboratories 1966).

(d) Potosi: Value reported for Potosi at Cabot Waste Injection Well in Tuscola, Illinois (see discussion in text for details).

(e) Ironton: Average of representative samples from side-wall core analyses (horizontal permeability, Klinkenberg from standard core permeability analysis and Swanson from high pressure mercury injection analysis) on samples from FGA#1 (stratigraphic characterization) borehole at the FutureGen 2.0 site (Whitney et al. 2012). Similar to geometric mean of a large number of samples (53) analyzed for air permeability from the Ironton Formation at the Waverly site (Core Laboratories 1966).

(f) ~~Reservoir~~Injection zone: Hydraulic properties (hydraulic conductivity and specific storage) based on fit of simulation pressure results from UIC Permit Injection model (see text for details).

Hydraulic conductivity and specific storage were adjusted in the ASLMA model for the composite Mount Simon/Elmhurst injection layer to fit the pressure responses from the UIC permit injection model at the FGA#1 borehole (2 km from the center of the injection-well laterals) and Waverly field Criswell borehole (26 km from the center of the injection-well laterals). A manual fitting process was used (see comparison in Figure 18). It was difficult to exactly fit both wells with the same parameters; therefore,

parameters were chosen so that the overall fit of the ASLMA pressure results for the FGA#1 and Waverly boreholes in the injection layer were mostly higher than the UIC permit model. This is conservative for this analysis because slightly greater pressures in the injection zone would lead to greater leakage at the well locations. The ASLMA model-predicted pressure at the injection well is much greater than the UIC

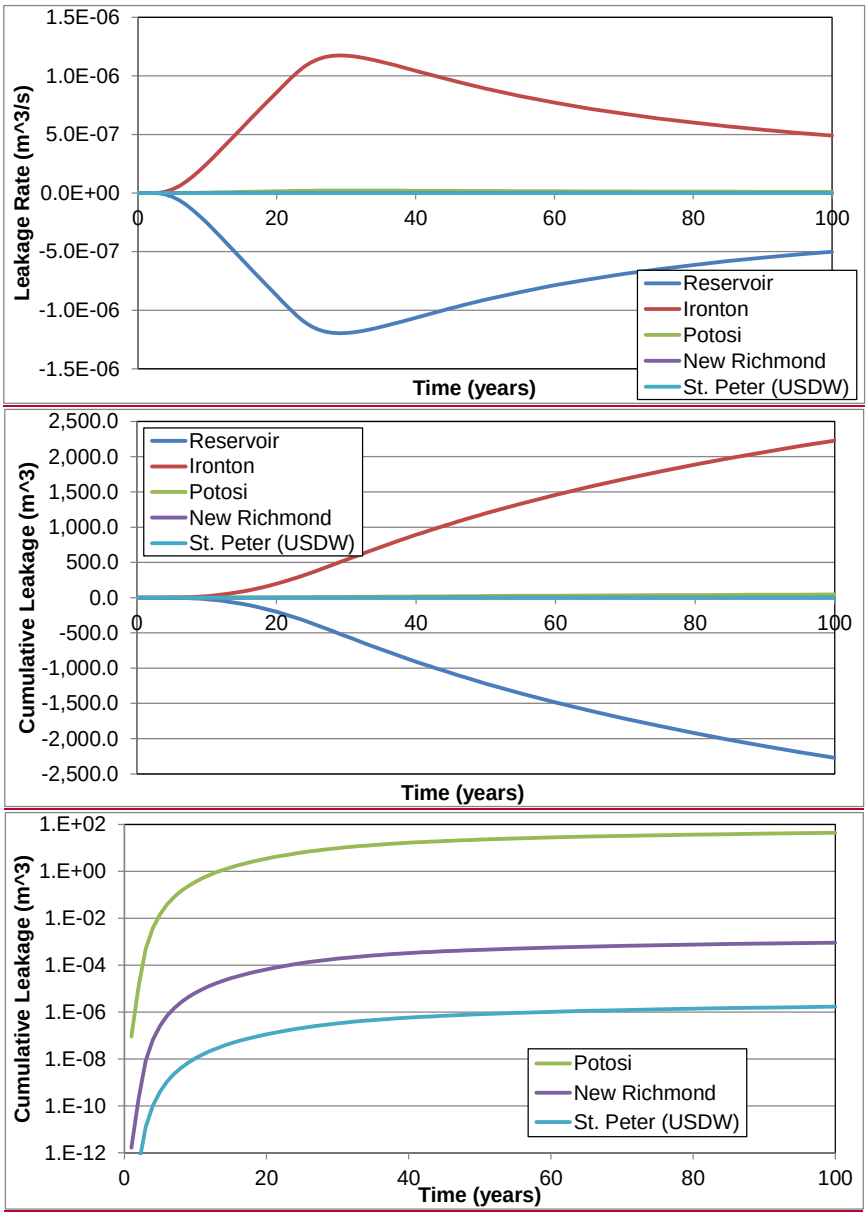

Figure 18. Waverly Field Well (26 km distance) − Top of Extreme Leakage Potential Category (10,000 mD).

permit model-predicted injection because we simulated only a single vertical well (instead of the four horizontal wells in the UIC permit model) and water injection (with a higher density and viscosity than $scCO_2$) with the equivalent injection zone displacement of the $scCO_2$. Leakage at the injection well was not part of this analysis, so this pressure difference did not affect the results (i.e., only transient pressures at the Waverly well and FGA#1 borehole were used in calculating the focused leakage into the upper units along these wells). Similar pressure buildup in the injection zone, as shown in Figure 18, was obtained from all the injection cases run in this study.

In Section 9.1.1, the hydraulic head difference calculated using the EPA method for the pressure differential was 34.1 m using the injection zone fluid density (see Table 12). For the cases run with ASLMA_V3_initialheads, the initial head for the injection zone was set to 34.1 m above hydrostatic pressure. The initial conditions for hydraulic heads in the aquifers above the injection zone were set to hydrostatic values.

9.1.2.3 Results and Discussion

Results for the simulated leakage for the Waverly field well (Criswell borehole, 26 km from the center of the injection-well laterals) are shown in Figure 19 for the Extreme Potential Leakage Category (10,000 mD). This extreme upper bound on the effective permeability for a plugged and abandoned or poorly constructed well is comparable to unconsolidated clean sand (see Table 2.2 of Freeze and Cherry [1979]). Figure 19 shows the total leakage from the injection zone and leakage into each of the permeable units above the confining zone up to the St. Peter (lowermost USDW). The plots in Figure 19 show the fluxes over the 100-year simulation period and the cumulative leakage volume. A plot also is included, using a log scale, of cumulative leakage for the units above the Ironton (Potosi, New Richmond, and St. Peter) because these values are much lower than those for the Ironton.

Similar results for the FGA#1 borehole (at the 2-km distance) for the Extreme Leakage Potential Category (10,000 mD) are shown in Figure 20. The simulated fluxes and cumulative leakage volume for the FGA#1 borehole are higher than those for the Waverly well, given the higher pressures at the closer location. Simulation results for the two simulated locations (Waverly and FGA#1, respectively) using the top of the High Potential Leakage Category (8 mD) had similar response shapes, but overall lower leakage rates than the Extreme Potential Leakage Category. Additional plots of these cases are provided in Williams et al. (2014).

Results for the non-hydrostatic case (initial head 34.1 m higher than hydrostatic in the injection zone) for the Extreme Leakage Potential Category at the Waverly well location are shown Figure 21. The results include the injection zone and Ironton Sandstone leakage rates for ambient (i.e., pre-injection) conditions. The constant leakage rates in the ambient flow cases for the injection zone and Ironton Sandstone are similar to estimates of the discharge calculated manually using Darcy's law with the site parameters. Note that the difference between the constant discharges in the non-hydrostatic cases for the two well locations in this study is related to the differences in the borehole radii. As shown in the three plots in Figure 21, the non-hydrostatic case leakage rate results are similar to the superposition of the ambient flow and the hydrostatic case results.

Table 14~~Table 14~~~~Table 13~~ and Table 15~~Table 15~~~~Table 14~~shows the simulated cumulative leakage volume estimates at 100 years for each of the permeable units for comparison of the hydrostatic and 34.1 m higher injection zone initial head case results. Also reported in Table 14~~Table 14~~~~Table 13~~ and 1Table

15~~Table 15~~~~Table 14~~ are the results for the sensitivity runs of the Extreme Potential Leakage Category, 34.1 m higher injection zone initial head cases for the two well locations. The Extreme Potential Leakage Category with 34.1 m higher injection zone head cases were selected for the sensitivity runs since these had the highest leakage rates into the lowermost USDW. As discussed in Section 9.1.2.2, the variations include a doubling of the permeability of the St. Peter Sandstone (the lowermost USDW), a 50 percent reduction of the Ironton Sandstone permeability (the first aquifer above the confining zone that has the greatest focused leakage), and reduction in the permeability of the Potosi Dolomite from 9,000 mD to 60 mD (the aquifer with the largest permeability). A composite case was also run for each of the well locations that combined all the sensitivity case permeability adjustments.

Simulation results from the base cases (High and Extreme Leakage Potential) for the closest well outside of the predicted extent of the $scCO_2$ plume (Waverly field, 26 km from the center of the injection area) show that the leakage of brine into the lowermost USDW from a damaged, plugged, and abandoned or poorly constructed well, even considering extremely conservative parameter estimates, is very small. As shown in the first two rows of Table 14~~Table 13~~, a volume of only 1.71×10^{-6} m^3 (0.00171 L) or less leaks into the lowermost USDW over a period of 100 years. The simulation results show that most of the focused leakage along a damaged borehole from the injection zone is captured in the permeable zones (thief zones), most notably the Ironton Sandstone, which is the first permeable zone above the confining zone (1,350 ft below the lowermost USDW [St. Peter Sandstone]). The simulated cumulative brine leakage volume from the injection zone over 100 years for the Extreme Leakage Potential Category (2,273 m^3 total or 62 L/day over this period) was mostly (i.e., 98 percent) into the Ironton Sandstone, as shown in Table 14~~Table 13~~. This injection zone leakage volume represents roughly 0.008 percent of the total $scCO_2$ injection volume (using an equivalent water-injection volume of 2.82×10^7 m^3 for 1.1 MMT/yr of $scCO_2$ based on $scCO_2$ densities discussed above over a 20-year period) for the Extreme Leakage Potential Category and much less for the High Leakage Potential Category.

Base-case simulation results for a well near the outer extent of the simulated $scCO_2$ plume (FGA#1, 2 km from the center of injection area) also resulted in very low volumes (4.16×10^{-5} m^3 [0.0416 L] or less over 100 years) of brine leakage into the lowermost USDW from a damaged, plugged, and abandoned or poorly constructed well. The Extreme Leakage Potential case at this well location did show significant leakage into the Ironton Sandstone and the Potosi Dolomite units, though both are well below the lowermost USDW. For the FGA#1 borehole, the simulated cumulative brine leakage volume from the injection zone over the 100-year period for the Extreme Leakage Potential Category (16,000 m^3 total) was also mostly (i.e., 97 percent) into the Ironton Formation (Table 15~~Table 15~~~~Table 14~~). This results in 2,190 L/day over a 20-year period, which is an average over a shorter time period than was used above for the Waverly well because fluxes drop off quickly after injection is over at this location. This injection zone leakage volume for the Extreme Leakage Potential Category represents roughly 0.06 percent of the total $scCO_2$ injection volume and a much smaller volume was predicted for the High Leakage Potential Category.

Results from the ASLMA_V3_initialheads variation runs, with the initial conditions for hydraulic heads in the injection zone set to 34.1 m greater than hydrostatic, are presented in Table 14~~Table 13~~ and Table 15~~Table 14~~ for the two well distances using the Extreme Leakage Potential Category. The cumulative leakage volumes over 100 years into the lowermost USDW are still very low for both wells (0.00631 L for Waverly and 0.0642 L for FGA#1). However, as shown in Table 14~~Table 13~~ and Table 15~~Table 14~~, there were large increases in the total loss from the injection zone and leakages into the Ironton Sandstone and Potosi Dolomite. It should be noted that the difference between the increased

fluxes in these cases compared to the base cases would roughly be equivalent to the natural leakage along a damaged, plugged, and

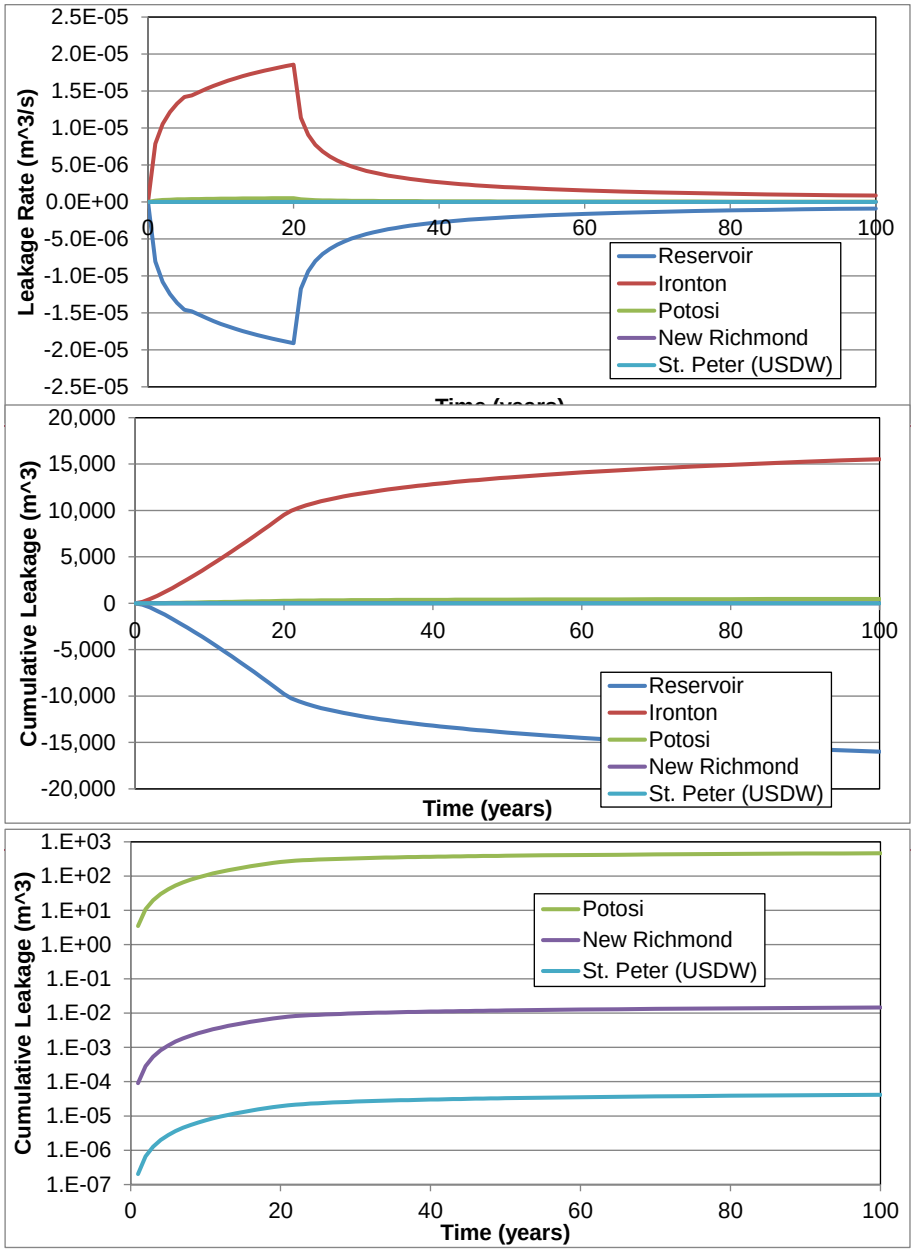

Figure 19. FGA#1 Borehole (2 km distance) – Top of Extreme Leakage Potential Category (10,000 mD).

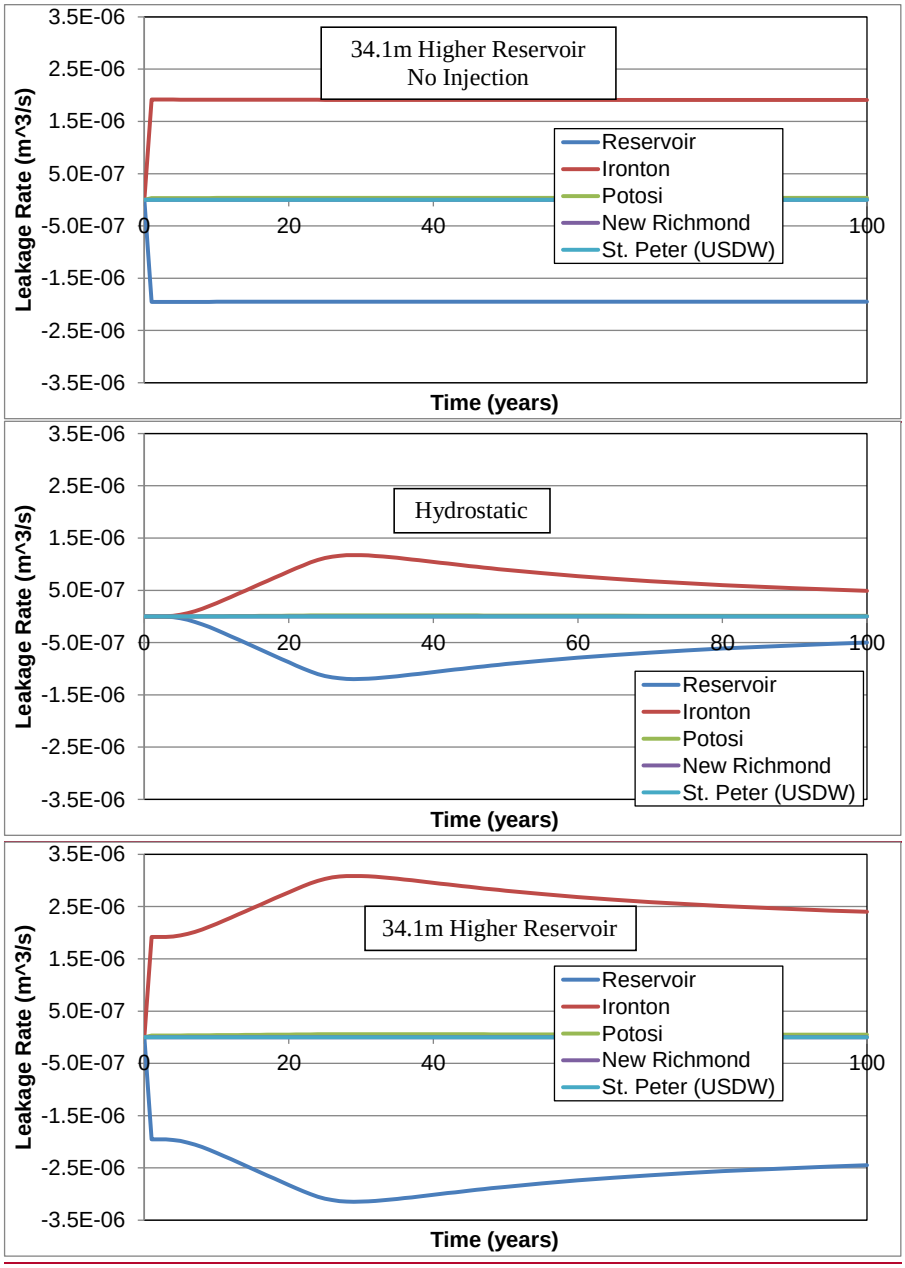

Figure 20. Comparison of Waverly Cases with Extreme Leakage Potential showing Ambient Leakage for Non-Hydrostatic Case (top), Hydrostatic Case (middle), and Non-Hydrostatic Case (bottom).

Table 141413. Waverly Well (26 km) Cases – Summary of Simulated Cumulative Fluxes after 100 Years

Case	Difference from Base Case	Injection zone Leakage Volume (m^3)	Ironton Sandstone Leakage Volume (m^3)	Potosi Dolomite Leakage Volume (m^3)	New Richmond Sandstone Leakage Volume (m^3)	St. Peter Sandstone Leakage Volume (m^3)
Base Case – High Leakage Potential	Base Case	-1.842	1.842	2.90E-05	4.86E-13	7.27E-19
Base Case – Extreme Leakage Potential		-2,273	2,229	43.92	9.15E-04	1.71E-06
Extreme Leakage Potential, Higher Initial Heads in Injection zone (34.1 m)		-8,426	8,263	162.5	3.38E-03	6.31E-06
Extreme Leakage Potential, Higher Initial Heads in Injection zone (34.1 m)	No Injection	-6,153	6,034	118.6	2.46E-03	4.60E-06
Extreme Leakage Potential, Higher Initial Heads in Injection zone (34.1 m)	200% St. Peter Permeability	-8,426	8,263	162.5	3.38E-03	6.31E-06
Extreme Leakage Potential, Higher Initial Heads in Injection zone (34.1 m)	50% Ironton Permeability	-8,341	8,034	306.9	6.38E-03	1.19E-05
Extreme Leakage Potential, Higher Initial Heads Injection zone (34.1 m)	0.67% Potosi Permeability	-8,426	8,264	161.4	0.4331	8.09E-04
Extreme Leakage Potential, Higher Initial Heads in Injection zone (34.1 m)	200% St. Peter Permeability, 50% Ironton Permeability, 0.67% Potosi Permeability	-8,341	8,035	304.9	0.8182	1.53E-03

Table 151514. FGA#1 Borehole (2 km) Cases – Summary of Simulated Cumulative Fluxes after 100 Years

Case	Difference from Base Case	Injection zone Leakage Volume (m^3)	Ironton Sandstone Leakage Volume (m^3)	Potosi Dolomite Leakage Volume (m^3)	New Richmond Sandstone Leakage Volume (m^3)	St. Peter Sandstone Leakage Volume (m^3)
Base Case – High Leakage Potential	Base Case	-13.04	13.04	3.13E-04	7.93E-12	1.80E-17
Base Case – Extreme Leakage Potential		-1.60E+04	1.55E+04	465.1	1.47E-02	4.16E-05
Extreme Leakage Potential, Higher Initial Heads in Injection zone (34.1 m)		-2.52E+04	2.45E+04	727	2.28E-02	6.42E-05
Extreme Leakage Potential, Higher Initial Heads in Injection zone (34.1 m)	No Injection	-9238	8976	261.8	8.09E-03	2.25E-05
Extreme Leakage Potential, Higher Initial Heads in Injection zone (34.1 m)	200% St. Peter Permeability	-2.52E+04	2.45E+04	727	2.28E-02	6.42E-05
Extreme Leakage Potential, Higher Initial Heads in Injection zone (34.1 m)	50% Ironton Permeability	-2.49E+04	2.35E+04	1355	4.24E-02	1.20E-04
Extreme Leakage Potential, Higher Initial Heads in Injection zone (34.1 m)	0.67% Potosi Permeability	-2.52E+04	2.45E+04	719.9	2.907	8.19E-03
Extreme Leakage Potential, Higher Initial Heads in Injection zone (34.1 m)	200% St. Peter Permeability, 50% Ironton Permeability, 0.67% Potosi Permeability	-2.49E+04	2.35E+04	1342	5.42	1.53E-02

abandoned or poorly constructed well prior to any $scCO_2$ injection at the FutureGen 2.0 site (i.e., driven by ambient conditions in the area as shown in Figure 21).

Cumulative leakage results over 100 years for the sensitivity case runs are also provided in Table 14~~Table 13~~ and Table 15~~Table 14~~ for the two well locations. The base case for these runs was the Extreme Leakage Potential Category with the initial heads in the injection zone set to 34.1 m higher than hydrostatic. These cases were selected since they had the largest predicted leakage into the lowermost USDW. As shown in Table 14~~Table 13~~ and Table 15~~Table 14~~, the doubling of the St. Peter Sandstone permeability had little or no impact on the predicted leakages. However reductions in the permeability of the Ironton Sandstone and Potosi Dolomite did increase the predicted brine leakage into the lowermost USDW. Results of the composite runs that included all the sensitivity parameter adjustments still showed very small amounts of leakage into the lowermost USDW over 100 years for both the Waverly field distance (1.53 L) and the FGA#1 borehole distance (15.3 L).

Results from this modeling evaluation indicated that, under site conditions, operations-related pressure increases will not result in brine migration through damaged, plugged, and abandoned or poorly constructed wells extending above overlying thief zones at appreciable levels near the outer extent of the simulated $scCO_2$ plume or at the closest well outside this zone that penetrates the confining zone. Therefore, the delineated $scCO_2$ AoR should also be protective of the lowermost USDW from pressure-induced brine migration under these leakage scenarios.

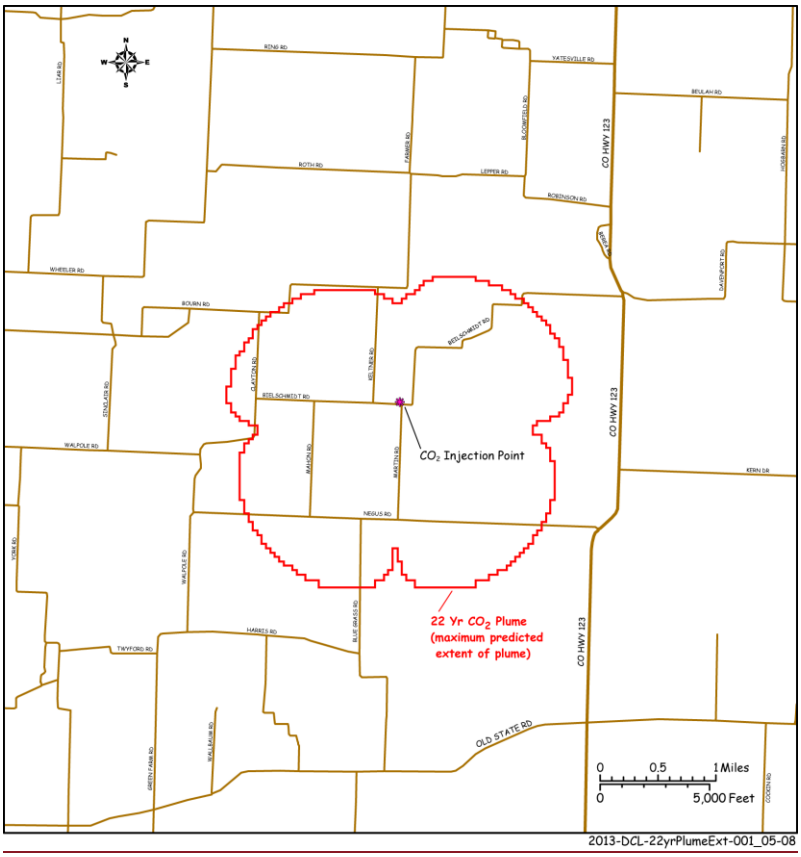

Figure 21. AoR for the Morgan County CO_2 Site

9.2 Separate-phase plume AoR delineation

Using the CO_2-rich phase saturation as a defining parameter for the CO_2 plume extent is subject to over-prediction due to numerical model choices such as grid spacing. Therefore, to accurately delineate the plume size, a methodology that used the vertically integrated mass per unit area (VIMPA) of CO_2 was developed. This ensures that the plume extent is defined based on the distribution of the mass of CO_2 in the injection zone. The VIMPA is calculated as follows:

$$VIMPA_{i,j} = \sum_{k} \frac{M_{i,j,k}}{A_{i,j,k}}$$

where M = the total CO_2 mass in a cell, A = the horizontal cross-sectional area of a cell, i and j = cell indices in the horizontal directions, and k = the index in the vertical direction.

For the purposes of AoR determination, the extent of the plume is defined as the contour line of VIMPA, within which 99.0 percent of the CO_2-rich phase (separate-phase) mass is contained. The acreage (areal extent in acres) of the plume is calculated by integrating all cells within the plume extent. Therefore, the CO_2 plume referred to in this document is defined as the area containing 99.0

percent of the separate- phase CO_2 mass. After 20 years of injection and 2 years of shut-in, the areal extent of the separate-phase CO_2 plume no longer increases significantly. Therefore, the AoR, shown in Figure ~~14~~ ~~15~~22 ~~(Figure 3.25)~~, is delineated based on the predicted areal extent of the separate-phase CO_2 plume at 22 years.

Corrective Action Plan and Schedule

With the exception of the FutureGen Stratigraphic well, no wells have been identified within the AoR that require corrective action.

Area of Review Reevaluation Plan and Schedule

Proposed Reevaluation Cycle

The Alliance will reevaluate the AoR on an annual basis for the first 5 years following the initiation of injection operations (Figure 23). After the fifth year of injection, the AoR will be updated at a minimum of every 5 years as required by 40 CFR 146.84(b)(2)(i). An annual reevaluation in the first 5 years is intended to account for any operational variation during the startup period.

Some conditions would warrant reevaluation prior to the next scheduled cycle. To meet the intent of the regulations and protect USDWs, the following six conditions would warrant reevaluation of the AoR:

1. **Exceeding Fracture Pressure Conditions:** Pressure in any of the injection or monitoring wells exceeding 90 percent of the geologic formation fracture pressure at the point of measurement. This would be a violation of the permit conditions. The Testing and Monitoring Plan provides discussion of pressure monitoring.

   Action: The computational model will be calibrated to match measured pressures. Model outputs that calculate the change in AoR would be provided to the EPA.

2. **Exceeding Established Baseline Hydrochemical/Physical Parameter Patterns:** A statistically significant difference between observed and baseline hydrochemical/physical parameter patterns (e.g., fluid conductivity, pressure, temperature) within the Ironton Formation immediately above the confining zone (ACZ1 and ACZ2 wells). The Student's t-test statistical procedure will be used to compare background (baseline) with observed results. The Testing and Monitoring Plan provides extended information regarding how pressure, temperature, and fluid conductivity will be monitored within the Ironton Formation.

   Action: If in the event that hydrochemical/physical parameter trends suggest that leakage may be occurring, either the computational model or other models may be used to understand the observational parameter behavior.

3. **Compromise in Injection Well Mechanical Integrity:** A significant change in pressure within the protective annular pressurization system surrounding each injection well that indicates a loss of mechanical integrity at an injection well.

   Action: Injection wells suspected of mechanical integrity issues would be shut down and the cause of the pressure deviation determined. Mechanical integrity testing would be conducted and the computational model would be updated with mechanical integrity results to determine the severity

and extent of the loss of containment. The Testing and Monitoring Plan provides extended information about the mechanical integrity tests that will be conducted in the injection wells.

4. **Departure in Anticipated Surface Deformation Conditions:** Surface deformation measurements that indicate an asymmetric or otherwise heterogeneous evolution of the injection zone pressure front, resulting in larger than predicted surface deformation outside the CO_2 plume. Areal surface deformation will be monitored using several technologies including differential synthetic aperture radar interferometry (DInSAR), which is a radar-based method that can measure very small changes in ground-surface elevation linked to pressure variations at depth. The area surveyed will extend beyond the predicted maximum extent of the CO_2 plume. If a measurable rise in the ground surface occurs outside the predicted extent, the AoR will be re-evaluated. The Testing and Monitoring Plan provides extended information about surface deformation monitoring.

   Action: The computational model will be calibrated to match calculated pressures if they vary from the predicted deformation/pressure calculations..

5. **Seismic Monitoring Identification of Subsurface Structural Features:** Seismic monitoring data indicate the possible presence of a fault or fracture near the CO_2 injection zone in the sedimentary cover or in the basement (concentration of microearthquakes of M<<1 in elongated clusters). The Testing and Monitoring Plan provides extended information about the microseismic monitoring network.

   Action: The cause of the indicated microseismicity patterns would be evaluated. In conjunction, various operational parameters would be tested using computational model to determine if the microseismic activity can be controlled to acceptable levels

6. **Seismic Monitoring Identification of Unexpected Plume Pattern:** Seismic monitoring data indicate a CO_2 plume migration outside the predicted extent. The observation of microearthquakes (M<<1) may also help define the actual shape of the maximum pressure field associated with the plume extensions.

   Action: The computational model will be calibrated to match the location of observed microseismicity patterns indicative of plume extensions.

Reevaluation Strategy

If any of these conditions occurs, the Alliance will reevaluate the AoR as described below. Ongoing direct and indirect monitoring data, which provide relevant information for understanding the development and evolution of the CO_2 plume, will be used to support re-evaluation of the AoR. These data include 1) the chemical and physical characteristics of the CO_2 injection stream based on sampling and analysis; 2) continuous monitoring of injection mass flow rate, pressure, temperature, and fluid volume; 3) measurements of pressure response at all site monitoring wells; and 4) CO_2 arrival and transport response at all site monitoring wells based on direct aqueous measurements and selected indirect monitoring method(s). The Alliance will compare these observational data with predicted responses from the computational model and if significant discrepancies between the observed and predicted responses exist, the monitoring data will be used to recalibrate the model (Figure 23). In cases where the observed monitoring data agree with model predictions, an AoR reevaluation will consist of a demonstration that monitoring data are consistent with modeled predictions. As additional characterization data are collected, the site conceptual model will be revised and the modeling steps described above will be repeated to incorporate new knowledge about the site.

The Alliance will submit a report notifying the UIC Program Director of the results of this reevaluation within 90 days of detection. At that time, the Alliance will either 1) submit the monitoring data and modeling results to demonstrate that no adjustment to the AoR is required, or 2) modify its Corrective Action, Emergency and Remedial Response and other plans to account for the revised AoR. All modeling inputs and data used to support AoR reevaluations will be retained by the Alliance for the period of the project.

To the extent that the reevaluated AoR is different from the one identified in this supporting documentation, the Alliance will identify all active and abandoned wells and underground mines that penetrate the confining zone (the Eau Claire Formation) in the reevaluated AoR and will perform corrective actions on those wells. As needed, the Alliance will revise all other plans, such as the Emergency and Remedial Response Plan, to take into account the reevaluated AoR and will submit those plans to the UIC Program Director for review and approval.

Note that seismic events are covered under the Emergency Response and Remediation Plan. A tiered approach to responding to seismic events will be based on magnitude and location. A notification procedure is provided in that plan.

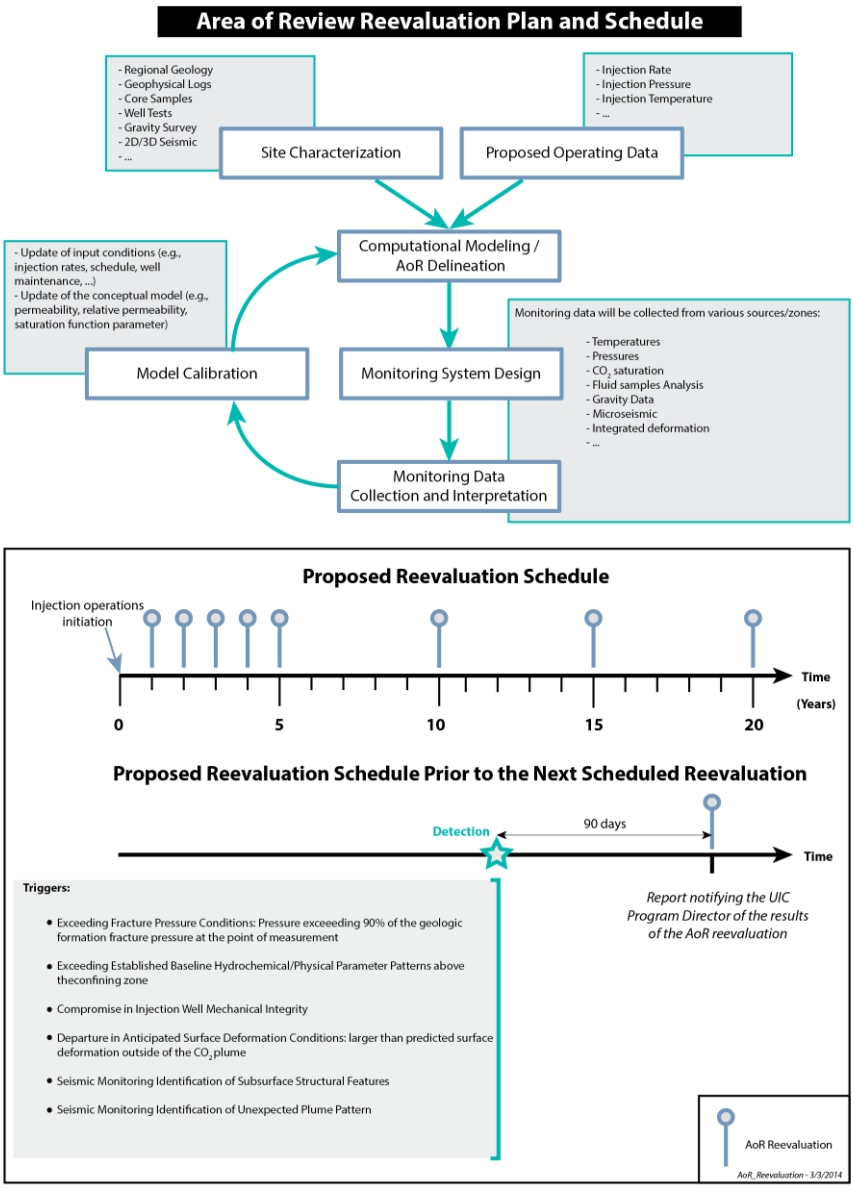

Figure 22. AoR Correction Action Plan Flowchart

References

~~FutureGen Alliance. 2006. Mattoon, Illinois Environmental Information Volume II Subsurface. PNWD-3768, prepared for the FutureGen Alliance by Battelle – Pacific Northwest Division, Richland, Washington.~~

~~White, S.P., R. Allis, J. Moore, T. Chidsey, C. Morgan, W. Gwynn, and M. Adams. 2005. Simulation of reactive transport of injected CO2 on the Colorado Plateau, Utah, USA. Chemical Geology 217:387–405.~~

Battelle (Pacific Northwest Division). 2012. Borehole Completion and Characterization Summary Report for the Stratigraphic Well, Morgan County, Illinois. PNWD-4343, Richland, Washington.

Bell AH. 1927. *Recent Developments in the Vicinity of Jacksonville*. Illinois Petroleum Report 11, Illinois State Geologic Survey, Urbana, Illinois.

Birkholzer JT, J Apps, L Zhenge, Y Zhang, T Xu and C Tzang. 2008. *Research Project on CO_2 Geological Storage and Groundwater Resources: Large-Scale Hydrological Evaluation and Modeling of the Impact on Groundwater Systems Annual Report: October 1, 2007, to September 30, 200*8. Lawrence Berkeley National Laboratory, Berkeley, California.

Birkholzer JT, JP Nicot, CM Oldenburg, Q Zhou, S Kraemer, and KW Bandilla. 2011. Brine Flow up a Borehole Caused by Pressure Perturbation from CO_2 Storage: Static and Dynamic Evaluations. *International Journal of Greenhouse Gas Control* 5(4):850-861.

Birkholzer JT, A Cihan, and KW Bandilla, and K. 2013. A Tiered Area-Of-Review Framework for Geologic Carbon Sequestration. *Greenhouse Gas Sci Technol*. doi: 10.1002/ghg.1393

Buschbach TC and DC Bond. 1967. Underground Storage of Natural Gas in Illinois − 1967. Illinois Petroleum 86. Illinois State Geological Survey, Champaign, Illinois.

Buschbach TC and DC Bond. 1974. Underground Storage of Natural Gas in Illinois – 1973 (updated). Illinois Petroleum 101. Illinois State Geological Survey, Champaign, Illinois.

Celia MA, JM Nordbotten, B Court, M Dobossy, and S Bachu. 2011. Field-scale Application of a Semi-Analytical Model for Estimation of CO_2 and Brine Leakage aong Old Wells. *International Journal of Greenhouse Gas Control* 5:257−269.

Cihan A, Q Zhou, and JT Birkholzer. 2011. Analytical solutions for pressure perturbation and fluid leakage through aquitards and wells in multilayered-aquifer systems. *Water Resour. Res.* 47.

Cihan A, JT Birkholzer, and Q Zhou. 2013. Pressure Buildup and Brine Migration During CO_2 Storage in Multilayered Aquifers. *Groundwater* 51(2).

Cihan A, JT Birkholzer, Q Zhou, and C Oldenburg. 2014. An Analytical Solution of Focused and Diffuse Leakage in Multilayered Aquifers (ASLMA): User Guide. LBNL-XXXXX (in press), Berkeley, CA.

Core Laboratories. 1966. Borehole Criswell No. 1-6 at the Waverly field: Core Laboratories, Inc. October 31, 1966, memo to Panhandle Eastern Pipeline Company, Liberal, Kansas (Waverly Field, Criswell 1-16), File #: SCAL-65269. Houston, Texas.

Crow W, JW Carey, S Gasda, B Williams, and MA Celia. 2010. Wellbore integrity analysis of a natural CO_2 producer. *International Journal of Greenhouse Gas Control* 4:186–197.

Duguid A, R Busch, JW Carey, MA Celia, N Chugunov, SE Gasda, TS Ramakrishnan, V Stamp, and JE Wang. 2013. Pre-Injection Baseline Data Collection to establish existing Well Leakage Properties. In Proceedings of the GHGT-11 Meeting, Kyoto, Japan, November 2013, *Energy Procedia*.

EPA (U.S. Environmental Protection Agency). 2013. Underground Injection Control (UIC) Program Class VI Well Area of Review Evaluation and Corrective Action Guidance. EPA 816-R-13-005, Office of Water, Washington, D.C.

EPA (U.S. Environmental Protection Agency). 2011a. "Underground Injection Control Permit Application IL-ICCS Project." Administrative Record for Underground Injection Control Permit Application from Archer Daniels Midland Company, EPA Region 5, Chicago Illinois.

EPA (U.S. Environmental Protection Agency). 2011b. "Underground Injection Control Permit Application IL-ICCS Project." Administrative Record for Underground Injection Control Permit Application from Christian County Generation, LLC of Taylorville, EPA Region 5, Chicago Illinois.

EPA (U.S. Environmental Protection Agency). 1994. "Determination of Maximum Injection Pressure for Class I Wells." Underground Injection Control Section Regional Guidance #7. EPA Region 5, Chicago, Illinois.

Freeze RA and JA Cherry. 1979. *Groundwater*. Published by Prentice-Hall, Inc., Englewood Cliffs, New Jersey.

FutureGen Alliance. 2006. *Mattoon, Illinois Environmental Information Volume II Subsurface*. PNWD-3768, prepared for the FutureGen Alliance by Battelle – Pacific Northwest Division, Richland, Washington.

Gasda SE, MA Celia, JE Wang, and A Duguid. 2013. Wellbore permeability estimates from vertical interference testing of existing wells. In Proceedings of the GHGT-11 Meeting, Kyoto, Japan, November 2013, *Energy Procedia*.

Greb SF, DC Harris, MP Solis, WH Anderson, JA Drahovzal, BC Nuttall, RA Riley, W Solano-Acosta, JA Rupp, and N Gupta. 2009. Cambrian–Ordovician Knox carbonate section as integrated reservoirs and seals for carbon sequestration in the eastern mid-continent United States. In M. Grobe, JC Pashin, and RL Dodge (eds.), Carbon dioxide sequestration in geological media—State of the science. *AAPG Studies in Geology* 59: 241–259.

Hornung J and T Aigner. 1999. "Reservoir and aquifer characterization of fluvial architectural elements: Stubensandstein, Upper Triassic, southwest Germany." *Sedimentary Geology* 129(3–4):215-280.

ISGS (Illinois State Geological Survey). 2012. Coal Mines, Coal Geology, and Resource Data Online,

County Coal Map and Data Series, Morgan County. Available at: http://www.isgs.uiuc.edu/maps-datapub/coal-maps/counties/morgan.shtml. Last accessed January 4, 2012.

Kerr DR, L Ye, A Bahar, BM Kelkar, and S Montgomery. 1999. "Glenn Pool Field, Oklahoma: A Case of Improved Production from a Mature Reservoir." *American Association of Petroleum Geologists Bulletin* 83(1):1-18.

Mandel, R.J., and Kontis, A.L., 1992, Simulation of Regional Ground-water Flow in the Cambrian-Ordovician Aquifer System in the Northern Midwest, United States: U.S. Geological Survey Professional Paper 1405–C.

Meents WF. 1981. *Analysis of Natural Gas in Illinois, Gas, Natural – Illinois*. Illinois State Geological Survey, Urbana, Illinois.

Meyer R and FF Krause. 2006. "Permeability Anisotropy and Heterogeneity of a Sandstone Reservoir Analogue: An Estuarine to Shoreface Depositional System in the Virgelle Member, Milk River Formation, Writing-On-Stone Provincial Park, Southern Alberta." *Bulletin of Canadian Petroleum Geology* 54(4):301-318.

Pruess K, J Garcia, T Kovscek, C Oldenburg, J Rutqvist, C Steefel, and T Xu. 2002. *Intercomparison of Numerical Simulation Codes for Geologic Disposal of CO_2*. LBNL-51813, Lawrence Berkeley National Laboratory, Berkeley, California.

Ringrose P, K Nordahl, and RJ Wen. 2005. "Vertical permeability estimation in heterolithic tidal deltaic sandstones." *Petroleum Geoscience* 11(1):29-36.

Saller AH, J Schwab, S Walden, S Robertson, R Nims, H Hagiwara, and S Mizohata. 2004. "Three-dimensional seismic imaging and reservoir modeling of an upper Paleozoic "reefal" buildup, Reinecke Field, west Texas, United States." Pp. 107-125 *in* GP Eberli, JL Masaferro, and JF Sarg (eds.), *Seismic Imaging of Carbonate Reservoirs and Systems*, Volume 81, American Association of Petroleum Geologists, Tulsa, Oklahoma.

Span R and W Wagner. 1996. "A New Equation of State for Carbon Dioxide Covering the Fluid Region from the Triple-Point Temperature to 1100 K at Pressures Up to 800 MPa." *J Phys Chem Ref Data* 25:1509-1596.

Spycher N and K Pruess. 2010. "A Phase-Partitioning Model for CO_2-Brine Mixtures at Elevated Temperatures and Pressures: Application to CO_2-Enhanced Geothermal Systems." *Transport in Porous Media* 82:173-196. doi:10.1007/s11242-009-9425-y.

Spycher N, K Pruess, and J Ennis-King. 2003. "CO_2-H_2O mixtures in geological sequestration of CO_2. I. Assessment and calculation of mutual solubilities from 12 to 100°C and up to 600 bar." *Geochimica et Cosmoschimica Acta* 67(16):3015-3031. doi:10.1016/s0016-7037(03)00273-4.

Texas World Operations, Inc. 1995. Drilling and Completion Report, Well No. 3. CABOT # 3 \ 12-0070, prepared by Texas World Operations for Cabot Corporation, Tuscola, Illinois.

Watson TL and S Bachu. 2008. Identification of Wells with High CO_2-Leakage Potential in Mature Oil Fields Developed for CO_2-Enhanced Oil Recovery. In: Paper SPE 11294, SPE Improved Oil Recovery Symposium, Tulsa, Oklahoma, USA, 19-23 April, 2008.

White, MD, DJ Watson, DH Bacon, SK White, BP McGrail, and ZF Zhang. 2013. *STOMP Subsurface Transport over Multiple Phases STOMP-CO2 and -CO2e Guide Version 1.1*, PNNL-21268, Pacific Northwest National Laboratory, Richland, WA.

White, MD and BP McGrail. 2005. *STOMP Subsurface Transport over Multiple Phases Version 1.0 Addendum: ECKEChem Equilibrium-Conservation-Kinetic Equation Chemistry and Reactive Transport*, PNNL-15482, Pacific Northwest National Laboratory, Richland, WA.

White MD and M Oostrom. 2006. *STOMP Subsurface Transport Over Multiple Phases, Version 4: User's Guide.* PNNL-15782, Pacific Northwest National Laboratory, Richland, Washington

White MD and M Oostrom. 2000. *STOMP Subsurface Transport Over Multiple Phases: Theory Guide*. PNNL-12030, Pacific Northwest National Laboratory, Richland, Washington.

Whitney CL, L Parris, D Jiao, and R Lee. 2012. Core Analysis Study: FutureGen Industrial Alliance (Battelle), FutureGen #1 Well, Wildcat Field, Morgan County, Illinois. Core Laboratories Report HOU-111568, Core Laboratories, Houston, Texas.

Williams MD, VR Vermeul, D Appriou, AHR Bonneville, JA Horner, FA Spane, and TJ Gilmore. 2014. Analysis of Impacts on Lowermost USDW from Focused Leakage of Brine from Plugged and Abandoned or Poorly Constructed Wells at the FutureGen 2.0 Site . PNWD-4414 Rev. 1, Battelle—Pacific Northwest Division, Richland, WA.

Young, H.L., 1992, Hydrogeology of the Cambrian-Ordovician Aquifer System in the Northern Midwest, United States: U.S. Geological Survey Professional Paper 1405–B.

Zhou Q, JT Birkholzer, E Mehnert, Y-F Lin, and K Zhang. 2010. "Modeling basin- and plume-scale processes of CO_2 storage for full-scale deployment." *Ground Water* 48(4):494–514.

~~References needed:~~

~~White et al. 2012;~~

~~White and McGrail 2005,~~

Formatted: Font:

Attachment A: Known Well Within the Survey Area and outside of the AoR.~~Attachment~~

Map ID	API Number	ISWS ID	Latitude (NAD 83)	Longitude (NAD 83)	Public Land Survey System (PLSS)	Total Depth (ft)	Elevation (ft)	Completion Date	Owner	Well #	Well Type	Status	Confining Zone Penetration Well
2	121372155200	237387	39.815638	-90.084967	T16N,R9W,Sec 23	41		19920313	Nickel, Gerald	1	Water	Private Water Well	No
3	121372182100	300966	39.815638	-90.084967	T16N,R9W,Sec 23	46		19971104	Nickel, Gerald & Diane	1	Water	Private Water Well	No
13	121372173400	297871	39.811987	-90.07805	T16N,R9W,Sec 26	37		19960213	Keltner, Dale		Water	Private Water Well	No
23	121370024000		39.780186	-90.094859	T15N,R9W,Sec 3	402	642	19230101	Trotter, L.B.	1	Oil & Gas	Dry and Abandoned, No Shows	No
24	121372097800		39.776078	-90.080727	T15N,R9W,Sec 3	327	632	0	Harris		Unknown / other	Unknown, Plugged	No
28		115642	39.82166	-90.041238	T16N,R8W,Sec 19	25		1870	W W Robertson		Water		No
38		116456	39.776761	-90.107843	T15N,R9W,Sec 4	30			Rayburn		Water		No
39		116457	39.776761	-90.107843	T15N,R9W,Sec 4	32			Greene		Water		No
40		115725	39.821959	-90.097446	T16N,R9W,Sec 22	18			K Brown		Water		No
41		115726	39.821959	-90.097446	T16N,R9W,Sec 22	30			E C Trotter		Water		No
52		115640	39.836203	-90.022343	T16N,R8W,Sec 17	25			J H Hubbs		Water		No
53		115641	39.83617	-90.041154	T16N,R8W,Sec 18	32		1850	H Robinson		Water		No
54		115643	39.821671	-90.022214	T16N,R8W,Sec 20	26		1900	S Weinfeldt		Water		No
55		115644	39.821671	-90.022214	T16N,R8W,Sec 20	30		1904	Robinson		Water		No
56		115649	39.807149	-90.022402	T16N,R8W,Sec 29	26			M Walbaum		Water		No
57		115653	39.793	-90.022	T16N,R8W,Sec 32	18			Beggs		Water		No
58	121372070800	116522	39.77156	-90.0878	T15N,R9W,Sec 3	50		19770320	Linebarger, David		Water		No
59	121372118300	116520	39.769673	-90.080523	T15N,R9W,Sec 3	42			Harris, Frank R.		Water	Private Water Well	No
60	121372070700	116521	39.769673	-90.080523	T15N,R9W,Sec 3	40			harris F R		Water		No
61		116458	39.777	-90.126	T15N,R9W,Sec 5	30			Gary S. B.		Water		No
62		116464	39.761	-90.126	T15N,R9W,Sec 8	30			Cleray W		Water		No
63		116465	39.761	-90.126	T15N,R9W,Sec 8	40			Coons A		Water		No
64		116466	39.761	-90.107	T15N,R9W,Sec 9	30			Wallbaum W M		Water		No
65		116467	39.761	-90.107	T15N,R9W,Sec 9	35			Trotter l B		Water		No
66		227314	39.761	-90.107	T15N,R9W,Sec 9	40			Carl Shinnall #1		Water		No
67		116468	39.761	-90.089	T15N,R9W,Sec 10	30			Orear R		Water		No
68	121372070900	116525	39.765755	-90.080645	T15N,R9W,Sec 10	40			Linebarger D		Water		No
69		116469	39.761	-90.07	T15N,R9W,Sec 11	30			Collins W		Water		No
70		116470	39.761	-90.07	T15N,R9W,Sec 11	32			Lockhart G		Water		No
71		116393	39.776799	-90.032936	T15N,R8W,Sec 6	25		1923			Water		No
72		116394	39.776799	-90.032936	T15N,R8W,Sec 6	28			C Smith		Water		No
73	121372116800	116436	39.784526	-90.041604	T15N,R8W,Sec 6	54		19770226	Becker, Carl J.	1	Water	Livestock Watering Well	No
74	121372116900	116435	39.784526	-90.041604	T15N,R8W,Sec 6	43		19781010	Becker, Carl J.	1	Water	Private Water Well	No
75	121372117000	116434	39.782453	-90.041567	T15N,R8W,Sec 6	27		19761213	Smith, Lloyd E.	1	Water	Livestock Watering Well	No
76	121372161900		39.766277	-90.041266	T15N,R8W,Sec 7	26			Walpole, Ron		Water		No
77		116395	39.763	-90.033	T15N,R8W,Sec 7	30					Water		No
78		115696	39.836221	-90.059875	T16N,R9W,Sec 13	25			V R Mc Clure		Water		No

Table 9. (contd)

Map ID	API Number	ISWS ID	Latitude (NAD 83)	Longitude (NAD 83)	Public Land Survey System (PLSS)	Total Depth (ft)	Elevation (ft)	Completion Date	Owner	Well #	Well Type	Status	Confining Zone Penetration Well
79		115697	39.836221	-90.059875	T16N,R9W,Sec 13	27			U B Fox		Water		No
80		115698	39.836221	-90.059875	T16N,R9W,Sec 13	27			G W Lewis		Water		No
81		115699	39.836362	-90.078662	T16N,R9W,Sec 14	30			J Parrat		Water		No
82		115700	39.836362	-90.078662	T16N,R9W,Sec 14	28			C W Lewis		Water		No
83		115701	39.836362	-90.078662	T16N,R9W,Sec 14	28			J W Parrat		Water		No
84		115702	39.836362	-90.078662	T16N,R9W,Sec 14	32			J Hodgeson		Water		No
85	121372203900	356742	39.830101	-90.102984	T16N,R9W,Sec 15	47		20030910	Lomar Hager Construction		Water	Private Water Well	No
86		115703	39.836486	-90.097369	T16N,R9W,Sec 15	24			G Noulty		Water		No
87		115704	39.836486	-90.097369	T16N,R9W,Sec 15	30			L Lamkaular		Water		No
88		115705	39.836486	-90.097369	T16N,R9W,Sec 15	35			E E Hart		Water		No
89		115706	39.8365	-90.116151	T16N,R9W,Sec 16	23			S Jumper		Water		No
90		115707	39.8365	-90.116151	T16N,R9W,Sec 16	25			H Wester		Water		No
91		115722	39.821967	-90.116263	T16N,R9W,Sec 21	30			T J Ward		Water		No
92		115724	39.821967	-90.116263	T16N,R9W,Sec 21	30			C Trotter		Water		No
93		216249	39.821967	-90.116263	T16N,R9W,Sec 21	28		1934	Wm Noulty		Water		No
94	121370028400		39.822767	-90.073164	T16N,R9W,Sec 23	405		19540301	Keltner	1	Water		No
95	121372155100	237377	39.820978	-90.077895	T16N,R9W,Sec 23	42		19920414	Allen, John D.	1	Water	Private Water Well	No
96	121372207600	365042	39.822764	-90.075515	T16N,R9W,Sec 23	46		20040715	Burton, Larry		Water	Private Water Well	No
97	121372128400	115776	39.826288	-90.058992	T16N,R9W,Sec 24	40		19760220	Robinson, Leroy A.	1	Water	Private Water Well	No
98	121372128500	115777	39.828869	-90.059535	T16N,R9W,Sec 24	37		19781214	Romine, Buddy	1	Water	Private Water Well	No
99	121372211600	420169	39.813876	-90.103667	T16N,R9W,Sec 27	35		20060809	Donnan, Jeff		Water	Private Water Well	No
100		115744	39.807541	-90.116512	T16N,R9W,Sec 28	110			Noah B Fox		Water		No
101		115745	39.807541	-90.116512	T16N,R9W,Sec 28	28			Noah B Fox		Water		No
102		115746	39.807541	-90.116512	T16N,R9W,Sec 28	30			C Holdbrook		Water		No
103		115723	39.807541	-90.116512	T16N,R9W,Sec 28	28			W Noulty		Water		No
104	121372203000	348692	39.806645	-90.122622	T16N,R9W,Sec 28	42			Kendra Swain		Water		No
105		115759	39.792956	-90.116724	T16N,R9W,Sec 33	30			H Swain		Water		No
106		115760	39.792956	-90.116724	T16N,R9W,Sec 33	28			L L Hart		Water		No
107	121372155000		39.822856	-90.119949	T16N,R9W,Sec 21				Spradlin, Jack		Water		No
108	121370011400		39.833775	-90.10777	T16N,R9W,Sec 16	385	616	19551101	Wolfe, Eliz	1	Oil & Gas	Dry and Abandoned, No Shows, Plugged	No
109	121370011500		39.80091	-90.040421	T16N,R8W,Sec 30	420	635	19560101	Beilschmidt	1	Oil & Gas	Dry and Abandoned, No Shows, Plugged	No
110	121370011600		39.815108	-90.028322	T16N,R8W,Sec 20	365	610	19551201	Robinson, Howard	1	Oil & Gas	Dry and Abandoned, No Shows, Plugged	No
111	121370018900		39.825408	-90.062536	T16N,R9W,Sec 24	200		19440101	Lewis, E. C.		Oil & Gas	Dry Hole	No
112	121370024100		39.769077	-90.111454	T15N,R9W,Sec 4	580			Rayborn	1	Oil & Gas	Gas Producer	No
113	121370044200		39.770193	-90.110273	T15N,R9W,Sec 4	350			Rayburn	1	Oil & Gas	Gas Producer	No
114	121372086900		39.769679	-90.098565	T15N,R9W,Sec 4	301					Coal Test		No
115	121370024200		39.778927	-90.119618	T15N,R9W,Sec 5	423			Green, Laura & Effie	1	Oil & Gas	Gas Producer	No
116	121370024600		39.764523	-90.098492	T15N,R9W,Sec 9	293			Baxter	2	Oil & Gas	Dry and Abandoned, Gas Shows	No
117	121372094800		39.767065	-90.11144	T15N,R9W,Sec 9	325			Beilschmidt	1	Oil&Gas	Temporarily Abandoned	No
118	121372105200		39.763524	-90.104346	T15N,R9W,Sec 9				Leinberger	2	Oil&Gas	Permit to Drill Issued	No
119	121370007900		39.766464	-90.091366	T15N,R9W,Sec 10	295			Dunlap	8	Oil & Gas	Gas Producer	No
120	121372084800		39.766422	-90.065678	T15N,R9W,Sec 11	243					Coal Test		No
121	121370030900		39.806625	-90.105838	T16N,R9W,Sec 27	324	610	19591001	Fox, Lyman	1	Oil & Gas	Dry and Abandoned, No Shows, Plugged	No
122	121370033200		39.788212	-90.03349	T16N,R8W,Sec 31	323	641	19271001	Corrington	1	Oil & Gas	Dry and Abandoned, No Shows	No

Table 8. (contd)

Map ID	API Number	ISWS ID	Latitude (NAD 83)	Longitude (NAD 83)	Public Land Survey System (PLSS)	Total Depth (ft)	Elevation (ft)	Completion Date	Owner	Well #	Well Type	Status	Confining Zone Penetration Well
123	121370062300		39.828772	-90.06935	T16N,R9W,Sec 24	814	624	19700701	#MA-3		Stratigraphic or Structure Test	Structure Test, Plugged	No
124	121372068000		39.792709	-90.039363	T16N,R8W,Sec 31	142	641	19700518	Flynn, Robert		Coal Test		No
125	121372088400		39.829096	-90.098826	T16N,R9W,Sec 22	318	621	0			Coal Test		No
126	121372088600		39.801122	-90.108499	T16N,R9W,Sec 28	301	621	0			Coal Test		No
127	121372067800		39.814431	-90.023514	T16N,R8W,Sec 20	130	610	19700507	Newberry, Lucille		Coal Test		No
128	121372086000		39.83138	-90.055009	T16N,R9W,Sec 13	301	619	0			Coal Test		No